UNIVERSITY OF CALIFORNIA,
IRVINE

The Impact of the Circadian Clock and Feeding Time on Skin Function

DISSERTATION

submitted in partial satisfaction of the requirements
for the degree of

DOCTOR OF PHILOSOPHY

in Biomedical Sciences

by

Elyse Noelani van Spyk

Dissertation Committee:
Professor Bogi Andersen, Chair
Professor Paolo Sassone-Corsi
Assistant Professor Scott Atwood
Professor Eric Pearlman

2017

DEDICATION

To my parents, who encouraged me to pursue my passion- whatever it may be. To Milton, for keeping my head on straight in the midst of chaos, and to my cat, who has been an endless source of comfort.

TABLE OF CONTENTS

LIST OF ABBREVIATIONS

ZT	zeitgeber time
Per1/2	*Period 1/2*
Cry1/2	*Cryptochrome 1/2*
SCN	suprachiasmatic nucleus
CCGs	Clock controlled genes
Ox. phos.	oxidative phosphorylation
GO	Gene ontology
ED	early day
MD	mid day
EN	early night
AD	ad libitum
RF	restricted feeding
XPA	*Xeroderma Pigmentosum, Complementation Group A*
(6-4)PPs	(6-4) photoproducts
CPDs	cyclobutane pyrimidine dimers
H&E	Hematoxylin and Eosin
UV	untraviolet
Irf7	*Interferon regulatory factor 7*
IMQ	Imiquimod
IFE	interfollicular epidermis
DC	dendritic cell
pDC	plasmacytoid dendritic cell

LC	Langerhan's cell
KC	keratinocyte
Mp	macrophage
FACS	Fluorescence-activated cell sorting
IFN-α/β	Interferon α/β
KO	knock out
Wt	Wildtype
ELISA	enzyme-linked immunosorbent assay
GSEA	Gene Set Enrichment Analysis
GO	Gene Ontology
EdU	5-ethynyl-2́ -deoxyuridine
IREs	interferon responsive elements
TSNE	t-distributed stochastic neighbor embedding
qPCR	quantitative polymerase chain reaction
ChIP	Chromatin Immunoprecipitation
PAMP	pathogen-associated molecular pattern
ISGs	interferon-sensitive genes
PRR	pattern recognition receptors
TLR	Toll-like receptor
DBP	D-box binding protein
Stat1	*signal transducer and activator of transcription 1*

LIST OF FIGURES

Page

LIST OF TABLES

Page

ACKNOWLEDGMENTS

I would like to express the deepest appreciation to my committee chair, Dr. Bogi Andersen. His insight and expansive knowledge have been invaluable to me throughout the years. From planning my first experiments, to interpreting sometimes-inconsistent results, to critically reviewing scholarly articles, Dr. Andersen has guided me every step of the way. Without his guidance and persistent aid this dissertation would not have been possible.

I would like to thank my committee members, Professor Dr. Paolo Sassone-Corsi, Dr. Eric Pearlman and Dr. Scott Atwood whose advice about not only my research, but also life in general, has been extremely helpful. Their passion for science and mentorship has been a true inspiration to me. I would also like to thank all the wonderful people that I have worked with in the Andersen laboratory and throughout the campus community. These include Dr. Melanie Oakes, Vanessa Scarfone, and Dr. Jennifer Atwood. Your patience, expansive knowledge, and dedication to helping others has been invaluable to my research goals and experience here at UCI.

I thank Springer International Publishing Company for permission to include copyrighted figures and text as Chapter one. I also thank Dr. Maksim Plikus for permission to include Figure 1.4, which was originally published in *Journal Biological Rhythms* (published by SAGE Publications), and Dr. Hong Wang for permission to include Chapter two, which was originally published in *Cell Reports* (published by Elsevier under licensed under this Public License Creative Commons Attribution (CC BY 4.0)). Financial support was provided by NSF GRFP Grant number DGE-1321846 and an ARCS/Roche predoctoral fellowship.

CURRICULUM VITAE

Elyse Noelani van Spyk

25 Palatine Apt 221
Irvine, CA 92612
(831) 236-4372
evanspyk@uci.edu

Education:

July 2013-December 2017: Ph.D. Candidate in Biomedical Sciences in the laboratory of Dr. Bogi Andersen, Department of Biological Chemistry, School of Medicine at University of California, Irvine. **Overall GPA: 3.9**

September 2012-July 2013: Graduate student in the Cellular and Molecular Biosciences gateway Ph.D. program at University of California, Irvine.

September 2007-June 2011. University of California, Davis
Graduated with honors in the College of Biological Sciences with a Bachelors of Science degree in Neurobiology, Physiology and Behavior (NPB). **Overall GPA**: **3.55**

Grants and Awards:

- **National Science Foundation (NSF) Graduate Research Program Fellow, June 2014-2017.**
- **ARCS/Roche Scholar for UC Irvine's School of Medicine September 2014-2017.**
- Travel grant recipient from Associated Graduate Students (AGS).
- Travel grant recipient from the UC Irvine School of Medicine.
- Recipient of the Office of Graduate Studies in the School of Medicine Individual Fellowship Bonus yearly from 2014-2017.
- UC Davis John H. and Jeanne Pryor scholarship recipient, September 2010
- UC Davis Community Service Award recipient, 2010
- UC Davis College of Letters and Science Dean's Honor list, Fall and Spring 2008

Publications:

1. Time-restricted feeding shifts the skin circadian clock and alters UVB-induced DNA damage. Wang H*, **van Spyk E N***, Liu Q, Geyfman M, Salmans M L, Kumar V, Ihler A, Li N, Takahashi J S, Andersen B. *Cell Reports*. **2017** Aug: 20(5): 1061-1071
   *equal contributors

2. **van Spyk E N**, Greenberg M, Mourad F, and Andersen B. (2016). Regulation of Cutaneous Stress Response Pathways by the Circadian Clock: From Molecular Pathways to Therapeutic Opportunities. Skin Stress Response Pathways, Springer International Publishing**:** 281-300.
3. The circadian clock in skin: Implications for adult stem cells, tissue regeneration, cancer aging, and immunity. Plikus M V, **van Spyk E N**, Pham K, Geyfman M, Kumar V, Takahashi J, Andersen B. *JBR*. 2015 Jun;30(3):163-82.
4. Increased levels of CD34+ cells are associated in patients with abdominal aortic aneurysms compared with patients with peripheral vascular disease. **van Spyk E N**, Chun K C, Samadzadeh K M, Irving C S, Peters J H, Lee E S. *J Surg Res*. 2013 Sep;184(1):638–43.
5. Monocytic adhesion molecule expression and monocyte–endothelial cell dysfunction are increased in patients with peripheral vascular disease *versus* patients with abdominal aortic aneurysms. Lee E S, **van Spyk E N**, Chun K C, Pitts R L, Wu M H, Yuan S Y. *J Surg Res*. 2012 Oct;177(2):373–81.
6. Outcomes of an abdominal aortic aneurysm screening program. Chun K C, Teng K Y, **van Spyk E N**, Carson J G, Lee E S. *J Vasc Surg*. 2013 Feb;57(2):376–81.
7. Implementation of the Screen for Abdominal Aortic Aneurysms Very Efficiently (SAAAVE) Act: A Five-Year Follow-up. Chun K C, Teng K Y, **van Spyk E N**, Carson J G, Lee E S. *J Vasc Surg*. 2012 June;55(6):5S.
8. Risk Factors Associated with the Diagnosis of Abdominal Aortic Aneurysm in Patients Screened at a Regional Veterans Affairs Health Care System. Chun K C, Teng K Y, Chavez L A, **van Spyk E N**, Samadzadeh K M, Carson J G, Lee E S. *Annals of Vascular Surgery*. 2013.
9. Dual EGFR/HER2 inhibition sensitizes prostate cancer cells to androgen withdrawal by suppressing ErbB3. Chen L, Mooso B A, Jathal M K, Madhav A, Johnson S D, **Van Spyk E N**, Mikhailova M, Zierenberg-Ripoll A, Xue L, Vinall RL, et al. *Clin Cancer Res*. 2011;17:6218–6228.

Published Abstracts and Oral Presentations:

1. **van Spyk, E N.** Video interview by Gary Kirwan (Biohackers Lab). "Ep26: Eating Too Late is Bad For Our Skin's Ability to Repair Research with Elyse van Spyk". http://www.biohackerslab.com/ep26-elyse-van-spyk/. Published online on September 3rd, 2017.
2. **van Spyk E N**, Wang H, Ihler A, Liu Q, Salmans M, Geyfman M, Cam E, Espitia F, Kumar V, Yu Z, Li N, Takahashi J S, Andersen B. "Time-restricted feeding uncouples the circadian clock and the cell cycle of epidermal stem cells, and alters the sensitivity to UVB-induced DNA damage". Presented at the 2017 winter quarter Cancer Biology Journal Club on May 15th, 2017 at Sprague Hall, UC Irvine, CA.
3. **van Spyk E N**, Wang H, Ihler A, Liu Q, Salmans M, Geyfman M, Cam E, Espitia F, Kumar V, Yu Z, Li N, Takahashi J S, Andersen B. "Time-restricted feeding uncouples the circadian clock and the cell cycle of epidermal stem cells, and alters the sensitivity to UVB-induced DNA damage". Presented at the 17thAnnual Orange County ARCS Scholar Awards Dinner. March 16, 2017 at The Arnold and Mabel

Beckman Center of the National Academy of Sciences and Engineering, UC Irvine, CA.

4. **van Spyk E N**, Wang H, Ihler A, Liu Q, Salmans M, Geyfman M, Cam E, Espitia F, Kumar V, Yu Z, Li N, Takahashi J S, Andersen B. Time-restricted feeding uncouples the circadian clock and the cell cycle of epidermal stem cells, and alters the sensitivity to UVB-induced DNA damage. Presented at the First Annual Skin Symposium on Genomic Approaches to Skin Regeneration and Wound Healing on Thursday, February 23, 2017. Sprague Hall at UC Irvine, CA.
5. Invited speaker for the Skin DOT meeting held at the UCI Medical Center in Orange, CA on May 2, 2016. Gave a talk entitled, "Circadian regulation of the type I Interferon Pathway in the skin".
6. **van Spyk E N**, Wang H, Ihler A, Liu Q, Salmans M, Geyfman M, Cam E, Espitia F, Kumar V, Yu Z, Li N, Takahashi J S, Andersen B. Time-restricted feeding uncouples the circadian clock and the cell cycle of epidermal stem cells, and alters the sensitivity to UVB-induced DNA damage. Gave a talk at the Society for Investigative Dermatology 75th Annual Meeting on May 11-14, 2016 at the Westin Kierland Resort & Spa in Scottsdale, AZ.
7. **van Spyk E N**, Wang H, Ihler A, Liu Q, Salmans M, Geyfman M, Cam E, Espitia F, Kumar V, Yu Z, Li N, Takahashi J S, Andersen B. Time-restricted feeding uncouples the circadian clock and the cell cycle of epidermal stem cells, and alters the sensitivity to UVB-induced DNA damage. Presented at the Gordon Research Seminar on Epithelial Differentiation & Keratinization (GRS) held July 11-12, 2015 at Sunday River in Newry ME.
8. Invited panelist for UCI's CMB NSF fellowship workshop October 1, 2014 in Sprague Hall at UC Irvine. Presented a talk entitled, "The Circadian Clock in the Mouse Skin".
9. **van Spyk E N**, Chun KS, Jami SA, Samadzadeh KM, Lee ES. Peripheral Vascular Disease Patients Have Lower Percent Positive Circulating Progenitor Cells Compared To Abdominal Aortic Aneurysms Patients And Age-Matched Controls. Presented at the Academic Surgical Congress Conference. February 6, 2013. New Orleans, LA.
10. Samadzadeh KM, **van Spyk E N**, Chun KC, Lee ES. Increased Monocyte Adhesion and Infiltrative Activity Inhibits Arteriovenous Fistula Maturation for Hemodialysis Access in Patients With End-stage Renal Disease. Presented at the Arteriosclerosis, Thrombosis Scientific Sessions 2013. May 1–3, 2013. Lake Buena Vista, FL.
11. Chun KC, Teng KY, **van Spyk EN**, Carson JG, Lee ES. Implementation of the Screen for Abdominal Aortic Aneurysms Very Efficiently (SAAAVE) Act: A 5-year follow up. Presented at the Peripheral Vascular Society and Vascular Surgery Annual Meeting, June 6, 2012, National Harbor, MD.
12. Chun KC, Teng KY, **Van Spyk EN**, Carson JG, Lee ES. Risk factors associated with the abdominal aortic aneurysm diagnosis in patients screened at a regional Veterans Affairs health care system. Presented at the 2013 Winter Peripheral Vascular Society and Vascular Surgery Annual Meeting, February 3, 2013, Park City, UT.

Research Experience:

Graduate Student Researcher, *Laboratory of Dr. Bogi Andersen, Department of Biological Chemistry, UC Irvine. Summer 2012-December 2017.*

- Elucidating the effect of time-restricted feeding on the skin circadian clock and sensitivity to UVB-induced DNA damage.
    - Experiments involved: daytime restricted feeding protocols, RNA isolation and qPCR on whole back skin, *in vivo* UVB radiation assays, DNA isolation from mouse back skin and DNA damage ELISAs.
- Examining the effect of time-of-day on anti-viral gene expression and psoriasiform inflammation in the skin in response to topical treatment with the immunomodulatory cream, Imiquimod (IMQ).
    - Experiments involved: transgenic mouse husbandry (3 strains), FACS cell sorting and RNA isolation/qPCR on freshly isolated mouse epidermal cells and ear skin cells, qPCR and microarray on whole back skin RNA, immunofluorescent staining and imaging of back skin sections, serum IFNα/b ELISAs, nuclear translocation assessment with ImageStream®X Mark II Imaging Flow Cytometer, quantification of cell surface and intranuclear staining on primary mouse skin cells using NovoCyte® flow cytometer, single-cell sequencing on adult mouse epidermis (Chromium™ Single Cell 3' Solution).
- Additional tasks include: refereeing 16 scholarly articles (approximately half requiring additional review), and writing for IACUC renewal.

Biological Science Laboratory Technician/Lab Manager/Research Coordinator, *VA Hospital, Mather, CA. Aug 2011-Sept 2012*

- Experimental protocols involving vein segments and leukocytes isolated from patient blood samples to investigate the role of matrix metalloproteinases (MMPs) and their co-regulators as well as leukocyte activity and adhesion molecule expression in patients with Abdominal Aortic Aneurysms, Peripheral Vascular Disease and end stage renal failure.
    - Experiments to assess MMP levels include: zymography, western blotting of vein segments and monocyte/neutrophil supernatants, and ELISA assays.
    - Experiments probing leukocyte activity and adhesion molecule expression include: flow cytometry for adhesion molecule markers, adhesion to and transendothelial migration, and chemotaxis assays.
- Used the aforementioned experiments to help define arteriovenous fistula (AVF) outcome for hemodialysis access in end stage renal failure patients.
- Experimental protocols for isolation/culture of endothelial progenitor cells from patient blood.
- Managed a $64,000 per annum career development grant.
- Wrote, edited, and aided in the submission of scholarly articles and grants.

Research Assistant, *VA Hospital, Mather, CA. Oct 2009-Jan 2010; June 2010-Oct 2010*

- Analyzed the effectiveness of certain prostate cancer drug treatments in reducing the upregulation of the Epidermal Growth Factor family of receptors involved in cancer cell growth and proliferation.

- Experiments involved: cell culture, MTT (growth) assays, gel electrophoresis, and Western blotting

---

Outreach activities:

- Guest lectured for BC207, Advanced Molecular Genetics graduate course April 11th, 2017.
- Supervised 3 Cellular and Molecular Bioscience graduate students at UC Irvine (Winter 2013, Fall 2014, Fall 2017).
- Mentored 10+ undergraduates through the BIO199 course at UC Irvine and 3 undergraduates from other institutions (Chapman University, Brown University, UC San Diego). Majority of students retained 1+ years. Three of the UC Irvine BIO199 students were awarded "Excellence in Science", and two of these students obtained Summer Undergraduate Research Program (SURP) and/or Undergraduate Research Opportunity Program(UROP) awards.
- Mentored high school students through:
  - The Southern California Academy of Sciences – Research Training Program 2015-2016.
  - The American Cancer Society program 2015-2016.
  - The UCI Cancer Research Institute Youth Science Fellowship Program 2014.
- Volunteered at "Ask-a-Scientist" night at Rancho San Joaquin Middle School 2013-2014.
- Judged science fair projects at the IUSD 34th Annual Science Fair

ABSTRACT OF THE DISSERTATION

The Impact of the Circadian Clock and Feeding Time on Skin Function

By

Elyse Noelani van Spyk

Doctor of Philosophy in Biomedical Sciences

University of California, Irvine, 2017

Professor Bogi Andersen, Chair

The circadian clock regulates many important aspects of physiology, allowing organisms to anticipate daily environmental changes in addition to gating cellular processes. The circadian clock in the skin regulates biological functions ranging from cell renewal, protection against DNA damage, and defense against pathogens. The goal of this dissertation is to explore the effect of the circadian clock and feeding time on skin biological functions. We find that approximately 10% of genes are diurnal in the skin, and the expression of approximately 2,000 genes are acutely affected by food-intake. While daytime-restricted feeding does not shift the phase of epidermal cell proliferation, it reverses the diurnal sensitivity to UVB-induced DNA damage.

Next, we sought to investigate the role of the circadian clock in the Toll-like receptor 7 (TLR7)-induced immune responses in the skin. The TLR7 pathway, in coordination with the type I IFN pathway, mediates the expression of key genes, termed “Interferon-sensitive genes” (ISGs) which encode important mediators for host defense against pathogens. We find that topical application of the TLR7 agonist Imiquimod (IMQ) during the daytime elicits a greater magnitude

of ISG expression. In addition, shifting the clock by daytime-restricted feeding reverses the diurnal rhythm of IMQ-induced ISG induction. Epidermal immune cells, and not keratinocytes, exhibit time-of-day dependent differences in the induction of the key ISG transcription factor *Interferon Regulatory Factor 7* (*Irf7*) after IMQ treatment. In parallel, IMQ-induced IRF7 activation, as measured by nuclear translocation of IRF7 and phosphorylated IRF7, is greater after IMQ treatment during the daytime in epidermal T cells and monocytes. Further supporting the clock's role in ISG responses, systemic *Bmal1* deletion, but not in keratinocyte- or dendritic cell-specific *Bmal1* deletion, results in exacerbated IMQ-induced ISG expression. We also investigate whether the circadian clock modulates IMQ-induced inflammation. Under homeostasis and/or after one IMQ dose, diurnal rhythms exist in epidermal cell proliferation and thickness, neutrophil recruitment, and spleen weight; however, these rhythms are ablated by repeated IMQ doses. Interestingly, systemic *Bmal1* deletion does not alter immune infiltration to the skin, splenomegaly, or epidermal proliferation after repeated IMQ doses. These results suggest that, while the circadian clock is a critical mediator of the early ISG response to IMQ, it does not significantly impact the robust inflammation observed after repeated IMQ doses.

Chapter 1: Regulation of Cutaneous Stress Response Pathways by the Circadian Clock: From Molecular Pathways to Therapeutic Opportunities

(van Spyk E N, 2016, Springer Books)

Abstract

The skin is a protective barrier that defends against harmful environmental stressors such as solar radiation, chemical toxins and pathogenic microbes. Our environment is highly dynamic, with robust time-of-day dependent fluctuations in temperature, solar radiation, and probability of injury and infections. In addition, oxidative metabolism and cell-cycle progression in epidermal stem cells show prominent diurnal rhythms. Accumulating evidence suggests that the skin's circadian clock optimizes its physiology to meet the demands of this changing environment. The responsiveness of the skin to external stressors such as UVB radiation from the sun, and toxic pollutants, is regulated in a circadian manner on multiple levels. Furthermore, the robustness of inflammatory responses following injury, infections, exposure to allergens, pollutants, and drugs is dependent on the time of day in which exposure occurs. The diurnal variation in the responsiveness to external stressors may be important for skin integrity and organismal health. We speculate that such circadian gating may be important as constitutively high activation of stress response pathways could be deleterious for health; for example constant high activity of the immune system could contribute to the development of autoimmune diseases.

1. The Circadian Clock and the Skin Stress Response

As a forefront barrier between us and the environment, the skin is exposed to externally-derived insults, including ultraviolet B (UVB) radiation, toxic chemicals, and pathogenic microbes. Within epidermal stem and progenitor cells, desynchronization of oxidative/reductive metabolism and cellular division may facilitate genomic damage, apoptosis, and proteolysis resulting in skin ageing and/or cancer (Sancar et al., 2015; Plikus et al., 2015; Wilking et al., 2013; Stringari et al., 2015; Pluquet et al., 2014). These external insults and perturbations in homeostasis activate the skin's stress response pathways, triggering diverse activities such as DNA damage repair, reactive oxygen species (ROS) extermination, and immune modulation (Valacchi et al., 2012).

The body-autonomous circadian clock harmonizes an organism's physiology with the daily light/dark cycle caused by the earth's rotation. Numerous physiological processes, including organismal metabolism and the sleep-wake cycle, are directly or indirectly regulated by an organism's circadian rhythm. The clock is an evolutionarily conserved mechanism -- all phyla possess an internal clock with a period of approximately 24 hours – indicating that the clock optimizes fitness and survival. While earlier studies assumed that the circadian clock was a property of the suprachiasmatic nucleus (SCN) only, work in the 1990s showed that most, if not all, cells of the body have active clocks (reviewed in Mohawk et al., 2012; Schibler et al., 2010; Dibner et al., 2010). Consistent with this idea, more recent work has demonstrated the existence of a skin circadian clock (Lin et al., 2009; Tanioka et al., 2008) with important roles in skin biology (Plikus et al., 2015). In addition to functional experiments in genetically modified mice, epidemiological research has illustrated the importance of the circadian clock in promoting human fitness. Disturbed circadian rhythms caused by abnormal lighting schedules, sleep

deprivation, and aberrant feeding times are thought to promote maladaptation and pathologies ranging from cancer to metabolic diseases, as well as early ageing (Sancar et al., 2015; Pluquet et al., 2014; Wilking et al., 2013; Kondratov et al., 2006; Sigurdardottir et al., 2012; Armstrong et al., 2013; Lengyel et al., 2013a; Libert et al., 2012).

Exposure to many external insults, including solar radiation and endogenous cellular stresses is highly diurnal. Therefore, it is reasonable to propose a stress response role for the circadian clock, an ancient system that has evolved to better adapt to environmental changes over the day. In this chapter we will highlight studies supporting this notion. While there is strong evidence supporting the role of the circadian clock in modulating certain stress response pathways in the skin, the clock's involvement in other stress-activated pathways is more speculative. In addition to outlining this evidence, we also discuss therapeutic implications of the skin circadian clock, and how dysregulation of clock mechanisms through altered sleep, eating and/or light exposure may impair the skin's capacity to cope with external stressors.

1.1 Structure of the Skin

In the cellularily complex skin several different cell types cooperate to maintain homeostasis in the face of an ever-changing environment and external stressors. The epidermis, the surface epithelium of the skin, is separated from the underlying dermis by a basement membrane. At the base of the epidermis, epidermal progenitor/stem cells divide and give rise to post-mitotic keratinocytes which migrate upwards as they differentiate and start expressing structural proteins, adhesion molecules, and lipid-producing enzymes, all required for the formation of an

effective epidermal barrier. At the top of the epidermis, these cells lose their nucleus, forming the outermost layer of the epidermis, the stratum corneum, a layer of cells with heavily crosslinked protein/lipid structure sealed with lipids. The epidermis also contains melanocytes that transfer melanin to keratinocytes, an important mechanism countering UVB-induced DNA damage.

Below the epidermis resides the dermis, composed mainly of fibroblasts, adipocytes, and macrophages. Fibroblasts secrete extracellular matrix components that support the tensile strength of the skin while adipocytes store energy and macrophages contribute to pathogen clearance; macrophages will be discussed later in the chapter. The dermis is divided into two layers, the papillary layer abutting the epidermis, and the reticular layer residing deeper under the papillary layer. Epidermal appendages extending into the dermis include hair follicles, sebaceous glands, and sweat glands. In addition, the dermis is richly innervated and vascularized.

The skin contains numerous hematopoietic cell types that contribute to inflammatory responses and the barrier role of the skin (Pasparakis et al., 2014). Under homeostasis, Langerhans cells (LCs) in the epidermis sample pathogens in the environment through dendritic projections, and epidermal T cells help maintain epithelial integrity, and protect against the development of cutaneous malignancies (Girardi et al., 2001). Upon skin infection or damage, both LCs and dermal dendritic cells (DDCs) phagocytose and present antigens to T cells, enabling adaptive immune responses. In addition, the skin's microbiome composition is highly complex and dynamic. Changes in signals from the skin commensal microorganisms remodel the skin immune landscape with potential implications for skin immunity and pathologies (Naik et al., 2015). While the microbiome composition is known to vary in a circadian manner in the gut epithelium

(Zarrinpar et al., 2014), diurnal variations in microbial populations in the skin and their effects on host defense, homeostasis, and chronic disease have not been extensively explored.

1.2 The Circadian Clock

1.2.1 The Circadian Clock at an Organismal Level

The circadian clock, a cell-intrinsic transcriptional network that is present in most, if not all, cells of the body, coordinates the organism's physiology with the day-night cycle. In vertebrates, the central circadian clock is located in the SCN of the hypothalamus. While this clock is highly autonomous, its phase is primarily set by light input that activates ganglionic cells in the retina, which in turn send signals through the retinohypothalamic tract (RHT) to the SCN. The SCN, composed of 15-20,000 neurons, acts as the central pacemaker by synchronizing the clocks in peripheral organs, presumably through neuronal and hormonal pathways (Reppert et al., 2002) (Fig. 1.1). Light input signaling to the SCN is not the only stimulus that can entrain the peripheral clocks as physical activity, timing of food intake, and the metabolic state have been shown to affect the rhythm of the circadian clock in the peripheral organs independent of the rhythm produced by the SCN (Schibler et al., 2010; Dibner et al., 2010). Work in recent years has established a role for peripheral clocks in most organs where about 10-20% of the genome exhibits diurnal change in expression. The diurnal transcriptome in each organ is relatively unique and often composed of genes that confer functions prototypical for each organ (Mohawk et al., 2012; Geyfman et al., 2012).

1.2.2 Molecular Mechanism of the Clock

The molecular clock is driven by the rhythmic transcriptional activity of two transcription factors, Circadian Locomotor Output Cycles Kaput (CLOCK) and Brain and Muscle Arylhydrocarbon receptor nuclear translocator-Like 1 (BMAL1). CLOCK and BMAL1 form a heterodimer via their respective PAS domains and bind to E-box sequences in gene promoters, activating the expression of clock-controlled genes (CCGs) (Mohawk, 2012). Among the CCGs, are genes encoding repressors of the CLOCK:BMAL1 complex, including *Period 1, Period 2 and Period 3 (PER1/2/3)* and cryptochrome 1 and cryptochrome 2 (*CRY1/2*). PER1/2/3 and CRY1/2 accumulate in the cytoplasm and then return to the nucleus to form heterodimers that inhibit the activity of CLOCK:BMAL1 on E boxes in the promoters of target genes, thus inhibiting their own expression. The time-length of this loop of CLOCK:BMAL1-mediated transcriptional activation followed by inhibition by PER:CRY1/2 heterodimers is approximately 24 hours, resulting in the rhythmic expression of CCGs. This rhythmicity is further sustained by an auxiliary loop whereby CCGs RORα/ß/γ and REV-ERBα activate and inhibit, respectively, *Bmal1* gene expression (Preitner et al., 2002) (Fig. 1.2). In addition, postranscriptional mechanisms controlling the stability of clock proteins play important roles in the circadian clock; for a more thorough review, see (Mohawk et al., 2012).

1.2.3 The Circadian Clock in the Skin

Like other peripheral organs, the skin possesses an intrinsic circadian clock that is entrained by signals originating from the core clock in the SCN (Lin et al., 2009; Tanioka et al. 2009; Geyfman et al., 2012; Plikus et al., 2013; Al-Nuaimi et al.; 2014). Based on studies in other organs, it has been assumed that the skin clock in mice develops rhythmicity within the first month of life (Sladek et al., 2007; Ansari et al., 2009). While the skin clock maintains

rhythmicity in the absence of light input, the rhythms depend on an intact SCN (Tanioka et al., 2009). How the SCN transmits its signals to the skin clock has not been established although it is assumed that both hormonal and neuronal signals are important. The circadian clock seems to be active throughout the skin, but particularly robust clock output has been noted in quiescent bulge stem cells, the hair matrix, the dermal papillae, the interfollicular epidermis, and the secondary hair germ (Lin et al., 2009; Plikus et al., 2013; Janich et al., 2011). The circadian clock in the skin is important for skin physiology; Bmal1-deleted mice have many skin-related pathologies including delayed wound healing (Kowalska et al., 2013), cellular senescence (Kondratov et al., 2006; Khapre et al., 2011), and delayed hair regrowth (Kondratov et al., 2006).

1.3 Role of the Circadian Clock in the Skin's Response to Endogenous and External Stressors

1.3.1 Circadian Regulation of Cellular Metabolism and the Cell Cycle

Skin, similar to gastrointestinal epithelium and bone marrow, requires high levels of progenitor cell proliferation for its maintenance. In mice, the fraction of epidermal progenitors in S-phase is higher during the night than during the day; this is opposite to the phase in human skin, which exhibits peak S-phase during the day (Brown, 1991; Clausen, 1979; Geyfman et al., 2012). The rhythmic cell proliferation is controlled by the circadian clock as circadian knockout mice have a constant fraction of epidermal progenitor cells in S-phase over the day (Geyfman et al., 2012; Plikus et al., 2013; Gaddameedhi et al., 2011). While the function of the prominent diurnal variation in cellular proliferation remains unknown, it is proposed that the circadian clock may have evolved to coordinate the phases of different cellular processes (Jouffe, 2013 et al.;

Geyfman et al., 2012; Panda et al., 2002; Gillette et al., 2005). For epidermal stem cells, the clock's function may be to synchronize the cell cycle with intermediary metabolism, thus minimizing cellular damage from ROS created through ox. phos. (Stringari et al., 2015). This idea is supported by a recent study in which diurnal metabolic oscillations in the ratio of bound to free NADH (indicative of the balance between ox. phos. and glycolysis) in stem cells of the interfollicular epidermis were measured by fluorescence lifetime imaging (Stringari et al., 2015). It was found that ox. phos. was anti-phasic to the rhythm of S-phase and that diurnal metabolic oscillations and rhythms of proliferation in skin progenitors were abolished and became constitutively upregulated in the absence of the clock. These findings are corroborated by previous studies in *Bmal1*-deleted mice showing that they have elevated levels of ROS (Stringari et al., 2015; Geyfman et al., 2012). High ROS levels present during S-phase might contribute to the deleterious phenotypes seen in circadian knockout mice including reduced lifespans (Libert et al., 2012) and various symptoms of premature aging (Kowalska et al., 2013; Kondratov et al., 2006; Khapre et al., 2011). The involvement of elevated ROS in the premature aging phenotypes of *Bmal1*-deleted mice is supported by a study showing that antioxidants could assuage the age-dependent weight loss and development of cataracts typically seen in *Bmal1*$^{-/-}$ mice (Kondratov et al., 2009). Interestingly, some of the aging phenotypes in *Bmal1*$^{-/-}$ mice, including the hair regrowth defect, require *Bmal1* to be ablated early in development before the clock machinery has matured, suggesting a potential non-circadian role of BMAL1 during development (Yang et al., 2016).

Apart from its detrimental effects, ROS also function as signaling molecules that regulate biological activities (Finkel et al., 2011). ROS are implicated in regulating normal homeostatic

maintenance in other stem cell niches (Le Belle et al., 2011). The question as to whether these signaling functions of ROS are regulated by the clock in epidermal progenitor cells merits further investigation.

1.3.2 Circadian Clock Control of the Unfolded Protein Response

In response to stressful conditions such as wounding, infections, UV exposure, hypoxia, nutrient deprivation and ROS accumulation, cells upregulate proteins that help prevent the accumulation of misfolded proteins in the endoplasmic reticulum; this response is called the Unfolded Protein Response (UPR). For example, the UPR is activated in proliferating fibroblasts during wound healing (Matsuzaki et al., 2015). Although the UPR is most commonly thought of as a response to perturbation, it is activated in differentiating keratinocytes of the skin in the most differentiated layers of the epidermis (Sugiura et al., 2013). Interestingly, in mouse skin, several mRNAs encoding UPR-associated proteins oscillate diurnally, with most of them exhibiting peak expression in the late night/early morning (Fig. 1.3A). One of these genes, *HERPUD1* is affected in *Bmal1*-deleted mice. Although no studies to date have investigated the functional significance of the diurnal expression of components of the UPR in the skin, studies in the liver have shown that circadian UPR activation is coordinated with the timing of maximum protein secretion in mouse liver (Cretenet et al., 2010; Mauvoisin et al., 2013). Moreover, $Cry1^{-/-}$;$Cry2^{-/-}$ mice exhibit dysregulation of endoplasmic reticulum-resident enzymes and perturbed lipid metabolism (Cretenet et al., 2010), suggesting a direct clock role in modulating the UPR in the liver. The potential role of the circadian clock in modulating the UPR in the skin is unknown and merits further investigation.

1.3.3 Response to Wounding

The skin has evolved highly effective regenerative mechanisms to close wound defects. The review of wound healing is beyond the scope of this chapter but suffice to say, complicated signaling networks that are activated in response to wounding promote closure of the wound through enhanced migration and proliferation of fibroblasts and keratinocytes. In addition, polarizing immune cells are recruited to the wound to clear up debris and kill off intruding microbes. Studies suggest that the clock facilitates proper wound healing as evidenced by less epithelial coverage and decreased fibroblast proliferation after wounding in *Bmal1*$^{-/-}$ mice (Kowalska et al., 2013). It is possible that healing defects observed in *Bmal1*$^{-/-}$ mice are at least partially related to the dampened ability of *Bmal1*$^{-/-}$ keratinocytes to respond to pro-proliferative signals in older mice (Janich et al., 2011).

The microenvironment of wounded tissues is hypoxic and has impaired nutrient supply due to vascular perturbation and high oxygen utilization by cells at the wound edge (Pai, 1972). Hypoxia induces the expression of heat shock proteins, which facilitate epithelial cell migration, thus contributing to re-epithelialization. The mRNA levels for heat shock proteins (*Hsp90* and *Hsp70*), as well as several other proteins involved in the response to hypoxia, exhibit diurnal expression rhythms in mouse skin under homeostasis (Fig. 1.3B).

1.3.4 UVB- and γ-irradiation-Induced DNA Damage

Intricately linked to the cell cycle, the susceptibility to UVB-induced DNA damage in mouse skin exhibits a diurnal rhythm. UVB-induced DNA damage in the form of (6-4) photoproducts and cyclobutane pyrimidine dimers is greater when UVB is applied at night compared to the day.

This effect may be explained at least in part by the diurnal expression of a rate-limiting protein essential for the NER pathway, Xeroderma pigmentosum complementation group A (XPA) (Cleaver, 1968), which is lowly expressed in mouse skin during the night compared to day. The stage of the cell cycle may also contribute to this effect, as DNA is most sensitive to UVB-induced damage during the S-phase of the cell cycle, which also peaks during the night in epidermal progenitors (Geyfman et al., 2012). Recently, other physiological aspects of the mouse skins' response to UVB-induced damage, including sunburn apoptosis, inflammatory cytokine production, and erythema were found to be time-of-day dependent, with maximal response induced by UVB exposure at night (Gaddameedhi et al., 2015). Most strikingly, the same group found that UVB-induced squamous cell carcinomas accrue more rapidly in mice exposed to UVB at night (Gaddameedhi et al., 2011). Notably, in mouse skin under homeostasis, multiple mRNAs encoding proteins in the "response to UV" gene set exhibit diurnal oscillations, suggesting the possibility that other genes play a role in the diurnal UVB response (Fig. 1.3C). These findings are all in nocturnal mice, which have opposite phase of the circadian clock compared to diurnal humans where the maximum sensitivity to UVB-induced DNA epidermal damage may be during the day, the time of maximum solar exposure (Geyfman et al., 2012; Gaddameedhi et al., 2011).

Studies have shown that cells in the M phase are most susceptible to γ-irradiation-induced DNA damage (Sinclair, 1965; Terasima, 1961). Consistent with this fact, γ-irradiation causes more extensive hair loss when applied to skin during the early morning versus in the afternoon (Plikus et al., 2013). $Cry1^{-/-}$;$Cry2^{-/-}$ mice, which are arrhythmic, exhibit similar and enhanced levels of hair loss in response to γ-irradiation regardless of time of day, implicating a role for the circadian

clock in this process (Plikus, 2013). Together, these studies support a role for the circadian clock in modulating the epidermal response to exogenous stressors in the form of UVB- and γ-irradiation radiation.

1.3.5 Antioxidant Defense

The skin possesses an intricate network of antioxidant mechanisms poised to assuage oxidant stress caused by exposure to solar radiation, chemicals, inflammation, and endogenous metabolic processes. Antioxidant systems in the skin include proteins that protect against ROS, such as catalase (CAT), glutathione peroxidase (GPx), and superoxide dismutase (SOD), as well as antioxidants like vitamins A, C, and E, melatonin, and glutathione (GSH). Many of these components exhibit diurnal rhythmicity throughout the body. For example, Melatonin, most well known for its role as a primary circadian effector hormone, is also a potent ROS- and NOS-scavenger. The structure of melatonin allows it to neutralize many forms of radicals such as H_2O_2, $^{\bullet}OH$, singlet oxygen ($^1O_2$), superoxide anion ($^{\bullet}O_2^-$), peroxynitrite anion ($ONOO^-$) and peroxyl radical ($LOO^{\bullet}$) (Tan et al., 2002). The neutralization of these oxidizing molecules is especially important for skin health due to the epidermis' high rate of cell proliferation, which correlates with its propensity to become cancerous (Tomasetti et al., 2015). Apart from its direct actions, melatonin also works in the skin by inhibiting the depletion of antioxidant enzymes including CAT, GPx, and SODs after UV radiation-mediated photodamage (Fischer et al., 2013).

Another mechanism by which the skin and other organs fight the accumulation of harmful free radicals is through the action of SODs, which catalyze the dismutation of O_2^- into O_2 and H_2O_2. SODs are integral to skin homeostasis, as heterozygous deletion of SOD2 results in an "immune-

ageing" phenotype, with enhanced T cell-mediated contact hypersensitivity (Scheurmann et al., 2014) as well as nuclear DNA damage, and cellular senescence in the mouse epidermis (Velarde et al., 2012). SODs are expressed in a diurnal manner in many tissues including rat intestine, lung, and cerebellum (Martin et al., 2003). *Per2* mutant mice show dampened SOD expression levels in the liver, while *Per1/2* double knockout mice have a shift in phase of SOD gene expression (Jang et al., 2011), suggesting that this mechanism is modulated by the circadian clock.

GSH is a critical antioxidant that neutralizes ROS in a process catalyzed by GPx proteins, in which GSH becomes oxidized to form glutathione disulfide (GSSG). GSH and GSSG, as well as other components of the GSH pathway, such as GPx, GR, and GST, are robustly diurnal in multiple tissues (Baydas et al., 2002; Lapenna et al., 1992; Maurice et al., 1991) with a peak expression of GSH during the light phase in mice and during the night in humans (Atkinson et al., 2009). A few Glutathione *S*-transferases, including GSTT1 and GSTA3, exhibit diurnal rhythmicity in their mRNA expression in the skin and are altered in *Bmal1*$^{-/-}$ mice (Geyfman et al., 2012). Although there are no studies to date investigating the physiological significance of the circadian rhythmicity of these GSH-associated genes in the skin, higher oxidized GSH levels are often seen in lesional and non-lesional skin from patients with chronic irritant dermatitis, suggesting this pathway is integral for maintaining skin homeostasis (Kaur et al., 2001).

1.3.6 Xenobiotic Detoxification

The skin protects against the effects of man-made genotoxic drugs and cytotoxic compounds found in nature. The Aryl hydrocarbon receptor (AhR) is a ligand-dependent transcription factor

that plays a critical role in metabolism of small molecules, including dioxins, polycyclic aromatic hydrocarbons, plant polyphenols, and tryptophan photoproducts (Rannug et al., 2006). Upon ligand binding, AhR translocates to the nucleus and dimerizes with ARNT, inducing transcription of xenobiotic-metabolizing enzymes, including cytochrome P450 (CYP) 1A1 and CYP1A2/B1. The CYP proteins then degrade chemical toxins and, as a by-product, produce ROS. AhR also activates the expression of nuclear factor-erythroid 2-related factor-2 (Nrf2), which regulates the expression of myriad of antioxidant proteins including NAD(P)H dehydrogenase [quinone] 1 (Nqo1) and Heme oxygenase 1 (HO-1) that protect against genotoxicity due to elevated ROS (Cho et al., 2002). In the mouse lung epithelium, circadian Nrf2 levels control the pulmonary response to oxidative injury in a lung fibrosis model, with greater fibrosis accruing during the early evening, corresponding to lowest Nrf2 levels (Perovic-Vaughan et al., 2014). Moreover, reduced Nrf2 and GSH expression in the lungs of $Clock^{\Delta 19}$ mice is linked to increased oxidative damage of proteins and spontaneous development of fibrosis in the airways (Perovic-Vaughan et al., 2014). In the mouse skin, the expression of Nrf2, Nqo1, and HO-1 is diurnal with a peak in expression a few hours prior to the onset of night; in addition, *Nqo1* and *Nrf2* mRNA expression are altered in $Bmal1^{-/-}$ mice (Geyfman et al., 2012), suggesting these genes are controlled by the CLOCK:BMAL1 complex.

The AhR pathway and the circadian clock exhibit a dynamic, reciprocal interaction. On the one hand, AhR expression and DNA binding activity have a 24-hour rhythmicity; core clock proteins regulate AhR-mediated enzyme expression and detoxification activity in the rat pituitary and liver (Huang et al., 2002; Tanimura et al., 2011). On the other hand, activation of the AhR pathway by dioxins impacts the expression of core clock genes in mouse liver and hematopoietic

stem cells (Xu et al., 2010). It is currently unknown whether this disruption occurs in epidermal and follicular progenitor cells. However, if it does, this would suggest yet another pathway by which dioxins (acting through AhR activation) exert their damaging effects on the skin.

AhR is expressed in the upper part of the hair follicle including the infundibulum (Ikuta et al., 2009). Although the mRNA expression of AhR itself is not circadian in mouse skin, transcripts for genes associated with the xenobiotic response such as CYP2E1 and epoxide hydrolase 1 exhibit diurnal rhythmicity, peaking around the onset of night in mouse skin under homeostasis (Geyfman et al., 2012) (Fig. 1.3D). The functional significance of the circadian regulation of xenobiotic metabolism within the skin may be to prepare for and/or respond to chemical toxins encountered during the night, when mice are most active.

1.4 Circadian Regulation of Skin Immunity

1.4.1 Circadian Rhythm in Skin Innate Immunity

In addition to the barrier mechanisms described above, a diverse army of inflammatory cells in the skin deals with environmental insults by reacting, attacking, and relaying danger signals to the rest of the body. Several immune function-related genes are expressed in a diurnal manner in mouse skin, suggesting that the skin's immune system could be regulated by the circadian clock (Figure 1.4 adapted from Plikus et al., 2015, Geyfman et al., 2012). Epidermal keratinocytes, which compose the bulk of cells in the skin, secrete antimicrobial defensin peptides to resist pathogenic microbial colonization. *Defensin β23* mRNA exhibits a striking circadian rhythmicity in mouse skin under homeostasis (Geyfman et al., 2012). Skin immunity also relies on evolutionarily conserved pattern recognition receptors (PRRs), including TLR 1, 2, 3, 5, 9, and

10 which enable innate inflammatory responses to a variety of immunogenic stimuli including bacterial, fungal, viral, and apoptotic molecules (Miller et al., 2005; Köllisch et al., 2005; Lebre et al., 2007). Skin-resident leukocytes derived from the hematopoietic system contribute to barrier defense, expressing a diverse array of PRRs, including TLRs 1-10 (Renn et al., 2006) and C-type lectin receptors. In healthy mouse whole skin, TLR 4, 7, 8, and 9 expression oscillates diurnally (Figure 1.4, Geyfman et al., 2012). PRR engagement induces nuclear translocation of inflammatory transcription factors, including nuclear factor κB (NF-κB), enabling pro-inflammatory gene expression. The circadian clock regulates the magnitude of these inflammatory responses following PRR engagement. The most profound example of the circadian regulation of PRR sensitivity is exhibited by the increased mortality following systemic lipopolysaccharide (LPS) administration immediately preceding or during the evening in mice (Silver et al., 2012); this effect is clock-dependent as *Per2* mutant mice are resistant to LPS-induced endotoxic shock (Liu et al., 2006). LPS is a microbial component of gram-negative bacteria which induces inflammatory cytokine secretion through activation of TLR4, and systemic administration results in endotoxic shock and sepsis. The results in the mouse LPS models are recapitulated in human sepsis, in which greater mortality is observed during the night (Langevine et al., 1994).

Immune cell sensitivity to pathogenic challenges is regulated in by the circadian clock in numerous epithelial barriers. Lung epithelium responds diurnally to challenge by LPS or *S. pneumoniae,* where inflammatory chemokine release and neutrophil recruitment peaks during the day in mice. This diurnal variation in reactivity to exogenous particulates in the lung epithelium may contribute to the potent early morning symptoms of wheezing in asthma patients (Barnes,

1985) and decreased lung function in COPD patients (Calverley et al., 2003). In addition, the ability of the gut epithelium to respond to, and defend against, ingested microbes is dependent on the circadian expression of defensins (Froy et al., 2005) and PPRs in intestinal epithelial cells that both peak at the intersection between late night and early day (Mukherji et al., 2013). The physiological outcome of the circadian regulation of these proteins was revealed in experiments where investigators fed mice with *Salmonella,* and found that mice infected during the day showed increased colonization levels and pathology scores compared to nighttime-infected mice (Bellet et al., 2013). These findings support the idea that the circadian clock in epithelia promotes immunity during night, when mice are active and feeding, and thus most likely to encounter pathogenic microorganisms.

1.4.2 Circadian Rhythm in Skin Adaptive Immunity

In addition to innate PRR-mediated immunity, the skin epithelium is home to a complex network of leukocytes which also permit adaptive humoral and cell-mediated immunity (Silver et al., 2012; Pasparakis et al., 2014). Allergic contact dermatitis occurs in the skin following exposure to environmental chemicals, e.g. poison ivy, resulting in delayed type hypersensitivity (DTH). DTH is a cell-mediated response, requiring leukocyte migration to the lymph nodes and antigen presentation by skin-resident macrophages and dendritic cells to T cells. DTH has become a favorite animal model for human chronic inflammatory disease as the inflammatory pathology that occurs in skin DTH mirrors numerous cellular processes which also occur in chronic autoimmune disease in multiple organs. Prendergast et al. (Prendergast et al., 2013) found that circadian trafficking of antigen presenting $CD11c^{+}$ dendritic cells in response to DTH became arrhythmic after a disruptive phase shift (DPS) procedure.

Psoriasis, a common chronic human autoimmune disease affecting 2% of the population, is characterized by increased epidermal proliferation, epidermal thickening, altered epidermal differentiation, and organized lymphoid infiltrates in the reticular dermis. Psoriasis pathology is thought to be initiated by immuno-triggering environmental exposures and infections in patients with susceptibility to immune de-regulation due to genetic risk factors (reviewed in Harden et al., 2015). Innate immune cells such as dendritic cells expressing PRRs become activated to migrate to lymph nodes where they stimulate the differentiation of T cells into inflammatory subsets which become competent to enter the skin. T cell cytokine and growth factor secretion in the skin alters the transcriptional profile of keratinocytes and endothelial cells, resulting in a hyperproliferative state and self-perpetuating chronic inflammatory responses. The diurnal rhythmicity of psoriasis immunopathology was first published in the 1980's where Pigatto et al. found a substantial diurnal rhythmicity in neutrophil recruitment to the psoriatic lesions.

Work with psoriasis animal models suggests a circadian regulation of skin immunopathology. The psoriasiform lesion-inducing drug Imiquimod (IMQ) functions as a pathogen-associated molecular pattern (PAMP) and activates TLR7 signaling in skin-resident dendritic cells, resulting in the influx of inflammatory cells, proinflammatory cytokine secretion, and epidermal alterations (acanthosis, parakeratosis) similar to human psoriasis. These symptoms are more pronounced when mice are treated with IMQ at night than during the day (Ando et al., 2015). Knockout studies and circadian disruption studies support the modulatory role of the circadian clock in maintaining proper immune responsiveness to external PAMPs and antigens. Mice with mutated *Clock* genes have damped psoriatic lesion formation in response to IMQ, while *Per2*

knockout mice have attenuated pathogenesis (Ando et al., 2015). In other studies, mice subjected to disrupted lighting cycles and treated with the psoriatic-inducing agent human neutrophil elastase developed exacerbated psoriatic histopathology and pro-inflammatory cytokine production compared to mice housed under normal 12L:12D conditions (Hirotsu et al., 2012).

Nocturnal pruritus, or increased itchiness at night, has been well described in patients with various dermatological disorders, including psoriasis (Yosipovitch et al., 2000), atopic dermatitis (Yosipovitch et al., 2002), lichen simplex chronicus (Koca et al., 2006) and scabies (Chouela et al., 2002). There are many factors that may contribute to this effect, one of them being histamine release by mast cells, which is modulated by the circadian clock (Baumann et al., 2013). Time-of-day–dependent variations in a mouse model of IgE/mast cell–mediated allergic reaction (passive cutaneous anaphylactic (PCA) reaction) peaked during at night. Furthermore, these rhythms in reactivity were reliant on a functional clock protein, *Per2* (Nakamura et al., 2011). Together, these studies illustrate the powerful modulatory role of the circadian clock on immune responses in the skin.

1.5 Conclusions and Opportunities for Chronotherapy

Our skin maintains a dynamic barrier, protecting us from harmful external stimuli like fluctuating temperatures, humidity levels, UV rays, pollution, and infections. Work on the role of the circadian clock in skin suggests that it has evolved to coordinate the skins' protective function with changes in the external environment, allowing for optimal response to external insults. The clock also functions to temporally gate internal cellular processes such as ox. phos.,

cell division, and antioxidant pathways within the skin, perhaps helping to keep ROS-induced DNA damage at bay (Fig. 1.5). Most of the experimental work on the skin role of the circadian clock has been performed in mice, which are nocturnal, while humans are diurnal. Therefore, a number of circadian clock-modulated processes described in this review may exhibit antiphasic patterns in humans. It will be important to take this fact into consideration when thinking about the implications of these findings in the realm of human physiology and disease.

This chapter highlights the importance of the circadian clock in gating skin's stress response. In part, this notion is well supported by experimental data, but in part, the evidence is more speculative, pointing to the importance of further work in this field. Circadian disruption, a common phenomenon in today's society, may impair the skin's ability to handle stressors and infections.

Understanding the mechanisms by which the clock gates the skin's responsiveness to external stimuli, as well as the physiological outcomes of this regulation, is of paramount importance for the development of chronotherapy. Chronotherapy aims to administer drugs at specific times of the day to maximize the beneficial effects of the treatment and/or to minimize side effects. For example, 5-fluorouricil treatment of tumor bearing mice wielded more potent anti-tumor effects when dosed in the early morning compared to other times of the day (Kojima et al., 1999). The pro-inflammatory effects of another anti-tumor/anti-viral drug, the TLR7 agonist IMQ, have recently been shown to be diurnal with peak activity induced after nighttime treatment in mice (Ando et al., 2015). Studies on skin active drugs should increasingly consider time of day as a potentially important variable affecting effectiveness and side effects.

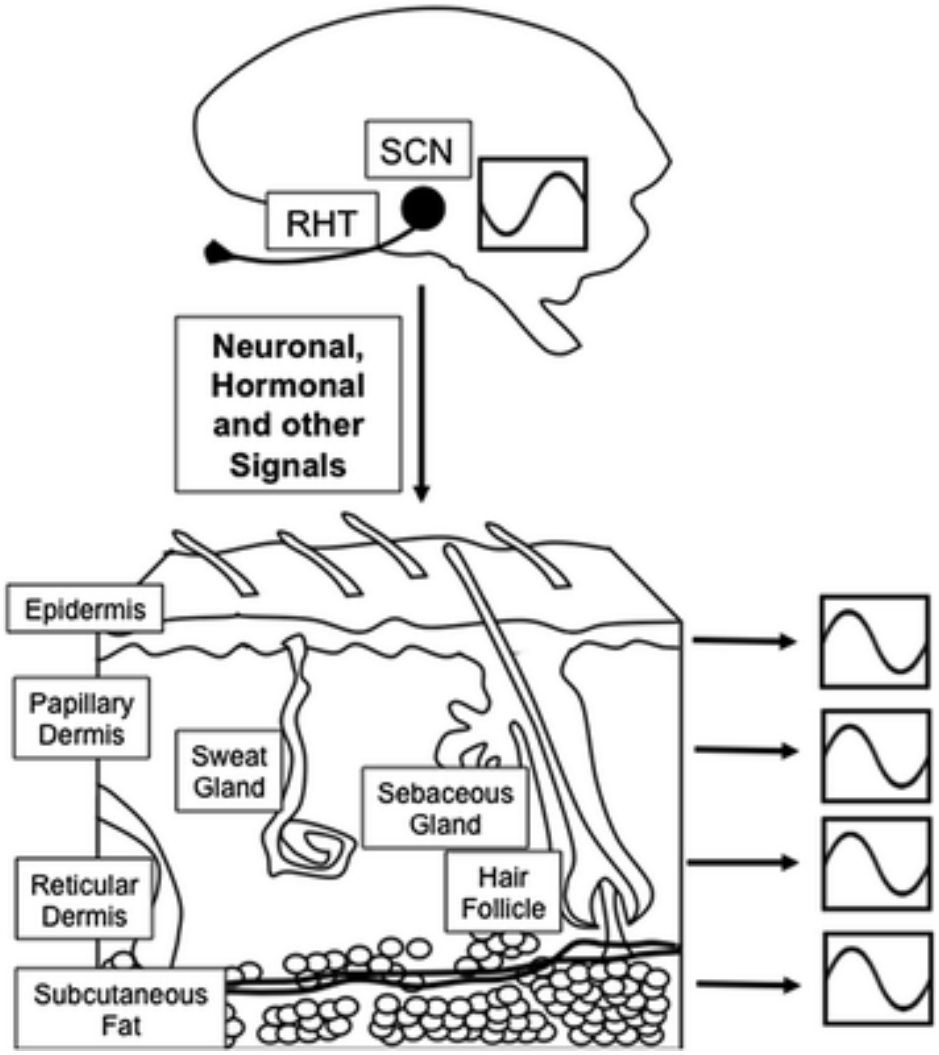

Figure 1.1 Organization of the skin circadian clock. Light input is received in the ganglion neurons in the retina, and signals are sent to the suprachiasmatic nucleus (SCN) in the hypothalamus via the retinohypothalamic tract (RHT). The SCN then transmits signals through neuronal efferents and hormonal pathways to other organ of the body, including the skin. These SCN-derived signals coordinate the circadian phase of different cell types in the skin.

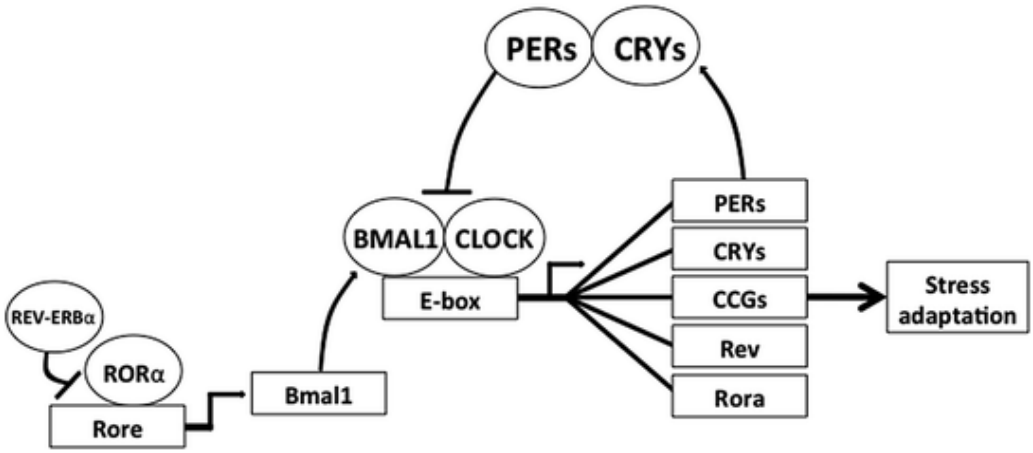

Figure 1.2 The molecular mechanism of the clock. CLOCK and BMAL1 form a heterodimer that initiates transcription of multiple genes through binding to E-box sequences in target gene promoters. An autoregulatory feedback loop is created, as BMAL1 and CLOCK promote the transcription of their own inhibitors (Per1/2/3 and Cry1/2). Furthermore, CLOCK:BMAL1 promotes the transcription of RORα and REV-ERBα which induce and repress, respectively, *Bmal1* expression. Other CLOCK:BMAL1 target genes encode for critical functions in peripheral organs, including genes regulating the response to stressors. CCGs, Clock-controlled genes.

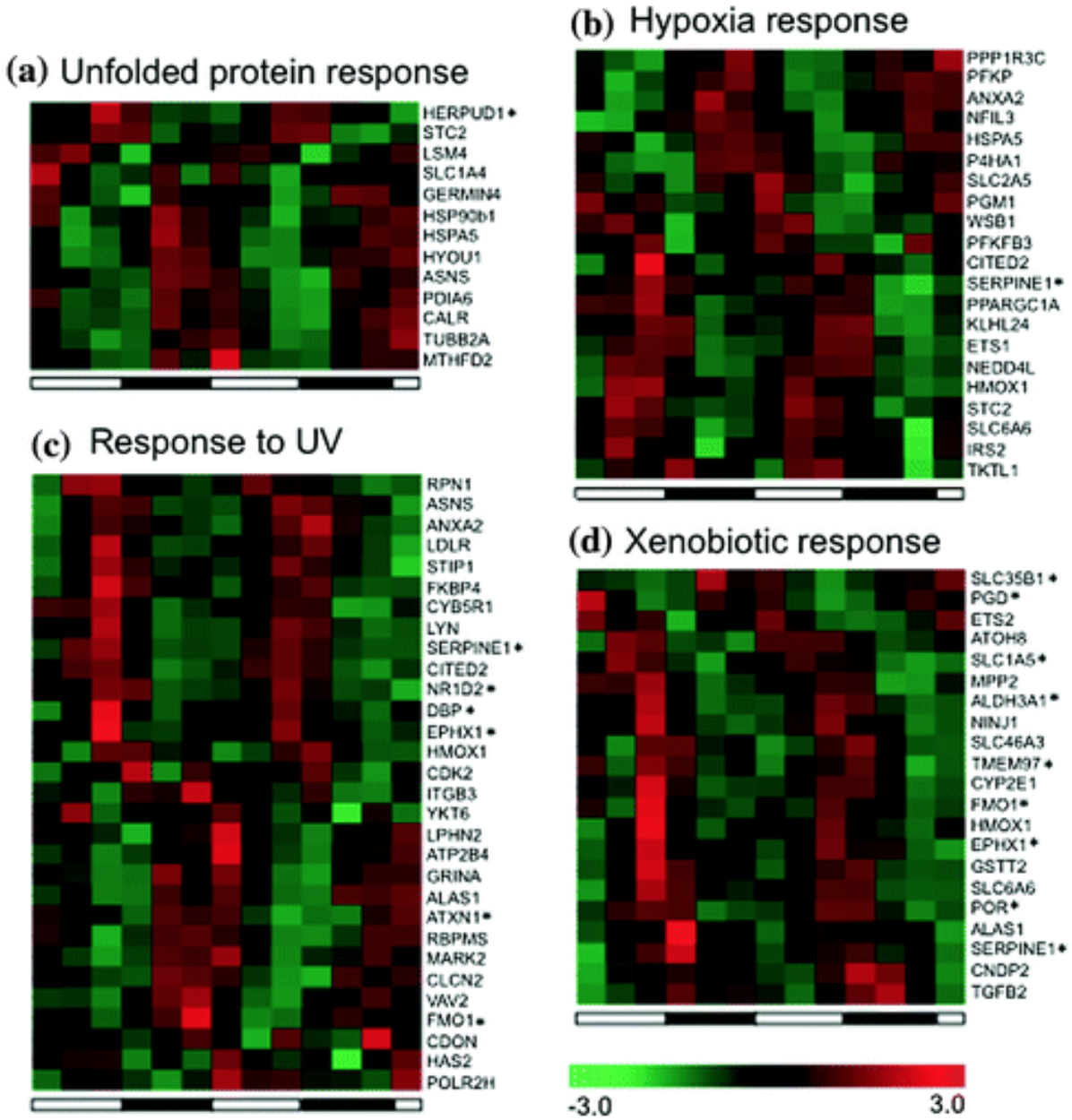

Figure 1.3 Circadian expression of stress response pathways in the skin. Heat maps showing the expression of genes in the skin over 2 days based on previously published whole skin microarrays performed in mice (Geyfman et al. 2012). The MSigDB database was used to identify significantly enriched stress response pathways. Shown are diurnal genes associated with unfolded protein response (**a**), hypoxia response (**b**), UV response (**c**), and xenobiotic response (**d**). Asterisks indicate genes whose expression is significantly different in the skin of systemic *Bmal1 KO* versus Wt mice (Geyfman et al. 2012), suggesting the possibility of direct clock regulation.

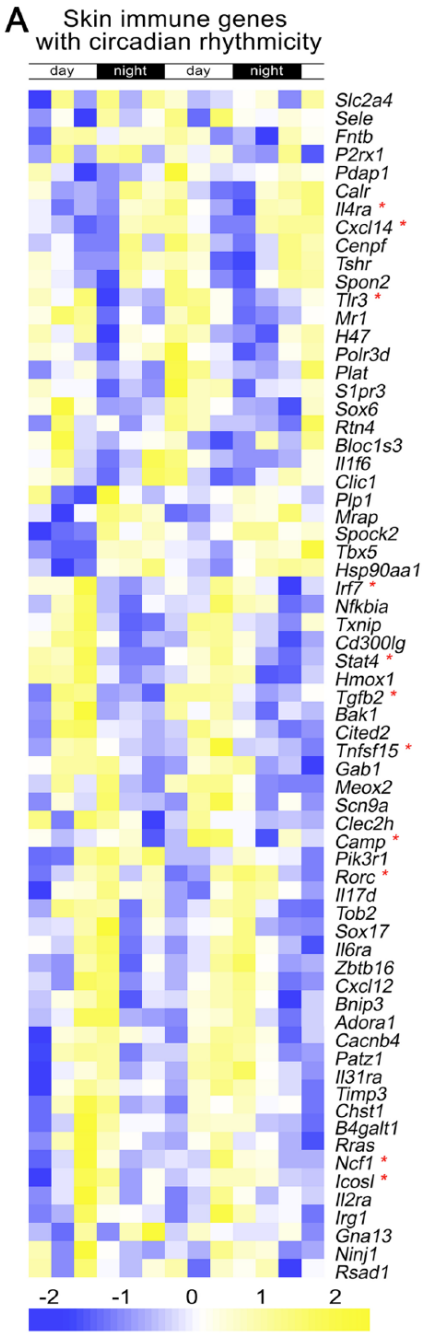

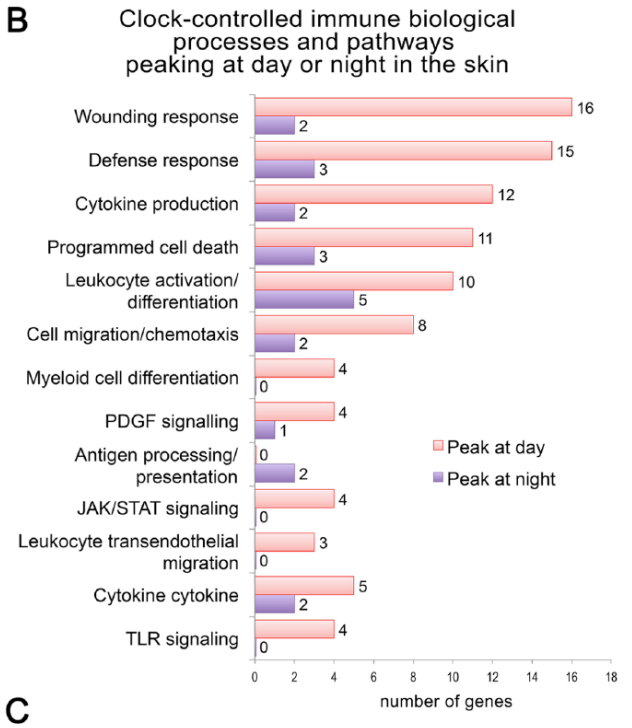

C

Gene	Classification	Known function
Il4ra	Anti-inflammatory cytokine	T_H2 differentiation; M2 polarization of macrophages post-wounding
RORC	Proinflammatory nuclear hormone receptor	T_H17 development
Icosl	Inducible costimulator ligand	Treg development/activity; Inflammatory cell infiltration, post-wounding
Tgfb2	Immunosupressive cytokine	Negative regulation of lymphocyte proliferation
Ncf1	NADPH oxidase	Phagocyte oxidative burst
Cxcl14	Monocyte chemoattractant	Immune surveillance; Antimicrobial
Stat4	Proinflammatory transcription factor	Innate host defense; T_H1 differentiation
Irf7	Transcription factor for type I interferons	Response to virus
TLR3	Double-stranded RNA recognition receptor	Antiviral host defense; Type I IFN induction; Post-wounding inflammation
CAMP	Cathelicidin antimicrobial peptide	Innate immunity defense against bacterial pathogens; Angiogenesis
TNFsf15	Proinflammatory cytokine	T cell activation; T_H1 cytokine production; Dendritic cell maturation

Figure 1.4 Many immune genes in skin display circadian rhythmicity, Adapted from Plikus et al., 2015. (A) A heat map showing the expression of immune-related genes in telogen over 2 days based on previously published whole skin microarray datasets generated in mice (Geyfman et al., 2012). Multiple genes with established immune functions exhibit circadian expression. The day and night periods are indicated at the top and gene expression strength indicated at the bottom. **(B)** Shown is the gene ontology for the circadian immune genes. The number at the end of the bars refers to the number of genes with the specific function. Genes that peak at day or night are indicated with the pink and purple color. **(C)** The function of selective immune genes is indicated. These genes are marked with an asterisk in (A).

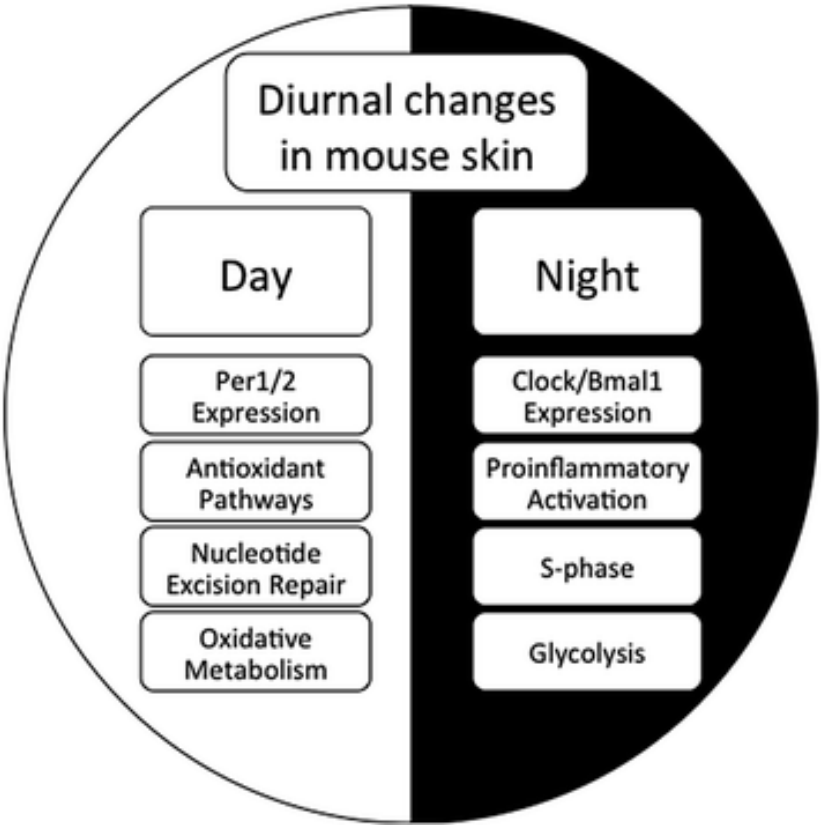

Figure 1.5 Diurnal activities of circadian stress response pathways in the skin. In mouse skin, circadian clock proteins, BMAL1 and CLOCK, exhibit peak expression during the night when most epidermal progenitor cells are in S-phase and glycolysis is the predominant metabolic pathway in these cells. The propensity for immune activation also peaks at night, which may help defend against invading pathogens encountered during the active phase. Conversely, oxidative metabolism and ROS production is higher during the day, coinciding with antioxidant pathway activity. DNA damage repair also peaks during the day in mice.

Chapter 2: Time-restricted feeding shifts the skin circadian clock and alters UVB-induced DNA damage

(Hong W*, van Spyk E N*)

***equal contributors**

Abstract

The epidermis is a highly regenerative barrier protecting organisms from environmental insults, including ultraviolet radiation, the main cause of skin cancer and skin aging. Here we show that time-restricted feeding (RF) shifts the phase and alters the amplitude of the skin circadian clock, and affects the expression of approximately 10% of the skin transcriptome. Furthermore, a large number of skin-expressed genes are acutely regulated by food intake. While the circadian clock is required for daily rhythms in DNA synthesis in epidermal progenitor cells, RF-induced shifts in clock phase do not alter the phase of DNA synthesis. Yet, RF alters both the diurnal sensitivity to UVB-induced DNA damage, and the expression of the key DNA repair gene *Xpa*. Together, our findings indicate an unexpected regulation of skin function by time of feeding and emphasize a link between circadian rhythm, food intake, and skin health.

2.1 Introduction

Acting as a strong barrier to physical, chemical and pathogen insults from the exterior, and to water loss from the interior, the epidermis, the outermost layer of the skin, is a stratified epithelium. Its homeostasis is balanced by stem-cell progeny production in the basal layer and loss of cells through terminal differentiation culminating in shedding of corneocytes at the skin's

surface (Blanpain and Fuchs, 2009). Skin biology research focuses largely on the responses to various forms of external injury, including UV irradiation, a major cause of DNA-damage, accelerated skin ageing, and cancer (Armstrong and Kricker, 2001; Fisher et al., 2002). Recent work, however, has unearthed an important role for the circadian clock in regulating skin function (Plikus et al., 2015). This raises the intriguing possibility that signals that influence circadian clocks, such as the time of feeding, could act as a regulator of skin function; the clocks in some peripheral tissues, especially metabolic organs, including the liver, can be entrained by time-restricted feeding (RF) (Damiola et al., 2000; Hara et al., 2001; Izumo et al., 2014; Kuroda et al., 2012; Stokkan et al., 2001).

The hierarchically organized mammalian circadian clock comprises the central clock, located in the suprachiasmatic nucleus (SCN), and peripheral clocks, possessed by almost all cells (Dibner et al., 2010; Mohawk et al., 2012). Entrained by the day-night cycle, the central clock synchronizes the phases of peripheral clocks, thus coordinating the locomotor and metabolic activity of the animal with the Earth's rotation. At a molecular level, the central and peripheral clocks are transcription-translation feedback loops wherein the heterodimeric CLOCK/BMAL1 transcription complex activates a large number of genes. These include PERs and CRYs that form heterodimers to inhibit CLOCK/BMAL1 activity, thus establishing an oscillating transcriptional output with a 24-hour periodicity (Dibner et al., 2010; Lowrey and Takahashi, 2011; Mohawk et al., 2012). The direct and indirect targets of the circadian clock encode key regulators of many, if not most, biological processes, including metabolism (Bass, 2012; Lamia et al., 2011), cell proliferation (Levi et al., 2007; Masri et al., 2013), and response to therapeutic treatment (Levi et al., 2007; Levi and Schibler, 2007).

Previous studies showed important roles for the circadian clock in skin biology (Plikus et al., 2015). The clock is highly active in the progenitor cells of the secondary hair germ where it plays a role in the initiation of the hair growth cycle (Lin et al., 2009). It also contributes to heterogeneity in hair follicle stem cells by regulating the sensitivity to activation signals (Janich et al., 2011). In addition, in the matrix of growing hair follicles, the clock determines diurnal variation in cell division which affects the sensitivity of hair follicles to external gamma radiation (Plikus et al., 2013). The circadian clock also gates the response to UVB-radiation in the skin (Gaddameedhi et al., 2011; Geyfman et al., 2012), at least in part by controlling the expression of *Xpa*, a rate limiting enzyme involved in the repair of UVB-induced DNA damage (Gaddameedhi et al., 2011; Khang et al., 2010). In fact, the skin is most sensitive to UVB-induced tumor induction at night when expression of *Xpa* is lowest (Gaddameedhi et al., 2011). Studies also showed a link between the circadian clock and skin aging as *Bmal1*-deleted mice exhibit accelerated skin aging (Janich et al., 2011; Kondratov et al., 2006), perhaps related to excessive reactive oxygen species (ROS) generation. In the interfollicular epidermal progenitor cells, the clock is required for a prominent diurnal variation in DNA synthesis (Gaddameedhi et al., 2011; Geyfman et al., 2012). While the function of these diurnal rhythms in epidermal progenitor cell DNA synthesis remains unknown, transcriptome studies from yeast to mammals have suggested that the circadian clock may coordinate the timing of different cellular processes (Geyfman et al., 2012; Gillette and Sejnowski, 2005; Jouffe et al., 2013; Panda et al., 2002); in the case of epidermal progenitor cells, its role may be to synchronize intermediary metabolism and the cell cycle, thus minimizing cellular damage from oxidative phosphorylation-generated ROS (Stringari et al., 2015). The circadian clock, then, may be a mediator of the long-

appreciated, yet incompletely understood cross-talk between metabolism and the cell cycle (Buchakjian and Kornbluth, 2010; Fritz and Fajas, 2010; Laporte et al., 2011).

Despite the circadian clock's multiple roles in skin biology, other than the SCN, little is known of the factors that entrain the skin circadian clock. Restriction of food intake to defined time periods is known to change the phase of the circadian clock and gene expression programs, especially in primary metabolic organs such as the liver (Adamovich et al., 2014; Damiola et al., 2000; Kuroda et al., 2012; Stokkan et al., 2001). But not all peripheral tissues are entrained by RF (Izumo et al., 2014), and the effect of RF on the skin has not been investigated. Hence, we examined whether RF can entrain the circadian clock in skin and affect skin function. We discovered that RF can shift the circadian clock of skin, but that the phase of the skin circadian clock is not as tightly coupled to feeding time as that of the liver. We found RF-schedule-specific changes in the skin transcriptome, including changes in the expression of multiple metabolic genes and the nucleotide excision repair factor, *Xpa*. Although the phase of the cell cycle was insensitive to changes in circadian clock phase, RF decreased overall progenitor proliferation rates, and day-time RF reversed diurnal rhythm of epidermal sensitivity to UVB-induced DNA damage. This study points to unexpected influences of time of feeding on the biology of skin, suggesting that time of feeding may affect UVB-induced conditions such as skin cancer and premature aging.

2.2 Results

2.2.1 RF entrains the skin circadian clock in a manner distinct from that of the liver

To determine whether RF can shift the phase of the skin circadian clock, we administered five different feeding schedules (Figure 2.2.1A). The *ad libitum* (AD) group of mice had unlimited access to food. The early daytime (ED) feeding group had access to food from zeitgeber time 0 (ZT0) for 4 hours. The midday (MD) feeding group had access to food from ZT5 for 4 hours. The early nighttime (EN) feeding group had access to food starting at ZT12. Finally, the long daytime (LD) feeding group had access to food from ZT3 for 8 hours. These feeding lengths and times were modeled on previous RF studies (Damiola et al., 2000; Stokkan et al., 2001).

To evaluate the effect of RF schedules on body weight and food intake, we recorded food intake daily and body weight immediately prior to food availability every other day for 21-26 days for the AD, EN, MD and ED groups (Figure 2.2.2A-B). Both MD and ED mice ate significantly less than the AD mice during the first two days of RF, but by the end of the experiment there was no significant difference in food intake across the groups (Figure 2.2.2A). All groups weighed approximately the same prior to the beginning of the RF (data not shown), but throughout the RF experiment, body weight was significantly affected by RF schedule: AD weighed more than all RF groups, ED and EN had approximately equal body weight, and MD weighed consistently less than all other groups (Figure 2.2.2B). We performed two RF experiments as described in the Methods section, with similar results for body weight and food intake in both experiments (data not shown). We also measured skin compartment width (epidermis; dermis, including dermal fat layer; and muscle layer) by histology and found no significant changes except that dermis width was decreased by about 16-17% in EN and MD compared to AD (Figure 2.2.2C-F).

After implementing these RF schedules for 18 to 21 days, we harvested skin and liver from cohorts of mice every 4 hours for 28 hours starting at ZT0. We then determined the circadian clock phase by analyzing the peak time of skin mRNA expression of *Per2*, a commonly used indicator of the circadian phase. The phase of *Per2* in mice fed during the night (EN) was equivalent to that of AD (Figure 2.2.1B). Using AD as a reference, we found that MD induced a phase advance on average of 4.19 ± 0.43 hours; in contrast, ED caused a phase delay on average of 4.72 ± 0.38 hours (Figure 2.2.1C, Figure 2.2.3A). The phase of *Per2*, then, was almost 9 hours apart for MD and ED, the groups with the most widely separated phases (Figure 2.2.1B). The magnitude of phase advances was the same in LD and MD (Figure 2.2.3A). We also found that the amplitude of *Per2* was significantly lower in day-fed mice compared to EN (Figure 2.2.1C). Using either AD or EN as a reference, the phase shift of *Per2* in ED was significantly different compared to LD and MD (Figure 2.2.3A). By contrast, in the liver, the phase of *Per2* expression in all feeding groups was tightly linked to the time of initiation of food intake (Figure 2.2.1D, Figure 2.2.3B) and the peak expression of neither ED nor LD were significantly different from EN (Figure 2.2.1E).

To determine if the shift in the phase of the circadian clock was consistent in the skin and liver, we compared the phase shift of *Per2* in the RF groups relative to AD or EN, and found that, while MD exhibited the same phase advance in skin and liver, the phase shifts for ED and LD were different in these organs (Figure 2.2.3C). Expression results for core clock genes *Dbp* (Figure 2.2.3D-F) and *Per1* (Figure 2.2.3G-I) matched the *Per2* results, indicating a true phase shift of the core clock machinery. We also studied the phase and peak expression of *Per2* in

isolated epidermis of EN and ED, finding that they are similar to that in whole skin (Figure 2.2.3J-K and Figure 2.2.1B-C).

Collectively, these data demonstrate that time of feeding influences the phase and peak expression of the skin circadian clock in manner distinct from that of the liver. While feeding appears to be a direct zeitgeber for the liver with *Per2* expression having a constant relation to feeding time, there is a less direct relationship between the initiation of feeding and the phase of the skin circadian clock.

2.2.2 Diverse but functionally similar diurnal transcriptomes under different RF schedules

To define the diurnal transcriptome of skin under different RF schedules, we performed RNA-Seq on telogen skin collected every 4 hours for 28 hours under the three 4-hour RF schedules: ED, MD and EN (Figure 2.2.1A and Table 2.2.1). We selected mice from these RF schedules for further study in order to minimize effects of differences in caloric intake (see Methods section). EN mice were selected as the control because their circadian phase and time of feeding is similar to that of AD mice (Figure 2.2.1A-B); AD mice feed mainly during the early night (Vollmers et al., 2009; Yoon et al., 2012). Analysis of ED and MD mice allows us to observe the effect of maximum diurnal phase shifts as their circadian phases are nearly 9 hours apart in skin (Figure 2.2.1B, Figure 2.2.3A).

To quantify RNA expression levels, we separately counted the reads in exons, introns and antisense strands of all genes in the UCSC canonical gene set (Figure 2.2.4A). Using a

combination of four algorithms (Figure 2.2.4B), we identified 2,997, 3,198 and 2,546 exon transcripts as diurnally oscillating (out of 22,583 detected) in the EN, ED and MD groups, respectively (Figure 2A; Table S2 from Wang et al., 2017). Surprisingly, for each feeding group, there were a large number of genes with diurnally oscillating expression unique to that group, and only 147 genes were common to all three feeding groups (Figure 2.2.5A; Table S2 from Wang et al., 2017). These common genes include the core clock regulators *Clock*, *Cry1/2*, *Per2/3*, *Dbp*, and *Npas2* (Figure 2.2.5B; Table S2 from Wang et al., 2017). The overall shift direction of the diurnal transcriptome common between any two RF schedules was consistent with the shift of the circadian clock (Figure 2.2.1B, Figure 2B-E; Table S2 from Wang et al., 2017). Specifically, compared to EN, the phase of most diurnal genes in MD advanced while the phase of most diurnal genes in ED delayed (Figure 2.2.5C-E; Table S2 from Wang et al., 2017). Whereas the specific genes overlapping between any two groups differ, their functional categories were conserved, including *cell death*, *redox regulation*, *cell cycle* and *circadian clock* (Figure 2.2.5B-E; Table S2 from Wang et al., 2017).

We also identified diurnal intron (Figure 2.2.4C) and antisense (Figure 2.2.4D) transcripts (Table S2 from Wang et al., 2017). As transcription affects both intron and exon components of transcripts, the comparison of phase shifts between introns and exons in a gene gives insights into the extent to which the phases of diurnal genes and biological processes under different RF schedules are controlled at a transcriptional or a post-transcriptional level. Overall, we found that the phase shift in peak expression in exons and introns of a gene was correlated (Pearson R = 0.68) suggesting that transcriptional regulation is an important mechanism underlying food entrainment in the skin (Figure 2.2.6A; Figure 2.2.4E-G; Table S2 from Wang et al., 2017). This

mode of regulation was reflected in our gene ontology (GO) analysis showing that the circadian clock genes are clearly regulated transcriptionally (Figure 2.2.6B). However, there were a number of genes that are exceptions to this general rule as exemplified by cytokinesis genes, which appear to be regulated post-transcriptionally (Figure 2.2.6B).

We found only 37 antisense transcripts with diurnal expression in all three feeding schedules (Figure 2.2.4D). Some of these, including the clock regulator *Dec2* (also known as *Bhlhe41*), show expression in phase with the exons (Figure 2.2.6C) while others, including *Erc2*, which is involved in regulation of neurotransmitter release, show antiphasic expression to the exons (Figure 2.2.6D).

Together, these data indicate that RF shifts the phase of most diurnal genes in skin by transcriptional mechanisms. The RF-affected genes, while participating in similar functions, are largely unique to each RF schedule. In addition, we identified two antisense transcripts that may have a regulatory relationship with the gene from which they are encoded.

2.2.3 Food intake acutely regulates a portion of the skin transcriptome

We next considered the possibility that food intake could acutely affect skin gene expression. To search for such effects in the data, we rearranged the RNA-seq reads across all three feeding schedules according to the feeding time (Figure 2.2.7A), generating feeding time (FT) series (FT0-FT4-FT8) where FT0 represents the initiation of feeding and FT4 and FT8 represent times 4 and 8 hours after the start of feeding.

We identified 2,026 exons differentially regulated by food intake (Figure 2.2.7B and Figure 2.2.8A, B). Exons showing the most significant change in response to feeding were linked to metabolism (Figure 2.2.7C), including *Pdk4*, *Ucp3* and *Scd2*. The food intake-affected exons fell into two groups: those that decreased (998) after food intake and those that increased (1,028) after food intake (Figure 2.2.7B-E, Figure 2.2.8A-B). Genes showing decreased expression after food intake were overrepresented in GO categories including *response to starvation*, *autophagy*, *response to oxidative stress, negative regulation of cell proliferation*, and *lipid oxidation* (Figure 2.2.7D; Table S3 from Wang et al., 2017) and those showing increased expression included *lipid biosynthesis* and *protein synthesis* (Figure 2.2.7E; Table S3 from Wang et al., 2017). These results indicate that the metabolism of skin is oxidative before feeding and becomes anabolic after feeding. We also identified 1,890 introns and 662 antisense transcripts affected by food intake (Figure 2.2.8A-B). About half of the food intake-affected genes were identified as having diurnal expression in one or more of the three feeding schedules (Figure 2.2.8C), suggesting that food intake contributes to regulation of the diurnal transcriptome in the skin. In conclusion, these data indicate that expression of many genes in the skin, including those involved in oxidative-reductive metabolism and cell proliferation, respond acutely to food intake, and that the metabolic status of skin is determined by feeding.

2.2.4 RF-induced phase shifts of the circadian clock do not affect the diurnal phase of epidermal progenitor cell S-phase

Previous studies showed diurnal changes in epidermal progenitor cell proliferation with 3- to 4-fold greater number of cells in S-phase during the night than during the day (Geyfman et al., 2012). Deletion of *Bmal1*, either constitutionally or selectively in epidermal cells, obliterates the diurnal variation in cell proliferation, indicating that the circadian clock controls the diurnal variation in epidermal progenitor cell proliferation (Geyfman et al., 2012).

To determine whether the RF-induced phase shifts in the skin's circadian clock alter the phase of the diurnal variation in epidermal progenitor cell proliferation, we measured the proportion of epidermal progenitor cells in S-phase by BrdU staining over a 28 hour period. The proportion of cells in S-phase is diurnal under each of the five RF schedules. Interestingly, despite the different phases in the circadian clock in different RF schedules, the phase of S-phase was not shifted by RF (Figure 2.2.9A). We also evaluated whether RF affects the proliferation rate of interfollicular epidermal progenitor cells, finding that each of the RF schedules resulted in a similar and decreased peak and overall progenitor cell proliferation compared to AD (Figure 2.2.9B). Together with previous findings showing that the circadian clock is required for diurnal DNA synthesis rhythms in epidermal progenitor cells (Geyfman et al., 2012), these results indicate that whereas the clock is critical for establishing diurnal variation in progenitor cell proliferation, it alone does not control the phase of the cell cycle.

2.2.5 Daytime feeding shifts skin sensitivity to UVB-induced DNA damage

Previous work in mice showed that sensitivity to UVB-induced DNA damage in the epidermis is diurnal with more damage when UVB is applied during the night than during the day

(Gaddameedhi et al., 2011; Geyfman et al., 2012). This diurnal variation depends on the circadian clock as mutations in *Bmal1* (Geyfman et al., 2012) and *Cry1/Cry2* (Gaddameedhi et al., 2011) obliterate the diurnal variation. To test whether daytime feeding, with its consequent shift in the phase of the clock, modulates the epidermal sensitivity to UVB-induced DNA damage, we applied UVB during the day (ZT9) and night (ZT21) to the shaved backs of AD, EN, ED, and MD mice, collecting the skin 15 minutes after UVB exposure. Consistent with previous studies (Gaddameedhi et al., 2011; Geyfman et al., 2012), mice that ate mainly (AD) or only (EN) at night formed more cyclobutane pyrimidine dimers (CPD) when exposed to UVB during the night than during the day (Figure 2.2.10A). By contrast, mice fed during the day (ED and MD) exhibited a reverse pattern, forming more CPD when exposed to UVB during the day than during the night (Figure 2.2.10A). Similar trends were observed in a earlier RF experiment with fewer mice in which we measured both CPDs and the second most common UVB-induced lesion, (6-4) Photoproducts ((6-4)PP) (Figure 2.2.11A). Thus, while not altering the phase of S-phase in epidermal progenitor cells, daytime RF reverses the diurnal rhythm of sensitivity to UVB-induced DNA damage. In addition, we found that the expression of *Xpa*, the gene encoding a rate-limiting protein necessary for nucleotide excision repair of UVB-induced DNA (Li et al., 2011; Miyamoto et al., 1992), is dampened in EN, MD, and ED compared to AD. Furthermore, *Xpa* expression oscillates in a diurnal fashion in AD but not as robustly in the RF schedules (Figure 2.2.10B).

In sum, these results demonstrate that daytime-restricted feeding affects the sensitivity to DNA damage in the skin of mice, and dampens the expression of a key DNA repair factor.

2.3 Discussion

This work shows that time of feeding is an important regulator of skin function. As summarized in Figure 2.2.10C, we found that: 1) RF shifts the phase of the skin circadian clock, in a pattern distinct from that of the liver; 2) RF alters the expression of many diurnally expressed genes in the skin, including that of the key DNA repair factor *Xpa*; 3) feeding acutely causes large scale gene expression changes in the skin, most prominently of metabolic genes; 4) day-time RF reverses the time-of-day-dependent sensitivity to UVB-induced DNA damage in the skin. These findings are summarized in Figure 2.2.12. Together, our results indicate that timing of food intake has a more pronounced influence on skin biology than previously recognized, representing a modifiable regulator of skin health.

Studies focusing on the liver, a key organ for organismal metabolism, showed that the phase of the circadian clock is entrained by RF (Damiola et al., 2000; Kuroda et al., 2012; Stokkan et al., 2001) and that a significant portion of the liver transcriptome is affected by the time of feeding (Vollmers et al., 2009). The effect of RF on clocks in peripheral organs not primarily involved in organismal metabolism is less well studied (Izumo et al., 2014; Reznick et al., 2013); in particular, there are no such studies in the skin. Our findings indicate that both the phase and peak expression of the skin circadian clock are distinct from that of the liver. In the skin, day-fed mice (MD, ED, LD) exhibit lower amplitude of the core clock gene *Per2* than mice fed during the night (EN), while in the liver, *Per2* amplitude does not seem to be sensitive to time of feeding. Furthermore, mice fed during the early daytime (ED) exhibited a 4.7-hour phase delay in *Per2* expression compared to AD mice in the skin, while in the liver the phase of *Per2*

expression is advanced by 10.9-hours, corresponding to the initiation of food intake. These findings suggest that RF controls the phase of the skin circadian clock by different mechanisms than in the liver where feeding appears to be a more direct and dominant cue (Figure 2.2.1). These observations suggest that, in addition to regulation of the skin clock by the SCN's central clock (Tanioka et al., 2009), the skin clock is independently modulated by the timing of food intake. The exact mechanism by which feeding time controls the skin clock likely involves many factors such as physical activity, sleep-wake cycles, metabolism, and circulating hormones.

Comparison of the telogen skin transcriptome under three different RF schedules (ED, MD, EN) reveals that feeding schedule dictates the diurnal expression of approximately 10% of the skin transcriptome (Figure 2.2.5). Specifically, RF schedules generate diurnal gene rhythms that are largely unique to each RF schedule while dampening diurnal expression of other genes that are diurnal in the other RF schedules (Figure 2.2.5). Furthermore, while feeding time largely defines the identity of individual genes with oscillating expression, the functional categories annotated to these genes are similar among the three RF schedules. We also found that some diurnally expressed genes are conserved in all the three RF schedules; these genes are enriched for regulators of the circadian clock. The phase shift of the clock-related transcripts under the three RF schedules correlates well with the phase shift of the core circadian clock as indicated by the peak time of *Per2* expression (Figure 2.2.1). In addition, the shift of expression of exons is linearly correlated with that of introns, indicating that shift of transcriptional activity is an important mechanism underlying the shift of the whole transcriptome (Figure 2.2.6). Genes annotated to regulation of circadian rhythm tend to be diurnally expressed in introns and exons while some genes annotated to the cell cycle, especially cytokinesis, tend to be diurnally

expressed in exons and not introns. These findings suggest that different diurnal processes may be regulated to varying extents by both transcriptional and/or post-transcriptional mechanisms.

In contrast to exons, there are very few diurnal antisense transcripts. Also, the expression of antisense transcripts is largely uncorrelated with the expression of either introns or exons of the corresponding diurnal genes. We have identified a few antisense genes, however, that exhibit unique diurnal expression in relation to their corresponding genes, indicating a potential regulatory role.

We observed striking changes in skin gene expression directly in response to food intake (Figure 2.2.7). This suggests that at least part of the RF schedule-mediated changes in gene expression are a direct feeding effect although we cannot rule out contributions by changes in rhythms of activity level and sleep caused by restricted food availability. An analysis of these gene expression changes indicates that after feeding, cellular metabolism becomes biosynthetic and reductive. Instead of oxidation of fatty acids, the skin transcriptome becomes more characteristic of the synthesis and import of lipids, especially steroids, which are involved in cellular membrane systems. In addition, in response to food intake, genes involved in transcription, translation, and protein folding and localization are up-regulated and those involved in apoptosis are down-regulated. This analysis indicates that components of the global diurnal gene expression program are acutely responsive to food-intake.

In previous studies, we showed that the circadian clock intrinsic to keratinocytes is required for the diurnal fluctuation in the proportion of epidermal progenitors undergoing S-phase (Geyfman

et al., 2012). Interestingly, in the current study we find that despite the shift in the phase of the circadian clock by RF, the rhythm of DNA synthesis in epidermal progenitors of the skin did not shift (Figure 2.2.9). Together these findings indicate that while an intact clock is required for the diurnal variation in DNA synthesis, the phase of the clock is not the dominant regulator of the phase of the S-phase oscillations in the mouse skin. These findings are in agreement with studies showing that the cell mitotic cycle can be uncoupled from the circadian clock in immortalized rat-1 fibroblasts (Yeom et al., 2010) and Lewis lung carcinoma cells (Pendergast et al., 2010), and a recent study showing that cell division cycles could be gated by WNT-signaling (Matsu-Ura et al., 2016). While a previous study showed that time restricted feeding can shift the daily proliferative rhythm of the digestive tract (Burholt et al., 1985), in the gut, cell proliferation may be mechanically stimulated by food.

Given our finding that oxidative metabolism in the skin is affected by time-restricted feeding, it is likely that a deviation in the time of food intake may lead to asynchrony between oxidative metabolism and DNA replication which normally is coordinated with cell cycle stages in epidermal progenitors (Stringari et al., 2015). We hypothesize that such asynchrony between the timing peak oxidative phosphorylation metabolism and cell division due to unusual feeding times could contribute to increased ROS-mediated DNA damage in progenitor and stem cells, leading to aging and carcinogenesis.

We also show that feeding at non-physiological times can alter the skin's susceptibility to UVB-induced DNA damage. Mice that eat during the normal time (night) have greater sensitivity to UVB-induced DNA damage at night compared to during the day, consistent with previous

studies (Figure 2.2.11; Geyfman et al., 2012; Gaddameedhi et al., 2011). This rhythm in DNA damage is attributed to the increased number of progenitors undergoing S-phase at night (Geyfman et al., 2012) and the diurnal variation in the efficacy of DNA excision repair mediated by the key nucleotide excision repair factor Xpa (Gaddameedhi et al., 2011). We found that daytime-fed mice had reversed diurnal rhythm of sensitivity to UVB-induced DNA damage with greater sensitivity during the day than during the night (Figure 2.2.10A). Since the phase of S-phase is not altered by RF, other factors may contribute to the RF-altered rhythm in the susceptibility to DNA damage. In fact, the expression of the key repair gene *Xpa* is diurnal, peaking during the day in AD mice (Figure 2.2.10B) (Gaddameedhi et al., 2011; Khang et al., 2010), but exhibiting dampened and less rhythmic expression under RF schedules (Figure 2.2.10B).

In conclusion, our findings show that time-restricted feeding (EN, ED, MD) decreases the proportion of cells in S-phase, and dampens expression of DNA repair factor Xpa. In addition to these changes, daytime-restricted feeding (ED and MD) also shifts the phase of core clock genes and oxidative metabolism genes, and reverses the rhythm of sensitivity to UVB-induced DNA damage. By disrupting the natural expression and diurnal variation of such important processes in the skin, abnormally-timed food intake may contribute to the development of skin pathologies involving sun damage, skin aging and skin cancer.

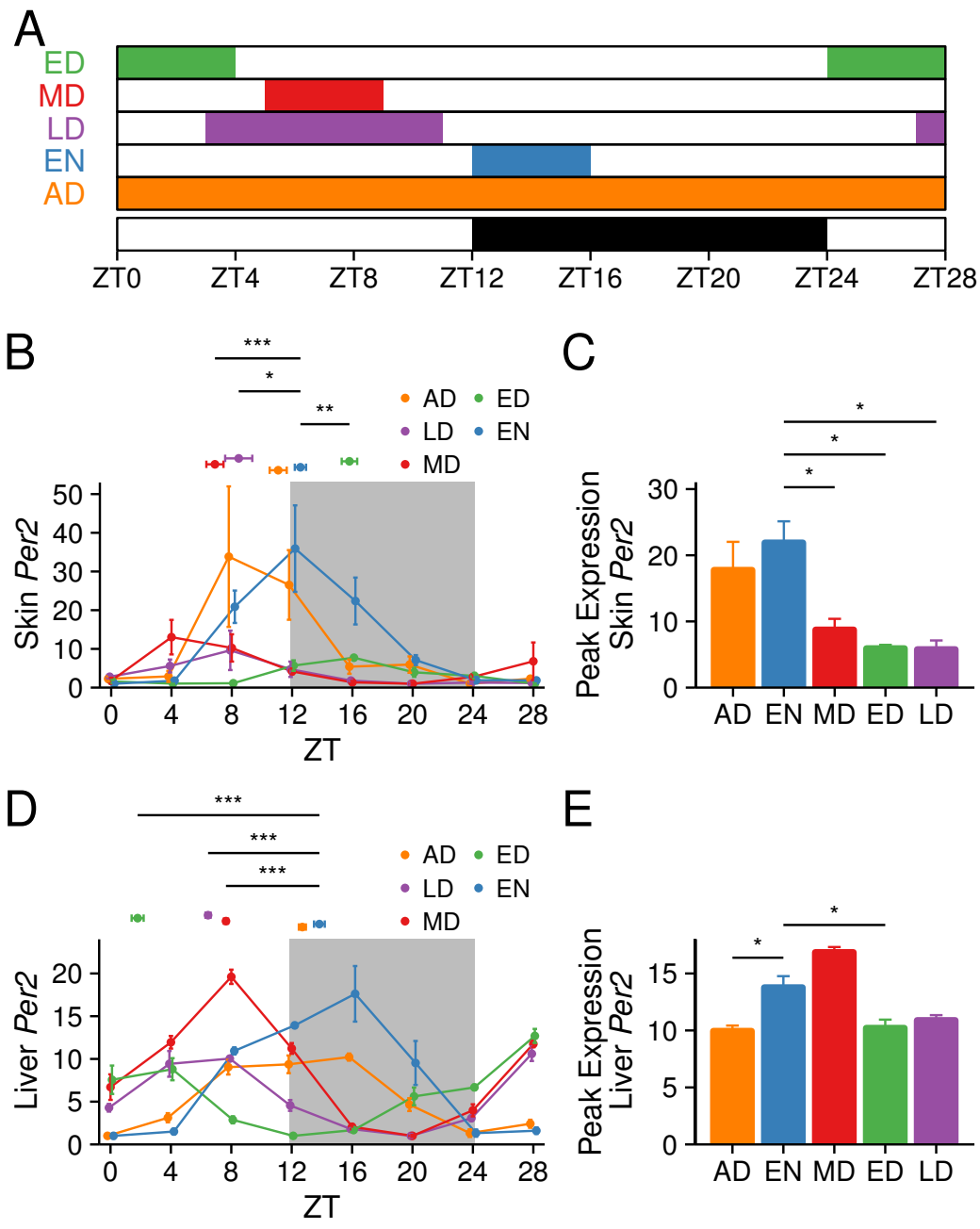

Figure 2.2.1. Entrainment of peripheral circadian clocks by time-restricted feeding.
(A) Schematic showing the RF schedules. Colored boxes indicate timing of food access: AD, ad libitum; ED, early day; MD, mid-day; EN, early night; and LD, long day. Day and night are indicated below with white and black bars. The sampling time points are indicated by ZT on the x-axis. *Per2* gene expression in the skin (B-C) and liver (D-E) as measured by qPCR. (B, D) The values represent mean ± SEM, N = 3-5. The peak time, a proxy for the circadian phase, is shown above the curves as mean ± SEM, N = 4. Watson-Williams test was used to compare the peak times. (C, E) The peak expression values are shown as mean ± SEM, N = 4. Statistical significance comparing peak expression values was determined by Welch's t-test, shown as *p < 0.05, **p < 0.01, *** P < 0.001. See also Figure 2.2.3.

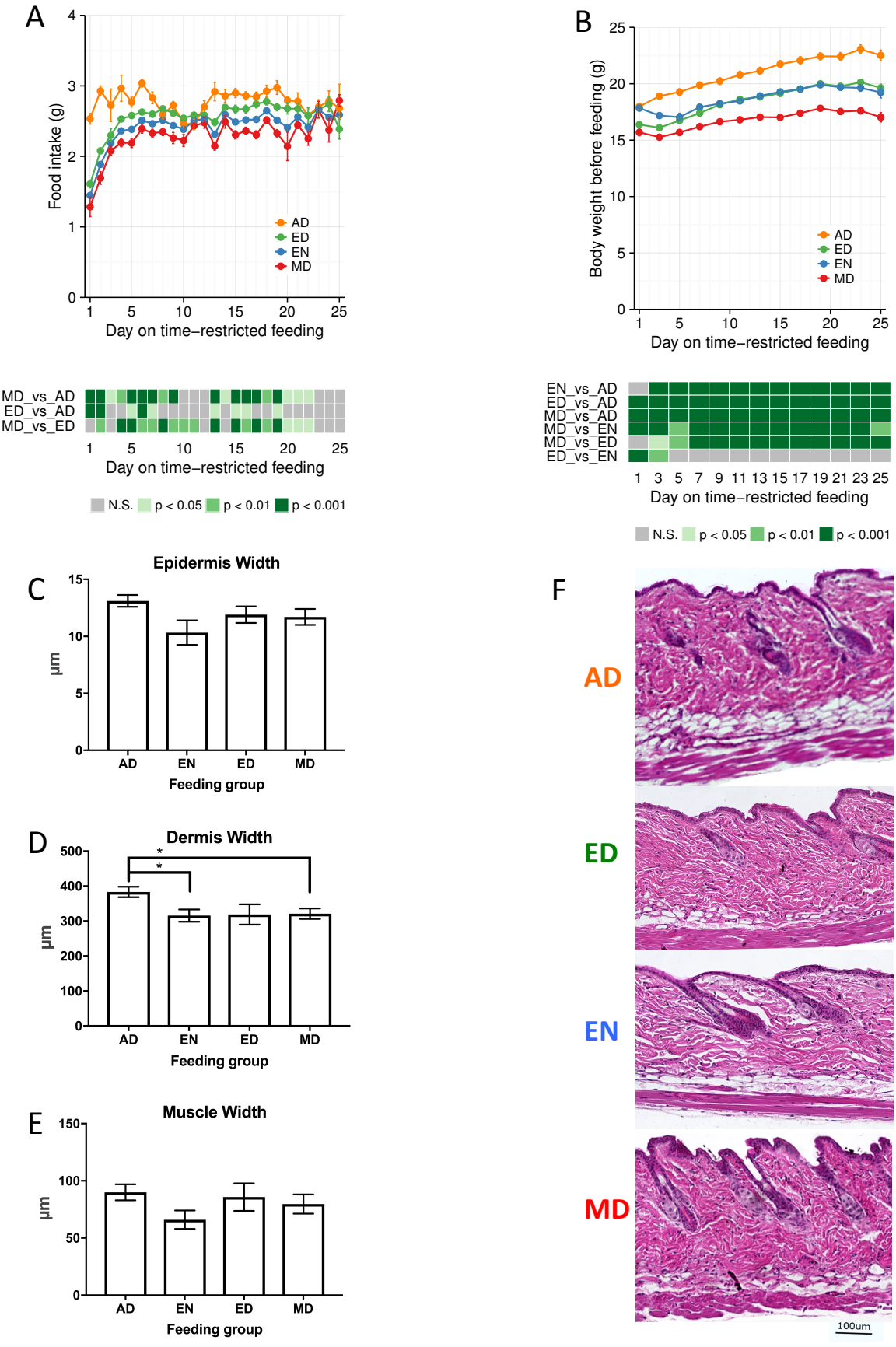
A
Food intake (g)
Day on time−restricted feeding
AD
ED
EN
MD
MD_vs_AD
ED_vs_AD
MD_vs_ED
N.S. p < 0.05 p < 0.01 p < 0.001
B
Body weight before feeding (g)
EN_vs_AD
ED_vs_AD
MD_vs_AD
MD_vs_EN
MD_vs_ED
ED_vs_EN
C
Epidermis Width
µm
Feeding group
D
Dermis Width
E
Muscle Width
F
100um

Figure 2.2.2. Food intake, body weight, and skin histology after RF schedules. (A) Food intake throughout the RF protocol. Two-way ANOVA (Group × Time): RF schedule ($p < 0.001$), ZT time ($p < 0.001$) and RF schedule × ZT time ($p < 0.001$). Data are represented as mean ± SEM, N = 15-18. (B) Body weights throughout the RF protocol. Two-way ANOVA: RF schedule ($p < 0.001$), ZT Time ($p < 0.001$) and RF schedule × ZT time ($p < 0.001$). Data are represented as mean ± SEM, N = 11-36. For (A) and (B), Welch's t-test p-values comparing feeding groups at each time point are listed below the graphs. Shade of green indicates significance, with darker green being more significant. (C-E) Skin histology measurements. Skin was collected, paraffin embedded, sectioned and stained with hematoxylin and 20x mosaic images were acquired. The thickness of (C) epidermis, (D) dermis (including the intradermal fat layer), and (E) subcutaneous muscle were measured. Data is presented as Mean ± SEM for N=10-18 mice per group. Significance was determined by one-way ANOVA (only dermis showed significance with P= 0.03), followed by Student's paired t-test, shown as *$p < 0.05$. (F) Representative cropped images of skin histology from the RF groups quantified in C-E. 100 um scale bar is shown.

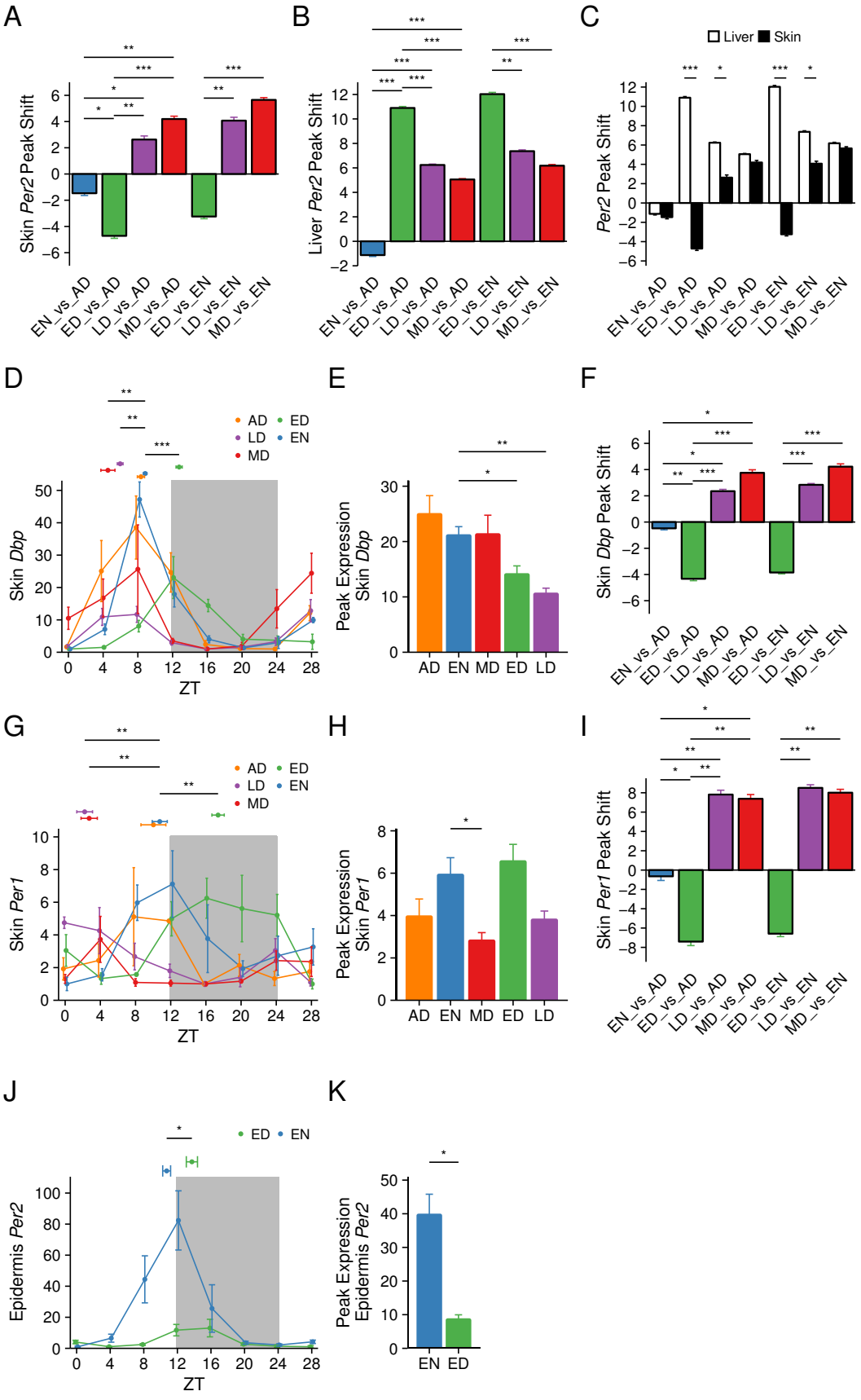
A
Skin Per2 Peak Shift
EN_vs_AD
ED_vs_AD
LD_vs_AD
MD_vs_AD
ED_vs_EN
LD_vs_EN
MD_vs_EN
B
Liver Per2 Peak Shift
C
Liver
Skin
Per2 Peak Shift
D
AD
ED
LD
EN
MD
Skin Dbp
ZT
E
Peak Expression Skin Dbp
AD EN MD ED LD
F
Skin Dbp Peak Shift
G
Skin Per1
ZT
H
Peak Expression Skin Per1
I
Skin Per1 Peak Shift
J
ED
EN
Epidermis Per2
ZT
K
Peak Expression Epidermis Per2
EN ED

Figure 2.2.3. *Per2*, *Dbp* and *Per1* expression and comparison of peak shifts. (*A*) Peak shift of skin *Per2* expression. (B) Peak shift of liver *Per2* expression. (C) Comparison of peak shifts of *Per2* expression in skin and liver. (D) *Dbp* gene expression in the skin measured by qPCR. (E) Peak expression of skin *Dbp*. (F) Comparison of the peak shifts of skin *Dbp* expression. (G) *Per1* gene expression in the skin measured by qPCR. (H) Peak expression of skin *Per1*. (I) Comparison of peak shifts of skin *Per1* expression. (J) *Per2* gene expression in the epidermis measured by qPCR. (K) Peak expression of epidermis *Per2*. (D, G, J) QPCR data is represented as mean ± SEM N = 3-5, after removal of outliers (Dixon's Q test, $Q_{99\%}$). The peak time of each group is shown above the curves represented as mean ± SEM N = 4. Watson-Williams test was used to compare the peak times (A-D, F, G, I, J) and Welch's t-test was used to peak expression levels (E, H, K). (A-K) For peak time and peak expression, the values represent mean ± SEM, N = 4. Statistical significance shown as *$p < 0.05$, **$p < 0.01$, *** $P < 0.001$.

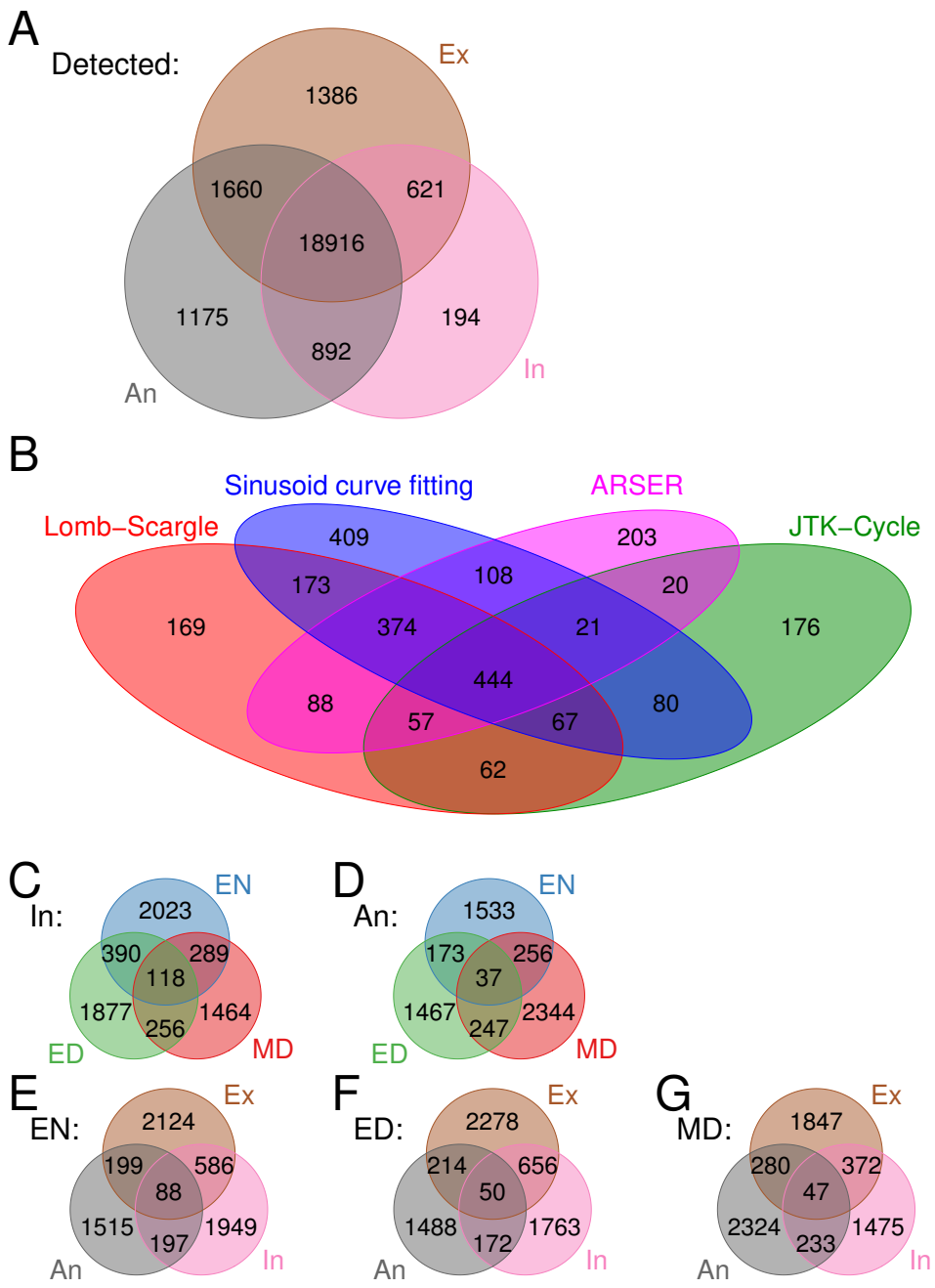

Figure 2.2.4. Identification of diurnal transcripts. (A) Overlap of detected exons, introns and antisense transcripts. (B) Overlap of diurnal exons of EN identified by different algorithms. Genes identified as diurnal by any algorithm(s) are included. (C-D) Overlap of diurnal introns (C) and antisense (D) transcripts in three feeding groups. (E-G) Overlap of diurnal transcripts in EN (E), ED (F) and MD (G) (A and C-G) Ex: exons; An: antisense; In: introns.

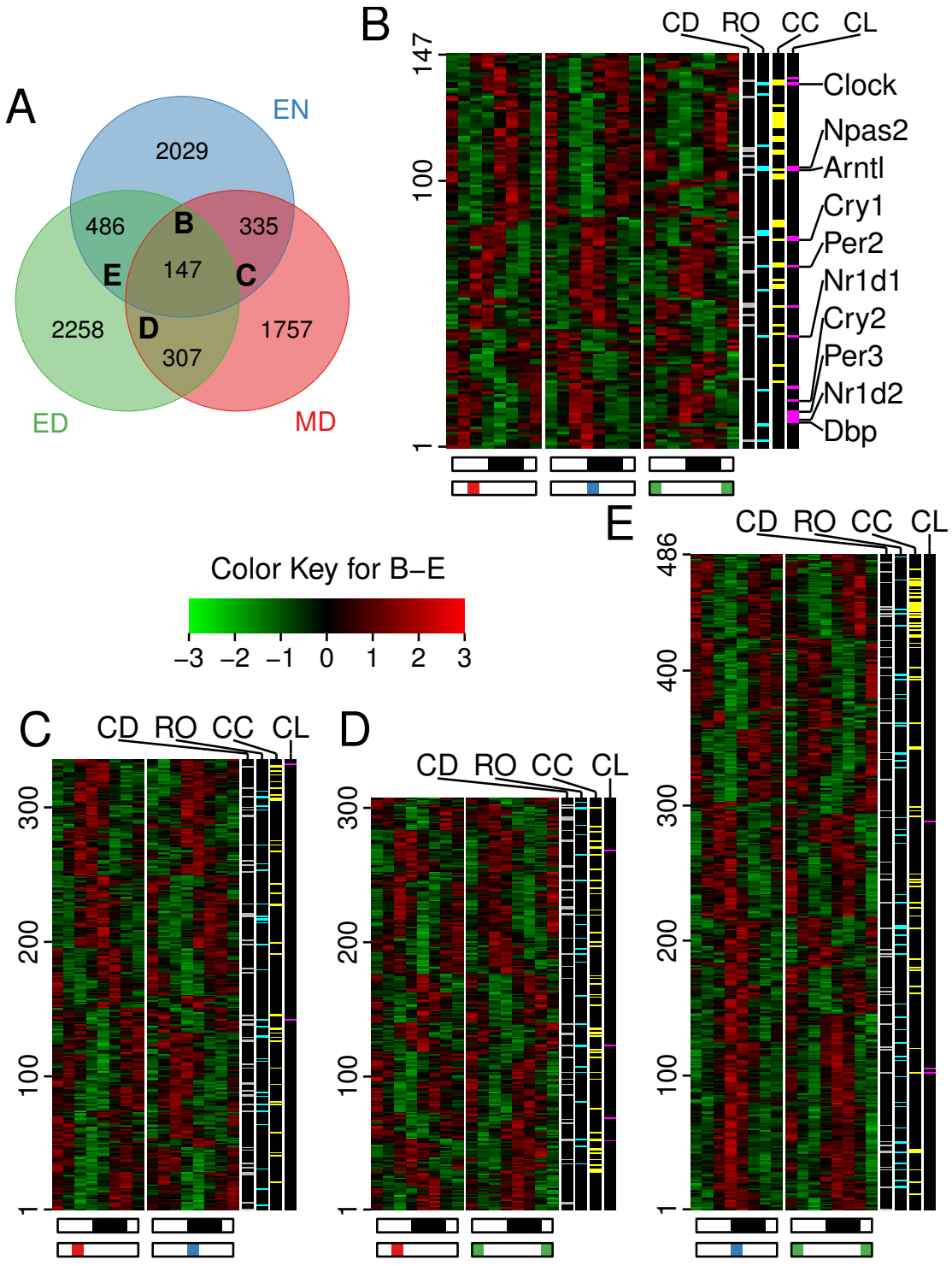

Figure 2.2.5. Diurnal transcriptome of skin under time-restricted feeding. (A) Venn diagram depicting the overlap of diurnal exons expressed in skin of mice after time-restricted feeding. Out of 7,317 total diurnally oscillating exon transcripts, 147 are common within all 3 RF schedules. Exons for core circadian clock genes (such as *Clock, Npas2,* and *Arntl*) maintained diurnal rhythm in all RF schedules (core clock gene examples listed in panel B, to the right). (B-E) Heatmaps of the diurnal exons common under all (B) or 2 (C, D and E) of the RF schedules

(corresponding to the B-E labels in (A)). Note that in B, most genes in MD are phase advanced while those in ED are phase delayed compared to EN. The white-black bars below indicate day and night, respectively. Colored bars under the heat maps indicate the time of food availability. The color key for the heat maps show the Z-score of expression value, where red is highly expressed and green is minimally expressed. The colored lines in black bars to the right of the heat maps indicate genes annotated to cell death (CD), reduction-oxidation (RO), cell cycle (CC), and circadian clock (CL) biological processes. See also Figure 2.2.4 and Table S2 from Wang et al., 2017.

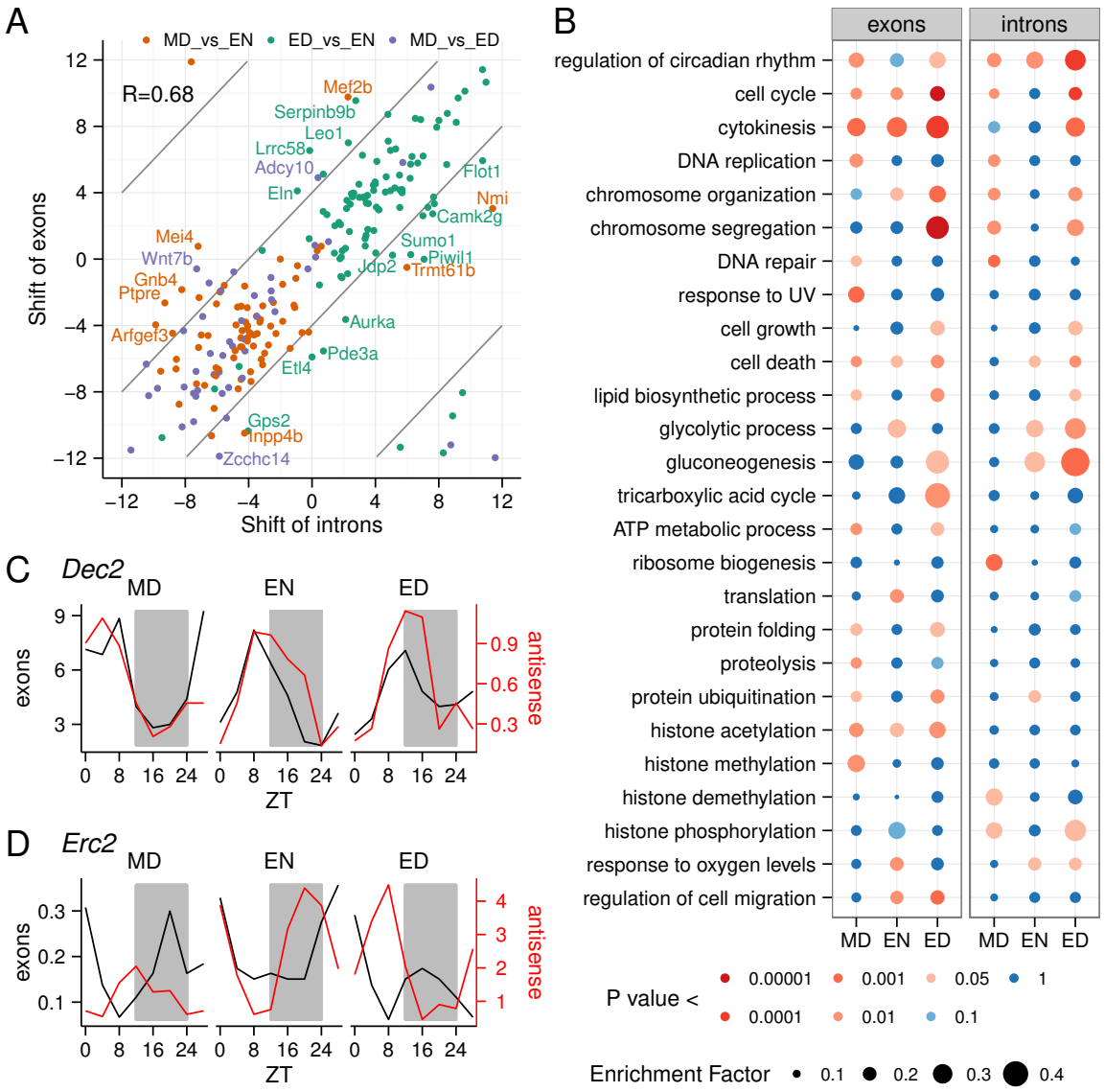

Figure 2.2.6. Functional and regulatory aspects of the skin diurnal transcriptome
(A) Linear correlation of the time-shift of exon and intron expression under different RF schedules. Examples of genes where the differential timing of intron and exon expression is greater than 4 hours are indicated with gene symbols. (B) Enrichment of biological processes was determined for genes with diurnally expressed introns and exons by Fisher's exact test. Rows are Gene ontology (GO) terms and columns are RF schedules. Enrichment factor was determined as the ratio of diurnal genes in a term over all genes in a term; this is represented by circle size. The color of the circles indicates p-value. This data suggests that genes annotated to "regulation of circadian rhythm" are mainly regulated at a transcriptional level, while genes annotated to "cell cycle", "cell death" and "histone acetylation" are mainly regulated post-transcriptionally. (C and D) The expression of the exon and antisense transcripts for two diurnally expressed genes, *Dec2* and *Erc2*, featuring diurnally expressed antisense transcripts in all three RF schedules. For *Dec2*, the exon and antisense oscillation is in phase, while for *Erc2*, the exon and antisense transcripts have antiphasic oscillations.

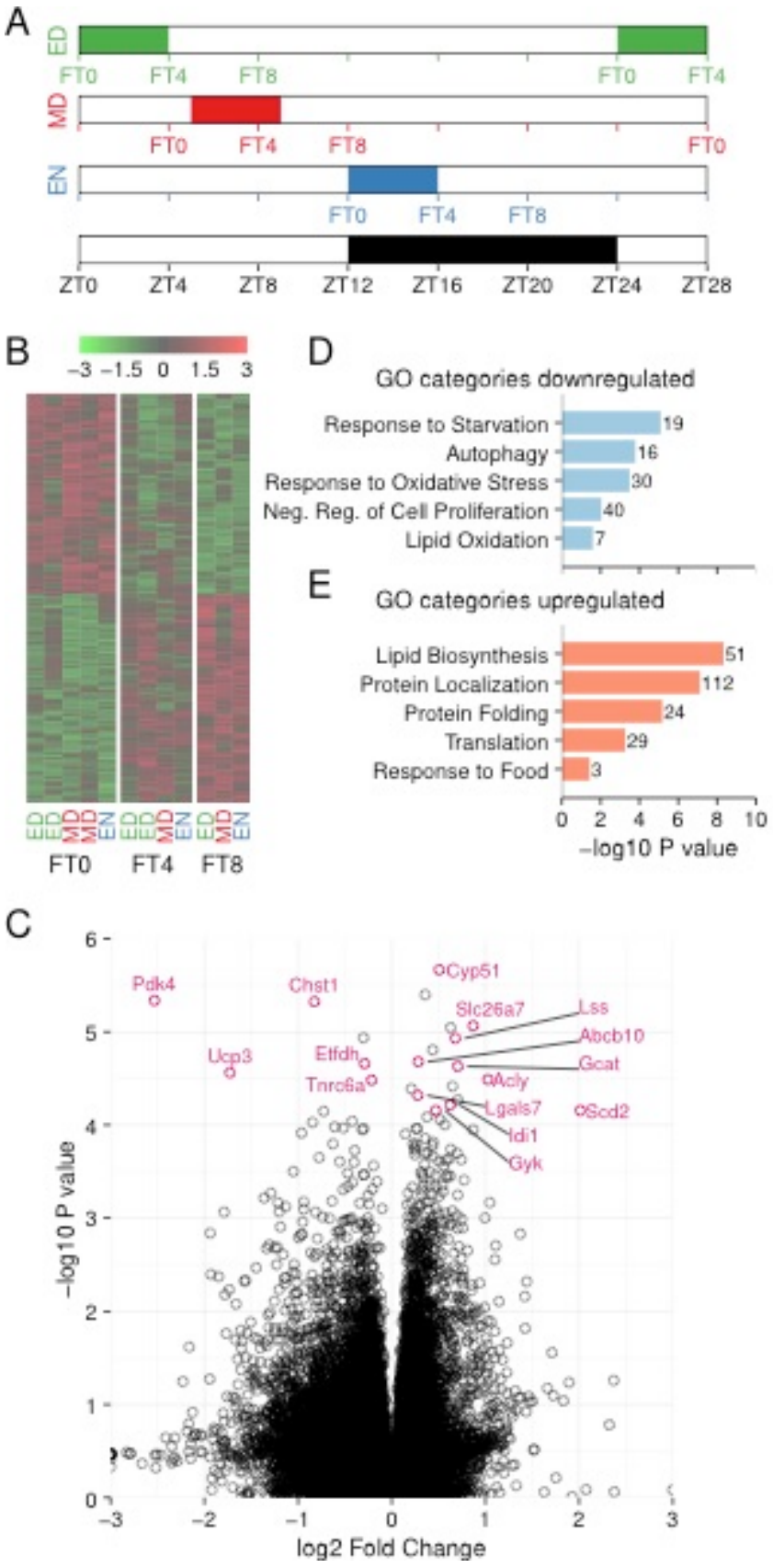
A
ED
FT0 FT4 FT8 FT0 FT4
MD
FT0 FT4 FT8 FT0
EN
FT0 FT4 FT8
ZT0 ZT4 ZT8 ZT12 ZT16 ZT20 ZT24 ZT28
B
−3 −1.5 0 1.5 3
ED MD EN ED MD EN ED MD EN
FT0 FT4 FT8
D
GO categories downregulated
Response to Starvation 19
Autophagy 16
Response to Oxidative Stress 30
Neg. Reg. of Cell Proliferation 40
Lipid Oxidation 7
E
GO categories upregulated
Lipid Biosynthesis 51
Protein Localization 112
Protein Folding 24
Translation 29
Response to Food 3
0 2 4 6 8 10
−log10 P value
C
Pdk4
Chst1
Cyp51
Slc26a7
Lss
Abcb10
Ucp3
Etfdh
Tnrc6a
Gcat
Acly
Lgals7
Scd2
Idi1
Gyk
−log10 P value
log2 Fold Change

Figure 2.2.7. Food intake alters the skin transcriptome. (A) A schematic showing how the RNA-seq reads from data presented in Figure 2.2.5 and 2.2.6 were regrouped and analyzed based on the timing of food availability. Feeding time zero (FT0) indicates reads immediately before food availability, feeding time 4 (FT4) indicates reads 4 hours after the onset of food availability, and feeding time 8 (FT8) indicates reads 8 hours after the onset of food availability, as described in the Methods section. Feeding groups are indicated below each column. The white-black bar indicates day and night, respectively. (B) 2,026 exons were affected by feeding based on the regrouping described in (A) (one-way ANOVA $P < 0.01$). Shown is the heat map of food intake-affected genes at FT0, FT4 and FT8. The color key represents the Z-score of expression value with red being highly expressed genes and green being minimally expressed genes. (C) Volcano plot showing feeding-affected exons. Representative, statistically significant metabolic genes are labeled. (D-E) Graphs of representative enriched GO categories for genes down-regulated (D) or up-regulated (E) after feeding. The numbers at the end of the bars refer to the number of genes affected in each category. See also Figure 2.2.8 and Table S3 from Wang et al., 2017.

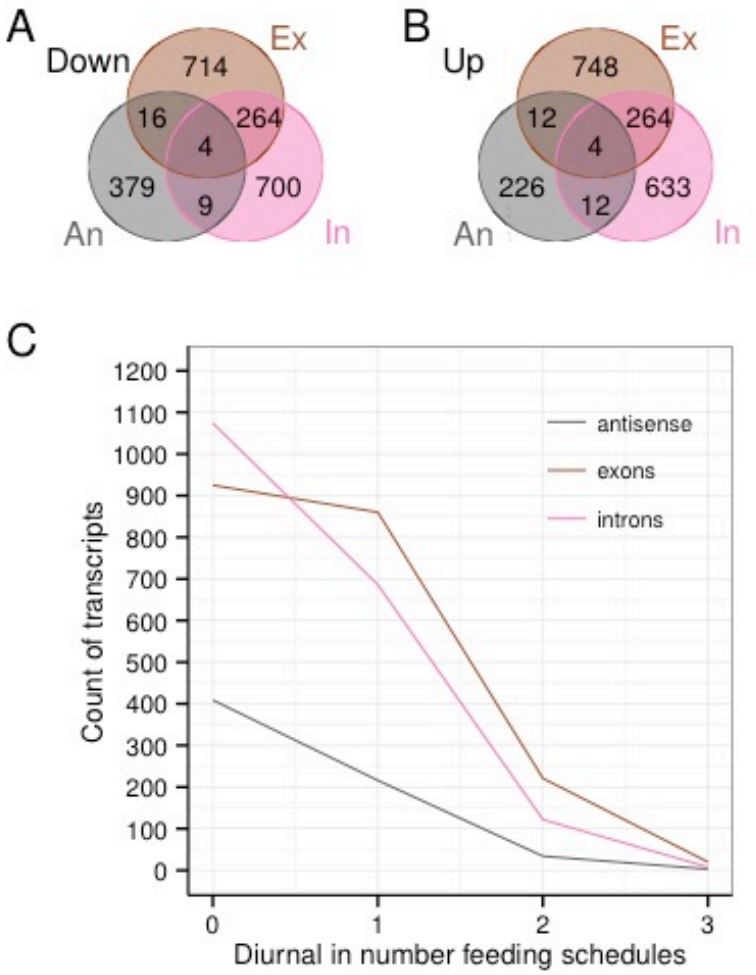

Figure 2.2.8. Genes affected by food intake. (A) Overlap of transcripts downregulated after feeding. (B) Overlap of transcripts upregulated after feeding. (A-B) Ex: exons; An: antisense; In: introns. (C) Graph depicting the number of feeding-affected transcripts that were identified as diurnal in 0, 1, 2, or 3 of the feeding groups.

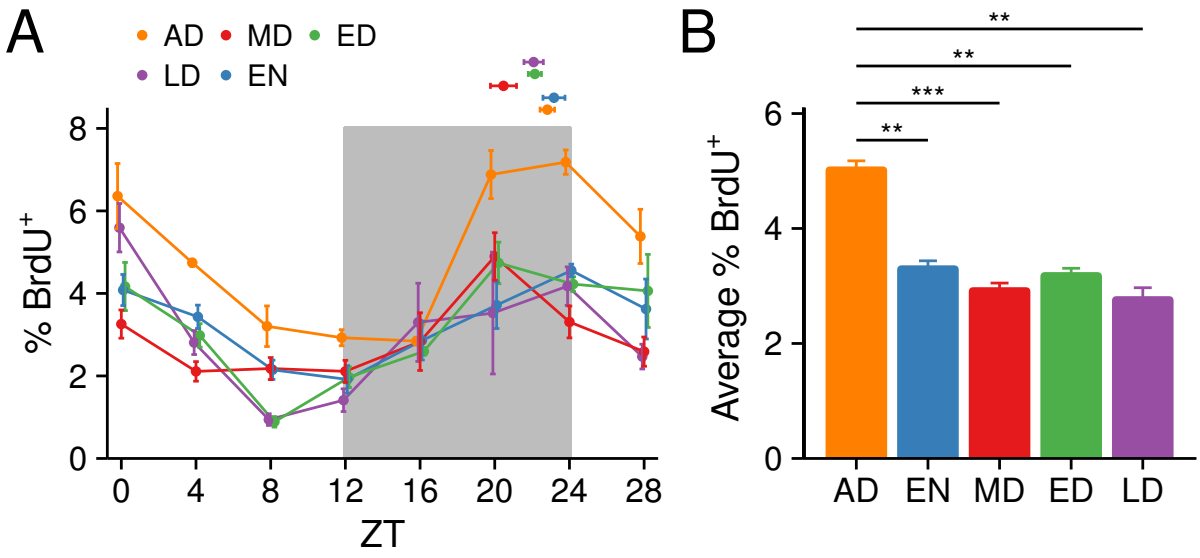

Figure 2.2.9. Effect of time-restricted feeding on epidermal cell proliferation. (A) BrdU-positive cells were counted in the epidermis by immunohistochemistry. Values represent mean ± SEM, N = 2-5. The proportion of cells in S-phase is diurnal under each of the five different RF schedules (one-way ANOVA $P < 0.01$). The dots above the curves indicate the peak time of BrdU incorporation. Values represent mean ± SEM, N = 4. Watson-Williams test was used to compare the peak times. The phase of diurnal rhythms of BrdU incorporation were unchanged among the four RF schedules. (B) The average percentage of BrdU-positive epidermal cells of each RF schedule. Values represent mean ± SEM, N = 4. AD had higher proliferation rate than all RF feeding schedules. Statistical significance was determined by Welch's t-test, shown as **$p < 0.01$, and ***$p < 0.001$.

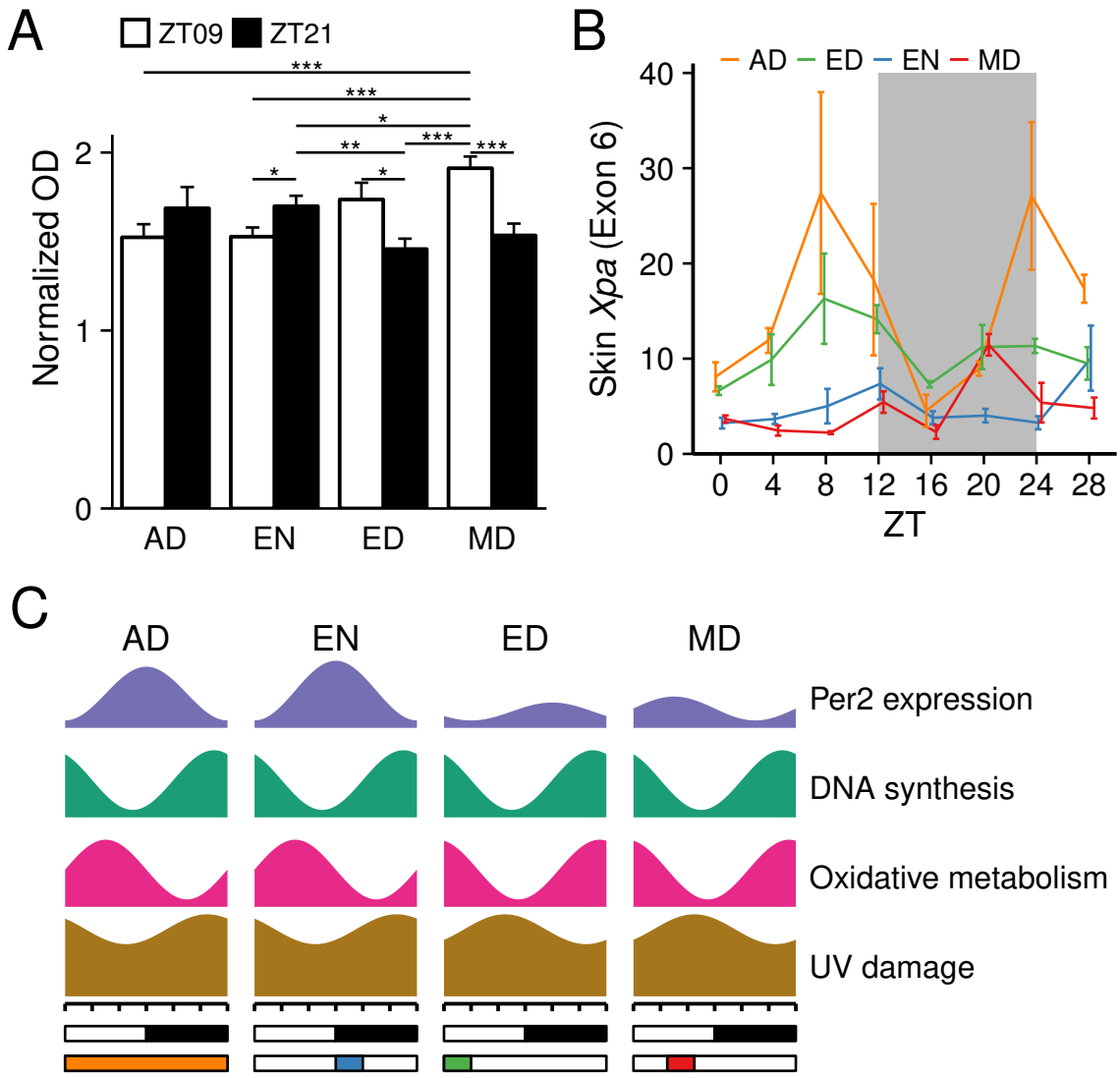

Figure 2.2.10. Diurnal sensitivity to UVB-induced DNA damage and Xpa gene expression in the skin. (A) Quantification of CPD photoproducts after UVB exposure at ZT9 and ZT21. The shaved back skins of mice from AD, EN, ED and MD feeding schedules were exposed to single dose of 500 J/m^2 UVB. Greater UVB-induced DNA damage is seen in AD and EN mice exposed to UVB at night versus the day, while mice fed during the day (ED and MD) have greater UVB-induced DNA damage when exposed to UVB during the day than during the night. Values represent mean ± SEM, N = 15. Statistical significance was determined by Welch's t-test, shown as *p < 0.05, **p < 0.01 and ***p < 0.001. (B) Skin *Xpa* expression is dampened under RF, as detected by qPCR. Values represent mean ± SEM (N = 3-5). Two-way ANOVA shows significance for RF group (p < 0.0001), ZT time (p < 0.002), and RF group X ZT time (p < 0.02). Tukey's post hoc test shows AD has greater *Xpa* expression compared to EN (p < 0.0001), and MD (p < 0.0001), while AD is not significantly different than ED (p < 0.056). (C) A schematic summarizing the effects of abnormal feeding time on diurnal rhythms UVB-induced DNA damage, expression of oxidative-reductive metabolic enzymes, DNA synthesis and *Per2* expression. See also Figure 2.2.1, Figure 2.2.5, Figure 2.2.9, Figure 2.2.10.

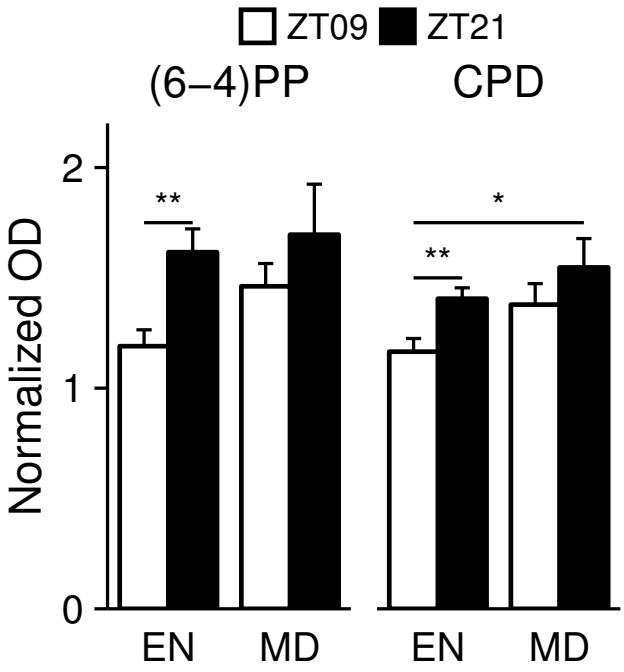

Figure 2.2.11. Skin sensitivity to UVB-induced DNA damage. Quantification of (6-4)PP (left) and CPD (right) photoproducts after UVB exposure at ZT9 and ZT21 presented as Mean ± SEM (N = 8 or 9). Statistical significance was determined by Welch's t-test, shown as *p < 0.05, **p < 0.01, *** P < 0.001.

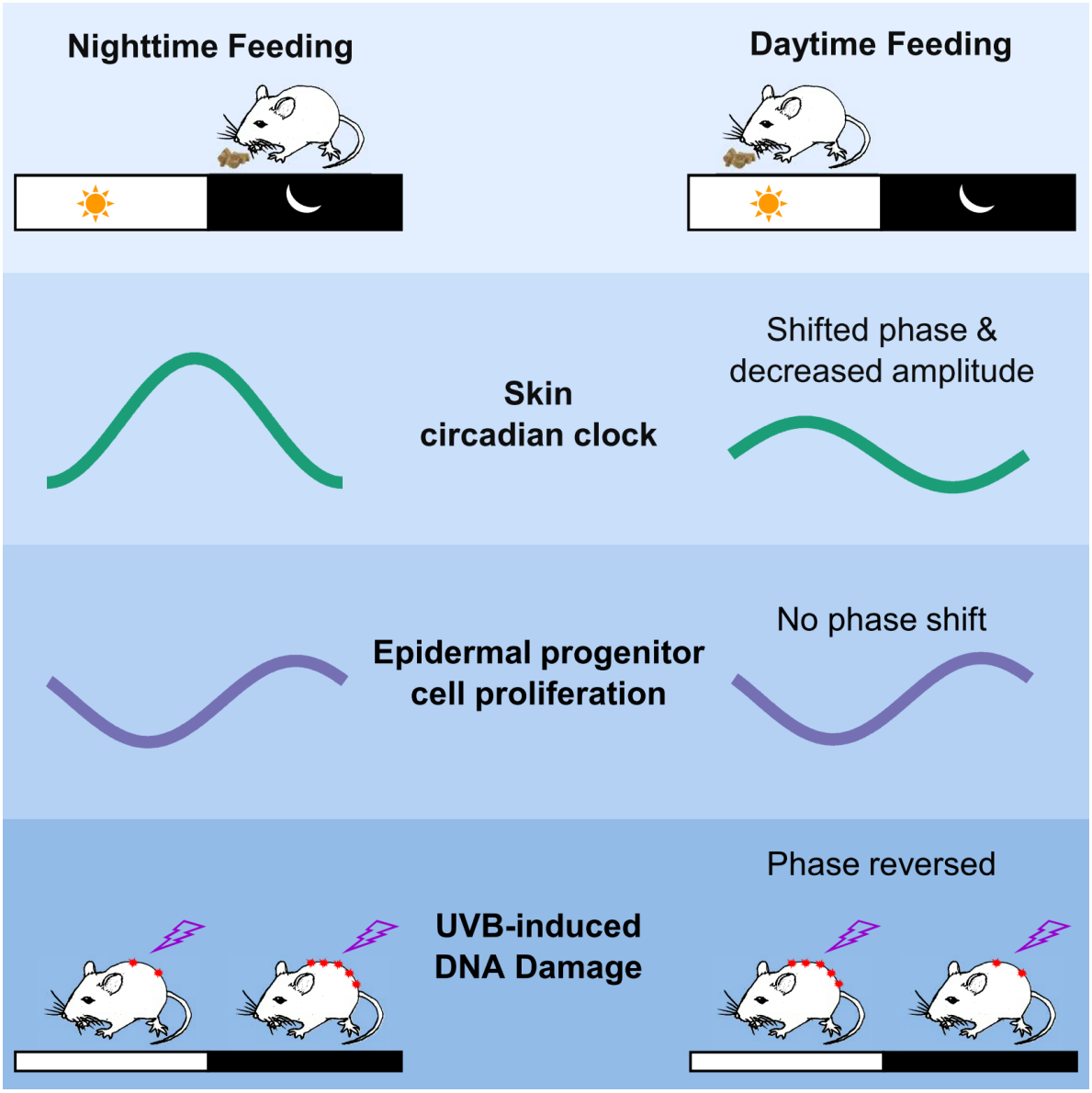

Figure 2.2.12. Graphical Summary: Daytime-restricted feeding shifts and dampens the skin circadian clock, dampens epidermal cell proliferation, and reverses the phase of UVB-induced DNA damage.

Table 2.2.1. Sequencing statistics for the RNA-seq.
Total reads, Mapped reads, percentage of reads mapped, non-rRNA reads, percentage of non-rRNA reads, reliable reads, and percentage of reliable reads, are indicated for RNA samples pooled from 2-4 mice per feeding group per time point as described in Methods section.

Table 2.2.1 Sequencing statistics for the RNA-seq

RNA sample		Total Reads	Mapped Reads	%	Non-rRNA Reads	%	Reliable Reads	%
MD	ZT0	53934987	50643956	94	47875030	89	43454124	81
	ZT4	58618045	51192377	87	46375200	79	39297337	67
	ZT8	63095384	52605332	83	44237151	70	33523750	53
	ZT12	56033285	48428388	86	41704141	74	31765142	57
	ZT16	59424906	52510958	88	46931580	79	38730040	65
	ZT20	63122441	53106139	84	47206698	75	37788061	60
	ZT24	58323439	51335336	88	47077225	81	41369525	71
	ZT28	53651833	47565580	89	42935111	80	36460548	68
ED	ZT0	64957607	56059860	86	50466217	78	39190824	60
	ZT4	62418183	52613181	84	45941760	74	33349770	53
	ZT8	63370673	53849389	85	46528867	73	32703877	52
	ZT12	54188794	45372675	84	38868470	72	24701796	46
	ZT16	59349340	47636646	80	41538428	70	27724999	47
	ZT20	61264210	53695629	88	48245655	79	35409323	58
	ZT24	53567052	45183962	84	39463990	74	25666218	48
	ZT28	64239934	52534714	82	45068850	70	32519483	51
EN	ZT0	63221149	50308240	80	43408139	69	28029993	44
	ZT4	60383655	51373718	85	43435890	72	30094176	50
	ZT8	62202466	53013034	85	46199673	74	31599842	51
	ZT12	67298866	54763533	81	46887244	70	29689138	44
	ZT16	59099629	47049092	80	39259630	66	25012802	42
	ZT20	99558258	80519391	81	69863732	70	47313932	48
	ZT24	59662234	47684780	80	40522893	68	27120354	45
	ZT28	63367104	50211616	79	41047157	65	26751407	42

Chapter 3: Circadian control of IMQ-induced Interferon-sensitive gene expression in the skin

Abstract

Recent studies suggest that the circadian clock in the skin modulates the skin's ability to protect against invading pathogens. The Toll-like receptor 7 (TLR7) pathway, in coordination with the IFN pathway, mediates the expression of key genes, termed "Interferon-sensitive genes" (ISGs) which are important for host defense against pathogens and cancer. We investigated the potential role of the circadian clock in regulating the ISG response in the mouse back skin after treatment with the synthetic TLR7 agonist, Imiquimod (IMQ). We found that after 1 day of IMQ treatment, ISGs including key ISG *Irf7* were more highly induced after treatment during the day than night, and this diurnal rhythmicity was eliminated following high dose or repeated IMQ doses. In support of the idea that the core clock controls the ISG response, altering core clock gene expression by daytime-restricted feeding reverses the diurnal rhythm of the IMQ-induced ISG expression in the skin. While we show several epidermal cell subsets that upregulate ISG/*Irf7* mRNA after IMQ, it is the immune cells, and not KCs, that upregulate *Irf7* in a diurnal manner after IMQ. Furthermore, we found that IMQ-induced nuclear localization of IRF7 and phosphorylated IRF7 (p-IRF7) is time-of-day dependent in epidermal monocytes and T cells, but not in dendritic cells (DCs) and keratinocytes (KCs). Mice lacking *Bmal1* systemically (*Bmal1* KOs) had exacerbated and arrhythmic *ISG/Irf7* expression after low dose IMQ, demonstrating that the core circadian clock protein regulates the initial diurnal ISG response. Interestingly, KC- and DC- specific *Bmal1* deletion had no effect on ISG induction, supporting the idea that the circadian clock in other cell types or the systemic IFN response is responsible for the rhythmic ISG expression in skin after IMQ. These results suggest a new role for BMAL1 as a negative

regulator of the IFN response. Since the IFN response is essential for the anti-viral and anti-tumor effects of TLR activation, these findings are consistent with the time-of-day dependent variability in the ability to fight viral and bacterial pathogens and tumor initiation.

3.1 Introduction

Recent evidence suggests that the circadian clock may regulate the ability of mice to defend against viral infections. Edgar and colleagues (2016) found that mice infected with herpes or influenza A viruses during the daytime had greater infection rates and mortality compared to mice infected at night and that *Bmal1* deletion resulted in exacerbated infection (Edgar et al., 2016). Another study showed that disruption of circadian function by jet lag or *Bmal1* deletion led to increased acute viral bronchiolitis after Sendai virus and influenza A viral infection (Ehlers et al., 2017). The mechanism by which the circadian clock, especially the core clock protein, *Bmal1,* contributes to host defense response against viruses is currently unknown. Using the viral single-stranded RNA mimic IMQ, we investigate the effect of the time-of-day and *Bmal1* deletion on the IMQ-induced expression of anti-viral genes (also known as interferon-sensitive genes (ISGs); ISGs are expressed after infection and help to mitigate the spread of infection through a variety of mechanisms.

IMQ as an immunomodulator

IMQ was developed as a topical treatment for the management of human papilloma virus-associated anogenital warts; however, it is currently approved for the treatment of actinic keratosis, superficial basal cell carcinomas, and many other off-label indications. It is currently

understood to be a specific ligand for TLR7/8 and is known to cause immune activation through the induction of anti-viral proteins, and pro-inflammatory cytokines and chemokines. The early response to topically applied IMQ involves the activation of epidermal Langerhan's cells (LCs) which when activated, leave the epidermis and travel to the skin draining lymph nodes to recruit other immune cell subtypes to the skin including activated monocytes, neutrophils and T cells. When IMQ is applied repetitively to mice, it induces robust inflammation, typified by symptoms including epidermal hyperproliferation, parakaratosis (nuclei retained in the stratum corneum), acanthosis (thickening of the epidermis), and formation of Munro microabcesses, similar to human psoriasis.

The TLR7 pathway

TLRs are pattern recognition receptors involved in sensing foreign antigens, most commonly from viral, microbial, or chemical agonists (such as IMQ), as well as self-DNA secreted by dying or infected cells. TLR activation by ligand binding leads to the production of proinflammatory cytokines necessary for initiating innate and enhancing adaptive inflammatory cascades. In this way, IMQ recruits cytotoxic effector cells that facilitate both the eradication of pathogens and the killing of tumor cells (Akira & Takeda, 2004). On the molecular level, IMQ induces immune activation by binding to the TLR7 receptors (and TLR8 in humans) located on the endosomes within a variety of different cell types including macrophages (Hemmi et al., 2002), keratinocytes (KCs) (Yin et al., 2014), mast cells (Heib et al., 2007), monocytes (Hornung et al., 2002), classic dendritic cells (cDCs) (Wohn et al., 2013), and plasmacytoid dendritic cells (pDCs) (Domizio et al., 2009). Upon IMQ binding, TLR7 dimerizes and the adaptor molecule MyD88 is recruited, leading to a signaling cascade involving PI3K (Guiducci et al., 2008),

IRAK1-, IKKα-, and/or LMP1-mediated phosphorylation of IRF7 and nuclear translocation. Once in the nucleus, IRF7 binds to interferon responsive elements (IREs) within promoters of type I IFN-encoding genes and other ISGs, including members of the RIG-I signaling pathway. While the majority of TLR-mediated ISG expression is induced as a result of secreted type I IFNs acting through the IFNAR1/2/JAK/STAT pathway (described below), recent studies show that ISGs can be induced by TLR7 activation independent of type I IFNs (Ning et al., 2005; Di Domizio et al., 2009; Li et al., 2017; Bego et al., 2012).

The IFNAR/JAK/STAT pathway

Type I IFNs (IFN-α IFN-β), produced through the activation of TLR7/8 signaling, bind to IFN receptors (composed of a heterodimer of IFNAR1/2) on the cell membrane of various cell types. Dimerization and activation of IFNAR1/2 activates two Janus family kinases, TYK2 and JAK1, resulting in recruitment of STAT1-STAT2 heterodimers that migrate into the nucleus and complex with IRF9 to form the ISGF3 complex, which binds to promoters of ISGs and activates their transcription. One key transcription factor induced by this pathway is IRF7, which acts in a feed-forward manner by facilitating the production of more ISGs and type I IFNs through the MyD88-dependant pathway. The increased levels of type I IFNs lead to a further increase in ISG expression through the IFN/JAK/STAT pathway. The end result of this feed forward loop is robust expression of ISGs which activates the immune system to kill off cancer, bacteria and viruses.

Cell type-specificity of IFN/ISG response

PDCs express TLR7 and they are able to produce large amounts of type I IFNs (10–100 times more than any other cell type) in the context of TLR activation and viral infections (Di Domizio et al., 2009). While pDCs are considered to be the main producers of type I IFNs after TLR7/8 activation in isolated cells, pDCs are extremely rare or absent in the skin, and it is unknown if other cell types contribute to type I IFN secretion in the skin following IMQ treatment. Other cell types including conventional DCs (cDCs) (Mancuso et al., 2008), myeloid-derived macrophages (Renn et al., 2006) and keratinocytes (KCs) (Zhang et al., 2016) secrete type I IFN under certain conditions. In most cell types, IRF7 is lowly expressed under homeostasis, while pDCs express IRF7 constitutively, making them capable of responding robustly to TLR7 activation. When most cells get activated by TLR stimulation, IRF7 expression is induced and plays a functional role in the feed-forward loop of the TLR7/IFN/ISG pathway (Durbin et al., 1998; Sato et al., 1998).

The goal of this study was to investigate the regulatory role of the circadian clock in the TLR7-induced immune response in the murine skin. We found that the early IMQ-induced ISG response is diurnal in Wt mouse skin, but becomes arrhythmic after repeated 1% IMQ treatments. We show that by shifting the core circadian clock by subjecting mice to daytime-restricted feeding schedules, we alter the rhythm of the IMQ-induced ISG response in the skin. To identify which cells are responsible for the diurnal IMQ-induced ISG response, we performed cell sorting and single cell sequencing. We found that epidermal immune cells (which are comprised of LCs, T cells, and monocytes) upregulate *Irf7* gene expression more potently after 1% IMQ during the day versus night. Using Imagestream flow cytometry, we found greater nuclear translocation of total and phosphorylated IRF7 (p-IRF7) in T cells and monocytes after

daytime 1% IMQ treatment. We show that systemic *Bmal1* deletion, but not KC- or DC- specific *Bmal1* deletion, results in exacerbated ISG expression in the skin after IMQ and elevated serum IFN-β levels. The results of this study suggest that BMAL1 is a negative regulator of ISG gene expression in immune cells, including, but not limited to, epidermal T cells and monocytes.

3.2 Results

3.2.1 Diurnal timing of treatment modulates transcriptional response to single and repetitive doses of IMQ

We first examined the circadian control of the IMQ-induced gene response in the skin. Mice were treated with 1% IMQ every 6 hours for 1 day, or daily at the same time of day for 5 consecutive days (Figure 3.2.1), and whole back skin was collected for microarray analysis. After filtering and normalization as described in Methods, we had 20,746 non-redundant exons. After 1 day of 1% IMQ, 890 genes were significantly different than control (Cyber T-test $P<0.05$). After 5 days of repeated IMQ doses, 8,831 genes were significantly altered (Cyber T-test $P<0.01$). We identified gene ontology categories that were enriched after 1 day or 5 consecutive days of 1% IMQ treatment using Gene Set Enrichment Analysis (GSEA) (False-Discovery Rate (FDR) Q-value of < 0.25; Nominal (NOM) P-value ≤ 0.05) (Table 3.2.1). After 1 day of 1% IMQ treatment, hallmark pathways associated with the immune system such as: allograft rejection, IL-6 Jak/Stat3 signaling, inflammatory response (including IFN-α/IFN-γ response), KRAS signaling-downregulated, and IL-2/Stat5 signaling were enriched (Table 3.2.1). Pathways enriched after 5 days of consecutive 1% IMQ treatment included protein secretion,

G2M checkpoint, and metabolic pathways such as cholesterol homeostasis and fatty acid metabolism (Table 3.2.1).

We further examined pathways that were enriched differentially depending on the time of day. Under homeostasis, genes downregulated by KRAS signaling were enriched during the night as opposed to the day, along with genes associated with pancreatic beta cells and spermatogenesis (Table 3.2.2). Conversely, pathways enriched under homeostasis during the day compared to the night include MYC and E2F targets, G2M checkpoint, and oxidative metabolism, among others (Table 3.2.2).

Out of 890 genes significantly altered after 1 day of IMQ, 249 genes were upregulated 1.2 fold or greater after IMQ during the day versus night, and only 28 genes were upregulated 1.2 fold or greater after IMQ during the night versus day. There were relatively few pathways enriched after 1 day of 1% IMQ applied at night compared to the day, which was similar to what was observed under homeostasis (Table 3.2.3). Conversely, many unique pathways were enriched after 1 day of daytime versus nighttime IMQ that were not identified as daytime enriched under homeostasis; these pathways included: adipogenesis, IFN-α response, IFN-γ response, fatty acid metabolism, and myogenesis (Table 3.2.3 and Figure 3.2.1B). After 5 days of repetitive IMQ treatment during the night, enriched pathways were associated with cell cycle regulation, E2F and Myc targets, TNFα signaling via NF-ϰB, and IL-2/STAT5 signaling (Table 3.2.4). On the other hand, there were few enriched pathways after 5 days of daytime IMQ treatment, and these pathways were associated with metabolic function including ox. phos., myogenesis, fatty acid metabolism and adipogenesis (Table 3.2.4). These findings suggest that the circadian clock gates

the early and late phases of IMQ-induced gene expression changes in a distinct manner, with greater IFN responses after 1 dose of 1% IMQ during the day, whereas by 5 days of 1% IMQ, cell cycle pathways are enriched after nighttime treatment.

Considering that many of IMQ's main immunogenic effects are facilitated through induction of IFN-α and IFN-γ pathways, we further investigated the genes associated with the IFN-α and IFN-γ response which were enriched after 1 dose of 1% IMQ during the daytime as opposed to nighttime IMQ (Figure 3.2.1B). The expression of 203 ISGs (identified in the MySig Database) illustrate that many ISGs lack expression under homeostasis but are induced after 1 day of 1% IMQ, while by 5 days of 1% IMQ, different groups of ISGs are induced (Figure 3.2.1C). Out of 203 total ISGs, we found 53 of these genes were upregulated on average by 1.2 fold after 1 day of 1% IMQ (Figure 3.2.1D). Expression of *Irf7*, a master regulator of ISG transcription, was confirmed by qPCR (Figure 3.2.1E). To more specifically define the biological processes that these genes could be regulating, we performed gene ontology analysis using the online database DAVID (Sherman et al., 2007). The majority of these genes were associated with anti-viral activities; examples include genes encoding anti-viral proteins known to inhibit replication of RNA viruses such as *Isg15, Ifit1, Mx1 and Oas1a*, as well as negative feedback factors that dampen pro-inflammatory responses, such as *Irgm1*, *Usp18*, and *Trim30*. These results suggest that the IMQ-induced ISG pathway exhibits a diurnal propensity for transcriptional activation with greater reactivity occurring during the day (ZT01, ZT07) compared to the night (ZT13, ZT19). As none of the IFN-α, -β, or -γ family member transcripts were induced after 1 day of 1% IMQ, we investigated whether IFNs were expressed earlier during the course of treatment by collecting mouse back skin and performing microarray and qPCR to measure gene expression at

0, 1, 2, 4, 6, and 24 hours after a single dose of 1% IMQ. We identified 3,108 genes significantly altered after IMQ (unpaired Cyber T-test, $P<0.05$). The majority of genes affected by IMQ were downregulated (2,206 genes); most of these genes encoded for proteins involved in cell cycle regulation. 902 genes were upregulated at 6 hours-post IMQ. While the 53 ISGs induced by IMQ consistently increased after treatment (Figure 3.2.1F), there was no induction of mRNA transcripts for IFN-α, -β, or -γ family members (data not shown). This time course also illustrated that *Irf7* expression overlapped well with the expression of other ISGs, thus we used it as a proxy of ISG expression throughout the study (Figure 3.2.1F and G).

3.2.2 Feeding schedules alter the type I IFN response after 1 day of 1% IMQ

In the RNA sequencing experiment described in Chapter 2, we identified genes in the skin that were affected by time-restricted feeding schedules. We found that the rhythmic expression of many immune-associated genes were shifted or perturbed after daytime-restricted food availability (Wang et al., 2017). Some of these genes encode for proteins that mediate the IMQ-induced ISG response, including *Tlr7, Ifnar2*, and *Irf7*. Therefore, we sought to determine if shifting the core clock by executing time-restricted feeding schedules could affect the rhythm of the ISG response. We performed time-restricted feeding with EN (early night), MD (mid-day) feeding groups (described in Chapter 2 and 6) and AD (ad libitum), as control, and treated these mice topically with 1% IMQ during the day (ZT07) or night (ZT19) for 1 day (Figure 3.2.2A). Whole skin RNA was pooled and subject to microarray as described in the Methods section. We confirmed that the core clock machinery was shifted in MD compared to AD by measuring expression of core clock gene, *Dbp*, in the whole back skin (Figure 3.2.2B). Consistent with our

previous findings (Figure 3.2.1), after 1 day of 1% IMQ, AD mice exhibited a diurnal rhythm of ISG induction after IMQ, with 1.2 fold or greater ISG expression after IMQ application during the day versus night (Figure 3.2.2C and D). Interestingly, MD mice exhibited the opposite, with greater ISG induction after IMQ treatment during the night (Figure 3.2.2C and D). QPCR for *Irf7* expression in individual mice (Figure 3.2.2E) confirmed the result from the microarray (Figure 3.2.2D).

3.2.3 IMQ upregulates ISG expression in keratinocytes, Langerhan's cells, T cells and monocytes within the epidermis

To hone in on exactly which epidermal cell types express the ISG signature after IMQ, we performed single cell sequencing using the Chromium 10x system on epidermal cells isolated from adult male mice under homeostasis or after treatment with 1% IMQ for 6 hours. We used the R package, Seurat, to cluster cells based on their gene expression profiles as described in the Methods section to produce t-distributed stochastic neighbor embedding (TSNE) plots (Figure 3.2.3). We annotated cell clusters manually based on previous studies, mainly the study by Jooste et al (2016). Differentially expressed genes from each identified population are shown in Table 3.2.5. Under homeostasis, LCs and T cells comprised 2.5% and 1.84%, respectively, of all live cells in the adult mouse epidermis. After 6 hours of 1% IMQ, the proportion of LCs and T cells out of live cells increased to 4.63% and 2.62%, respectively. There was a small group of immune cells that we defined as monocytes after searching the top 50 genes that were differentially expressed in this group compared to other epidermal populations in the Immgen database (Heng et al., 2008), and observing that most of these genes were most highly expressed in monocytes

followed by macrophages, and only lowly expressed in B cells, T cells, DCs, and innate lymphoid cells (Figure 3.2.3B). Genes enriched in the monocyte population included myeloid-associated genes (*Ly6e, CD14, Lyz2* (encodes LysM), M2 polarization markers (*CD16, Adgre1* (F4/80)), phagolysosomes/oxidative burst (*Coro1a, Ctss, Cyba, Cybb, fcgr3*) and chemokines (*Ccl6 (MCP-3)*, *Ccl4* (MIP-1β), *Ccl3* (MIP-1α), *Ccl9* (data not shown). The monocyte population comprised 0.5% of live epidermal cells under homeostasis, and increased to 1.2% after IMQ (Figure 3.2.3A and C).

Under homeostasis, there were very few *Irf7* positive cells (Figure 3.2.3C). After 6 hours of 1% IMQ, we identified 4 main cell populations that expressed the ISG signature after IMQ: a small group of KCs, LCs, T cells, and monocytes (Figure 3.2.3C). The small group of monocytes expressed *Irf7* most robustly out of all cell types. Forty percent of monocytes expressed *Irf7* under homeostasis, and 82% expressed *Irf7* after IMQ (Figure 3.2.3D). Out of the differentiated KC (*Krt1*$^{+}$) population, 4% of cells express *Irf7* under homeostasis, and this increases to 15% after IMQ. The same trend was observed in the basal KC population (*Col17a1*$^{+}$) (Figure 3.2.3D). In T cells (*Cd3g*$^{+}$), and LCs (*Cd207*$^{+}$), 7% and 4% of cells expressed *Irf7* under homeostasis, and this increased to 36% and 17%, respectively, after IMQ (Figure 3.2.3D).

To confirm that our diurnal ISG results were due to gene expression changes, and not diurnal differences in recruitment of monocytes (the main IRF7-expressing cells) to the epidermis, we performed flow cytometry on dissociated epidermis collected after 1 day of IMQ during the day or the night (Figure 3.2.3E). There were no differences in the proportion of T cell or DCs after

IMQ. There was a trend towards increased monocytes after IMQ at both times of the day, with no time-of-day dependent difference (Figure 3.2.3E).

Taken together, these results show that multiple cell types within the skin respond to IMQ by upregulating ISG expression. Immune cells, mainly monocytes and T cells, are the most potent responders, followed by LCs and a small population of KCs. Since there is no significant diurnal difference in monocyte recruitment to the epidermis after IMQ, our results suggest that the diurnal rhythm in the IMQ-induced ISG response is regulated on the transcriptional level.

3.2.4 Epidermal immune cells have diurnal induction of *Irf7* expression after 1 day of IMQ, while KCs do not

We wanted to determine the extent to which cells from different compartments of the mouse skin are induced to express ISGs after IMQ. Thus we FACS-sorted whole ears, and dorsal dermis and epidermis from mice treated with 1% IMQ for 1 day at ZT09, and performed qPCR to determine the level of *Irf7* expression in purified cell populations. We found that out of the cell types analyzed, $CD11c^+$ DCs from the whole ears were induced to express *Irf7* most robustly, approximately 3.5 fold more than KCs. In other immune cells (e.g. T cells and MPs), *Irf7* was induced 2 fold more than in KCs (Figure 3.2.4A). In the epidermis, we see that total immune cells in the epidermis upregulate *Irf7* 3 fold more than KCs ($CD45^-$); while in the dermis, the opposite is seen – there was approximately 3 fold greater ISG expression in dermal non-immune cells (e.g. fibroblasts, muscle, and/or endothelial cells) compared to dermal immune cells (Figure 3.2.4A).

Next, we sought to determine the contribution of different cell subsets to the diurnal ISG signature observed in the whole skin after IMQ treatment at different times of the day (Figure 3.2.1 and 3.2.2). We FACS-sorted back skin epidermal cells from mice treated with 1% IMQ for 1 day during the day (ZT0) or night (ZT12), and measured *Irf7* gene expression in total immune cells ($CD45^+$) and KCs ($CD49f^+CD45^-Lin^-$) (gating strategy shown in Figure 3.2.4B). We found that epidermal immune cells expressed 2 fold greater *Irf7* mRNA after 1 day of 1% IMQ compared to KCs (Figure 3.2.4C and D). Importantly, *Irf7* induction was diurnal in immune cells, with approximately 2-3 fold more *Irf7* expressed after IMQ treatment during the day compared to treatment at night. This trend is consistent with the rhythm of *Irf7* expression in whole skin after 1 day of 1% IMQ treatment shown in Figure 3.2.1D.

3.2.5 1% IMQ induces total and phosphorylated IRF7 protein nuclear translocation in epidermal cell subsets

In order to activate ISG expression, IRF7 must be phosphorylated and translocate into the nucleus. We wanted to see whether IRF7 nuclear translocation differed depending on the time of day in which IMQ is applied. To achieve this, we treated mice topically with 1% IMQ during the day or night, collected epidermal cells 6 hours or 24 hours later, stained the cells as described in the Methods section, and analyzed the samples on the ImageStream®X Mark II Imaging Flow Cytometer (Figure 3.2.5A and B). This assay combines high-resolution digital imaging with flow cytometry, allowing for quantitative image-based analysis of nuclear translocation in both rare and plentiful subpopulations (George et al., 2006). We measured nuclear similarity index (a

measurement of the relative nuclear localization of a given marker) of total IRF7 and phosphorylated IRF7 (p-IRF7) using IDEAS® software. We found that monocytes ($CD11c^{-}$ $CD3e^{-}CD45^{+}$) had greater nuclear localization of total and p-IRF7 after 6 hours of 1% IMQ during the day versus night. By 1 day of treatment, p-IRF7 nuclear localization was significantly increased at both treatment times (Figure 3.2.5C). Similar results are seen in T cells (Figure 3.2.5D). Nuclear localization of total IRF7 and p-IRF7 was increased in KCs after 1 day of 1% IMQ with greater nuclear localization of total IRF7 seen after daytime IMQ treatment (Figure 3.2.5E). In DCs, there was no significant increase in nuclear localization of total or p-IRF7 after 6 hours of IMQ, but by 24 hours, nuclear localization of total and p-IRF7 was significantly increased with no time-of-day dependence (Figure 3.2.5F).

In summary, nuclear localization of total and p-IRF7 is increased after 1% IMQ in epidermal KCs, T cells, and monocytes, and is time-of-day dependent in T cells and monocytes.

3.2.6 Systemic deletion of *Bmal1* exacerbates early skin IMQ-induced ISG expression

To explore whether the circadian clock plays a direct role in the rhythmic ISG expression in response to IMQ, and to confirm whether the diurnal differences in ISG induction are recapitulated with shorter treatment durations, we performed experiments in which we treated Wt and *Bmal1* KO mice topically with 1% IMQ for 6 hours or 1 day, and collected dorsal skin during the day (ZT07) or night (ZT19). We found that Wt mice had greater induction of *Irf7* after 6 hours of IMQ during the night, as opposed to the day (Figure 3.2.6A), which contrasts what we observed after 1 day of treatment (Figure 3.2.1D). Interestingly, 6 hours of 5% IMQ treatment

(the typical published dosage) yielded the same induction of *Irf7* regardless of the time of day in which treatment occurred (data not shown). These findings suggest that in Wt mice, the ISG response elicited by 1% IMQ is dynamic and time-of-day dependent, with greater initial response after IMQ at night; however, by 24 hours (the time at which *Irf7* expression peaks after IMQ), there is higher expression during the day (Figure 3.2.6A).

Bmal1 KO mice had exacerbated *Irf7* gene expression in their skin compared to Wt after 6 hours of IMQ treatment during the day, while there was no difference between the genotypes after 6 hours of IMQ at night. By 1 day of 1% IMQ treatment, however, *Bmal1* KO mice had significantly greater *Irf7* expression compared to Wt after IMQ during the day and night (Figure 3.2.6A). In epidermis isolated from Wt mice, *Irf7* mRNA was induced by approximately 4 fold after 1 day of 1% IMQ, with no diurnal difference (Figure 3.2.6B). Interestingly, *Irf7* mRNA in the epidermis of *Bmal1* KO mice was exacerbated almost 4 fold after IMQ compared to Wt (Figure 3.2.6B).

To determine whether systemic type I IFN activity was affected by *Bmal1* deletion, we measured serum IFN-β levels in Wt and *Bmal1* KO mice treated topically with IMQ for 2 hours or 6 hours during the day or night. We found no significant IFN-β induction after 2 hours of 1% IMQ in either genotype, while IFN-β levels were significantly upregulated after 6 hours of daytime IMQ in the *Bmal1* KO mice compared to control, and after 6 hours of nighttime IMQ in the *Bmal1* KO mice compared to Wt mice and control (Figure 3.2.6C). We also measured serum IFN-β levels after 24 hours of 1% IMQ and found that, while IFN-β levels were similar to control levels in the Wt, *Bmal1* KO mice had elevated IFN-β levels at this time point (Figure 3.2.6D). These results

suggest that the exacerbated ISG response we see in the skin of *Bmal1* KO mice is not unique to the skin, and may be a consequence of systemic IFN activity.

We further asked whether the exacerbated IMQ-induced ISG response we see in the skin and epidermis of *Bmal1* KO mice could be due to differences in cellular composition. Since our single cell sequencing data on dissociated epidermis shows that the population expressing *Irf7* most robustly, the monocytes, increase in frequency after 1% IMQ (Figure 3.2.3), we performed flow cytometry on isolated epidermis and measured the proportion of these cells and other immune cell populations out of all live cells after 6 hours of 1% IMQ treatment during the day or night in Wt and *Bmal1* KO mice (Figure 3.2.6E). We found no significant change in the percentage of all immune cells, T cells, DCs or monocytes in Wt compared to *Bmal1* KOs under homeostasis or after 1% IMQ (Figure 3.2.6E).

In summary, these results illustrate that deletion of *Bmal1* on the systemic level results in an exacerbated IMQ-induced ISG response in the skin and isolated epidermis, as well elevated levels of systemic IFN-β.

3.2.7 KC- or DC-cell type specific *Bmal1* deletion is not sufficient to cause exacerbated IMQ-induced ISG expression

Previous experiments have shown that both KCs and DCs in the epidermis upregulate ISG expression in response to IMQ (Figure 3.2.3, Figure 3.2.4); thus we wanted to determine whether *Bmal1* deletion in one of these two cell types could recapitulate the exacerbated IMQ-induced

ISG expression we observed in the systemic *Bmal1* KO mice. We generated KC-specific knockout mice and DC-specific *Bmal1* KO mice, as described in the Methods section. Genotypes were determined by PCR using Cre and *Bmal1* Flox primers as described in the Methods section. To confirm that we did indeed delete the circadian clock in the respective cell types specifically, we performed FACS sorting on $CD49f^{+}CD45^{-}Lin^{-}$ cells (KCs) and $CD11c^{+}$ DCs collected from the epidermis of these mice during the day (ZT07) and night (ZT19) and confirmed downregulation of *Dbp*, a representative clock-controlled gene (Figure 3.2.7A and B). We next treated the KC- and DC- *Bmal1* KO mice with 1% IMQ for 1 day during the day (ZT07) or night (ZT19) and collected the whole skin for qPCR analysis. We found that the expression of *Irf7*, a proxy of the ISG response, was lower in DC-specific *Bmal1* KO mice after daytime IMQ compared to Wt, while no other differences in IMQ-induced *Irf7* expression were observed in the different genotypes (Figure 3.2.7C). To see whether there were any differences in IMQ-induced *Irf7* expression in KCs specifically from the KC-specific *Bmal1* KO mice, which might have been masked by the robust ISG expression in the immune cells, we FACS-sorted $CD49^{+}$ KCs (and $CD45^{+}$ immune cells as a control) from the epidermis after 1 day of 1% IMQ treatment and measured *Irf7* by qPCR. We found that there was no difference in IMQ-induced *Irf7* gene expression in either the immune cells or KCs isolated from the epidermis of KC-specific *Bmal1* KO compared to Wt (Figure 3.2.7 D and E).

3.3 Discussion

In the skin, topical IMQ treatment induces the production of ISG gene products which facilitate pro-inflammatory and anti-viral immunity and help steer the host innate and adaptive immune

system to defend against pathogens and cancers. Our results show that the acute ISG response in the skin elicited by IMQ is time-of-day dependent, while chronic treatment results in ablation of rhythmic ISG expression (Figure 3.2.1). We observe greater ISG induction after 6 hours of IMQ treatment during the nighttime compared to the daytime, while by 24 hours after treatment, ISGs are higher during the day compared to the night. This temporally dynamic rhythm in ISG expression is supported by a previous study in which systemic injection of IFN produced greater IFN-induced myelosupressive activity during the night at early (12 hour) time points, whereas by 24-48 hours after injection, myelosupressive activity was greater during the day (Koren et al., 1993). Moreover, IFN administration during the day yielded higher anti-tumor activity than IFN administered at night, highlighting the functional significance of circadian IFN activity (Koren et al., 1993). We are the first to show that shifting the clock by daytime-restricted feeding reverses the phase in ISG pathway activation in the skin, suggesting that meal-timing may be a previously unknown modulator of skin immune responses (Figure 3.2.2).

Studies using intranasal influenza A, Herpesvirus, and Sendai virus infections illustrate that mice are more sensitive to viral infection during the day as opposed to the night, and mice lacking the core clock have greater infection titers and mortality (Edgar et al., 2015; Ehlers et al., 2017). Furthermore, there is evidence that BMAL1 inhibits replication of respiratory syncytial virus and parainfluenza virus type 3 viruses in a cell-intrinsic manner (Majumdar et al., 2017). All of these studies suggest that the circadian clock protein BMAL1 must be a positive regulator of anti-viral responses, while our results suggest the opposite, in that *Bmal1* deletion exacerbates the expression of ISGs. While these studies using viral models are complicated by ongoing viral replication, activation of multiple PRRs, and in the case of in vivo models, both innate and

adaptive immune activity, our study focuses on the early transcriptional response to activation of a single specific TLR. The potential mechanisms responsible for the increased susceptibility to viral infections seen in *Bmal1* KO mice are discussed further in Chapter 5.

In order to fully understand the impact of the circadian phase on TLR/IFN pathway activation in the skin, it is necessary to determine what cell types mediate this response. We found that the immune cells of the epidermis express 2-3 fold as much *Irf7* mRNA as KCs and do so in a diurnal fashion, matching what is seen in the whole skin (Figure 3.2.4). To the best of our knowledge, this study is the first to identify a population of activated monocytes within the mouse epidermis under homeostasis; as this population turns on ISG expression most robustly out of all cell types studied (Figure 3.2.3), it is temping to consider that these cells may be key initiators of defense responses in the skin. In epidermal T cells and monocytes, p-IRF7 exhibits greater nuclear localization after 6 hours of 1% IMQ during the day as opposed to night (Figure 3.2.5), supporting the idea that IRF7 regulates the activation of ISG expression by becoming phosphorylated and translocating into the nucleus in a time-of-day dependent manner early on after IMQ treatment in these cell types.

We found that systemic *Bmal1* KO mice have an exacerbated IMQ-induced ISG response in skin and isolated epidermis, while *Bmal1* deletion specifically in KC or DC had no effect (Figure 3.2.7). Considering the *Bmal1* KO phenotype is observed in isolated epidermis, and that the composition of immune cells within the epidermis does not exhibit diurnal changes after 1 dose of 1% IMQ (Figure 3.2.3E), we propose that BMAL1 acts as a negative transcriptional regulator of ISGs in a cell-type specific manner, mainly in epidermal monocytes and T cells and not KCs

or DCs. This hypothesis does not exclude the possibility that BMAL1 also regulates the ISG response in other immune cells; considering that we observe exacerbated serum IFN-β levels after IMQ in *Bmal1* KO mice, it is likely that BMAL1 plays this regulatory role in other immune populations throughout the body as well. Future experiments will focus on exploring which genes involved in the TLR7/IFN pathway are bound by BMAL1 after IMQ treatment (discussed in Chapter 5).

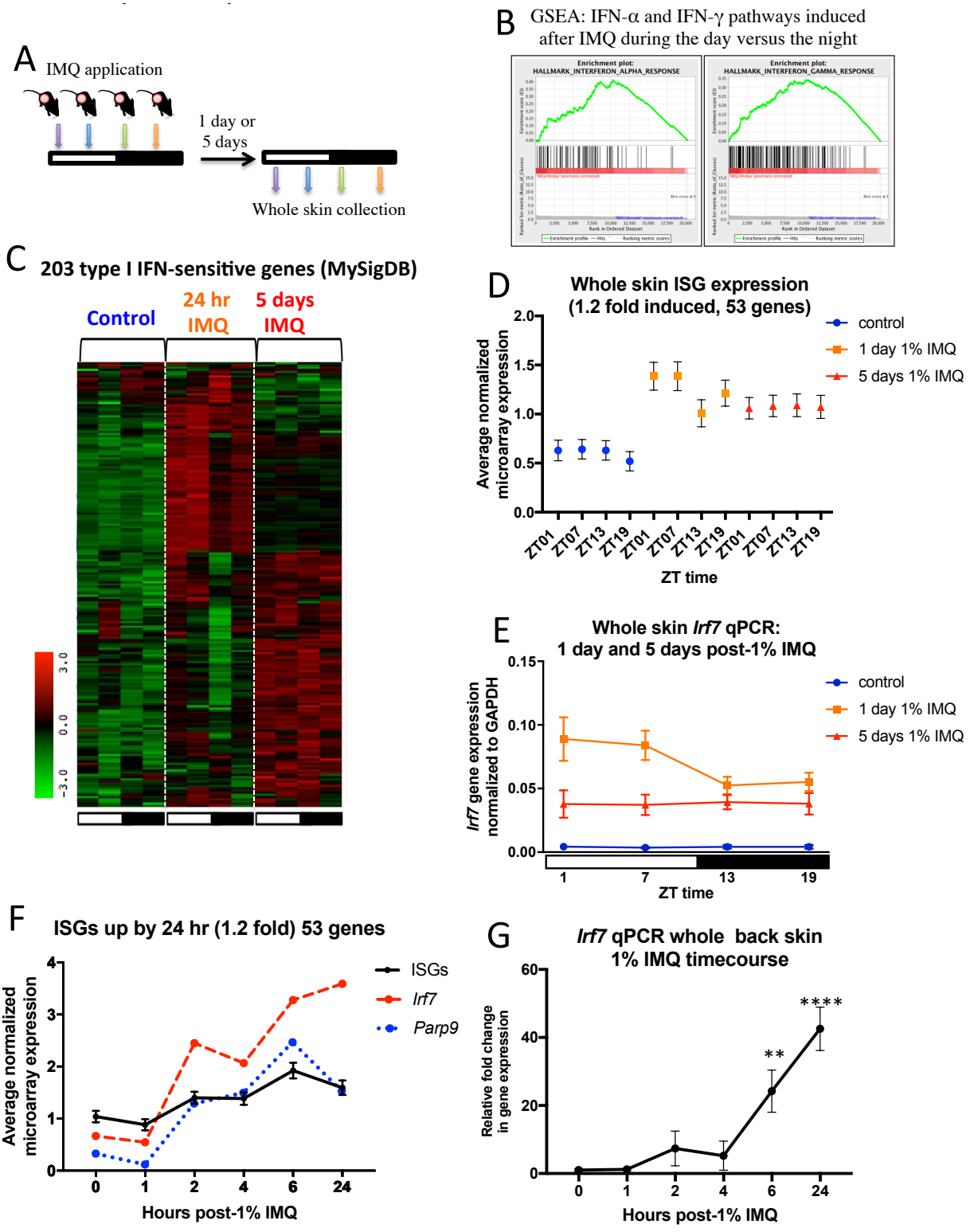

Figure 3.2.1 Diurnal timing of 1% IMQ treatment results in rhythmic interferon-sensitive gene (ISG) expression in the skin after 1 day but not 5 days of 1% IMQ treatment. (A) IMQ treatment protocol. Groups of mice were shaved and treated topically with 1% IMQ (colored arrows) at 6 hour time points throughout the day/night cycle (indicated by white and back bars)

for either 1 day, or each day for 5 consecutive days, and collected 1 day after the last treatment and pooled samples were subject to microarray analysis. **(B)** Gene set enrichment plot for IFN-α and IFN-γ hallmark pathways shows a significant enrichment of these pathways after 1 day of 1% IMQ during the day versus night. **(C)** Heatmap of 203 ISGs (from MysigDB) from the samples collected in (A). Green = lowly expressed genes and red = highly expressed genes. **(D)** Average normalized whole skin microarray expression of ISGs induced by 1.2 fold or more after IMQ, under homeostasis (blue), 1 day 1% IMQ (orange), and 5 day 1% IMQ (red). One-way ANOVA, control $P = 0.001$, 1 day 1% IMQ $P < 0.0001$, 5 day IMQ $P = 0.56$ **(E)** Expression of *Irf7* is diurnal after 1 day of 1% IMQ but not 5 days of IMQ. Whole skin RNA samples from the experiment described in A were subject to qPCR for *Irf7*. Two-way ANOVA shows significant difference between treatments ($p < 0.0001$). Tukey's post-hoc test showed significance between control versus 1% IMQ 1 day ($p < 0.0001$), control vs 5 days 1% IMQ ($P = 0.0002$) and 1% IMQ 1 day versus 1% IMQ 5 days ($p < 0.0001$). One-way ANOVA for control $P = 0.99$, for 1 day 1% IMQ $P = 0.07$, for 5 day 1% IMQ $P = 0.65$. Data represents mean + SEM of N = 5-7 mice per group. **(F)** Time course of ISG expression after IMQ treatment. Mice were treated with 1% IMQ and whole skin was collected after 0, 1, 2, 4, 6 or 24 hours. Average whole skin microarray expression of ISGs identified in (C). Average ISG expression (black line, error bars represent SEM), and the expression of representative ISGs, *Irf7* (red dashed line), and *Parp9* (blue dotted line), is shown. **(G)** *Irf7* qPCR validation on individual whole skin samples pooled and subject to microarray in (C). Data presented as Mean ± SEM for N = 5-7. Statistical significance was determined by one-way ANOVA ($P < 0.0001$) and for Tukey's post-hoc test, *$P < 0.05$, **$P < 0.001$, ***$P < 0.0001$, ****$P < 0.0001$.

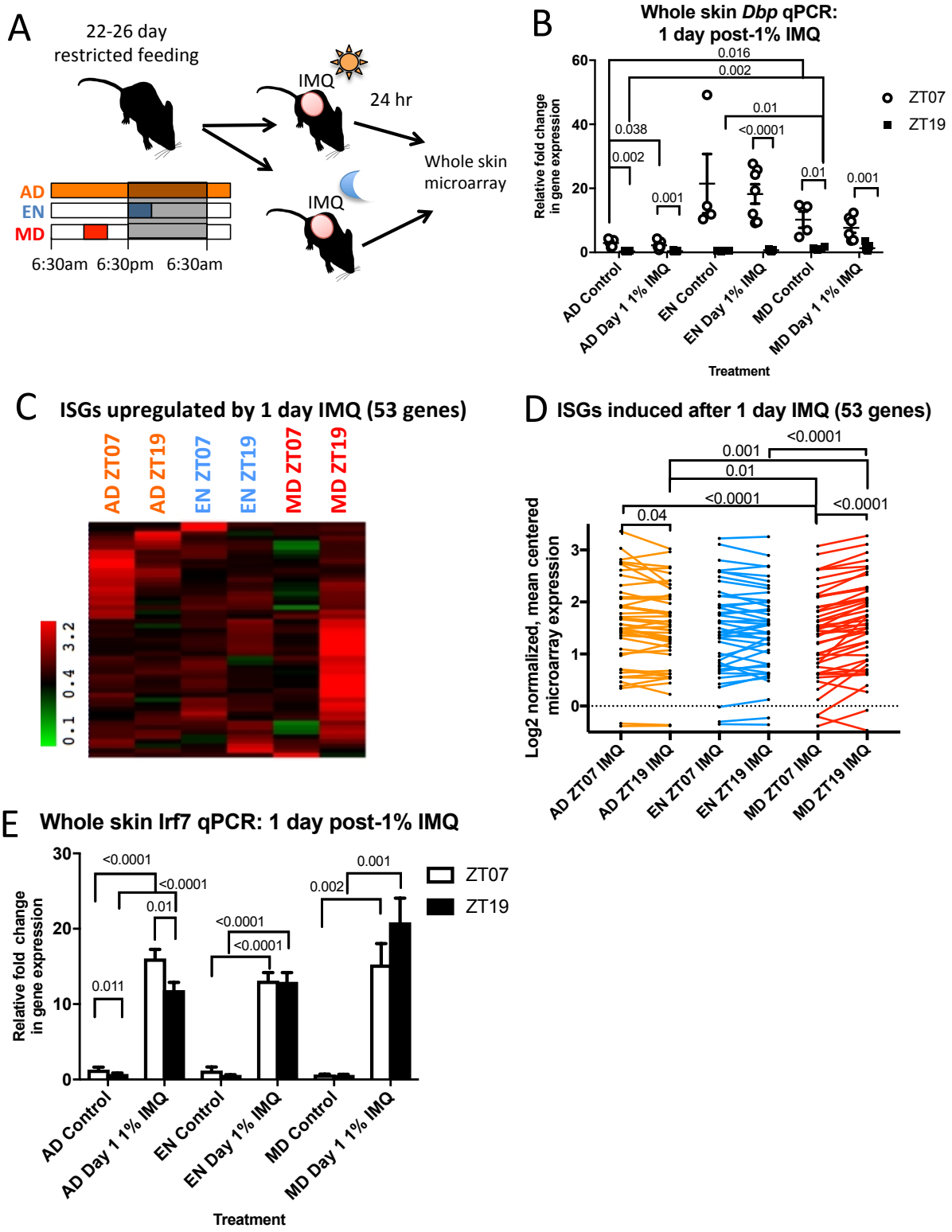

Figure 3.2.2 Shifting the clock by daytime-restricted feeding alters the diurnal rhythm of IMQ-induced ISG expression. **(A)** Restricted feeding followed by IMQ treatment protocol. Mice were subjected to RF feeding schedules as described in the Methods section, and then shaved and treated with 1% IMQ during the day (ZT07) or night (ZT19) for 1 day and then

whole skin was collected for qPCR and pooled for microarray analysis. **(B)** Daytime RF alters the expression of core clock gene, *Dbp*, in the skin as measured by qPCR. **(C)** Heatmap of 203 ISGs (from MysigDB) from the samples collected in (A). Green = lowly expressed genes and red = highly expressed genes. **(D)** Whole skin microarray expression of ISGs identified by MySig database, upregulated by 1.2 fold or more after 1 day of treatment, is plotted. Data points indicate individual ISG expression values after IMQ, with average ISG expression per group indicated by colored lines (AD = orange, EN = blue, MD = red). Statistical significance was measured by one-way ANOVA and significant p-values are shown. **(E)** Rhythmic *Irf7* expression after IMQ is altered in MD compared to AD. Whole skin RNA samples from (A) were subject to qPCR for *Irf7* (N = 5-14 per group). Data presented as Mean ± SEM. Statistical significance was determined by Student's paired t-test, and significant P-values are shown.

A TSNE Control

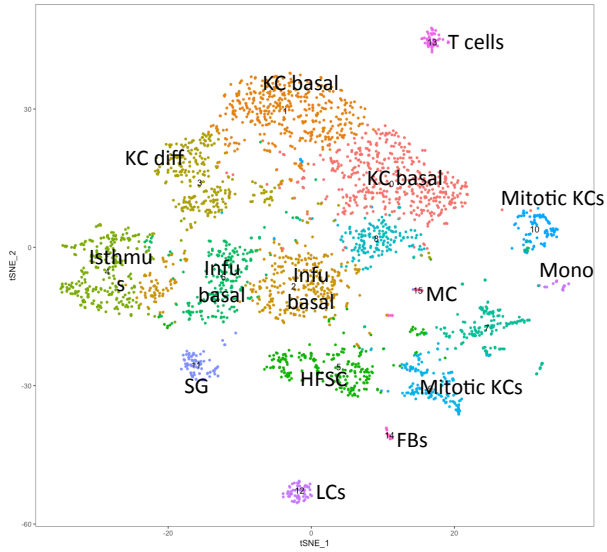

TSNE 6 hour 1% IMQ

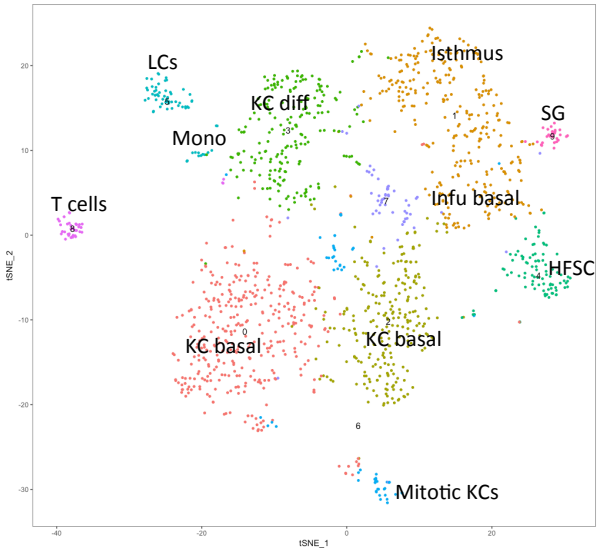

B Means-normalized expression value

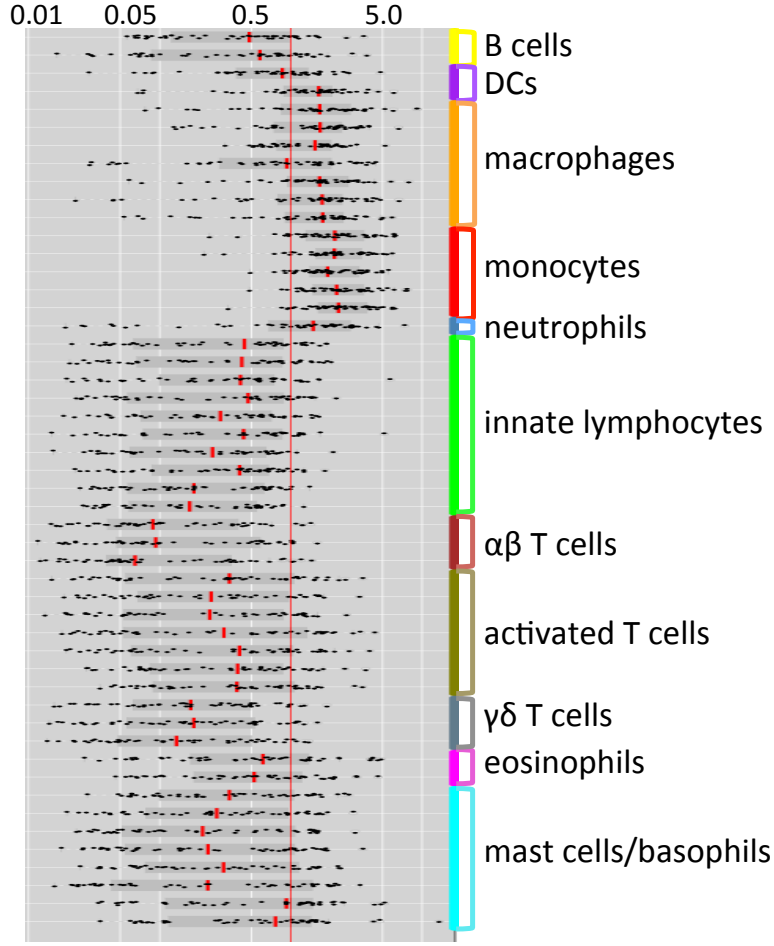

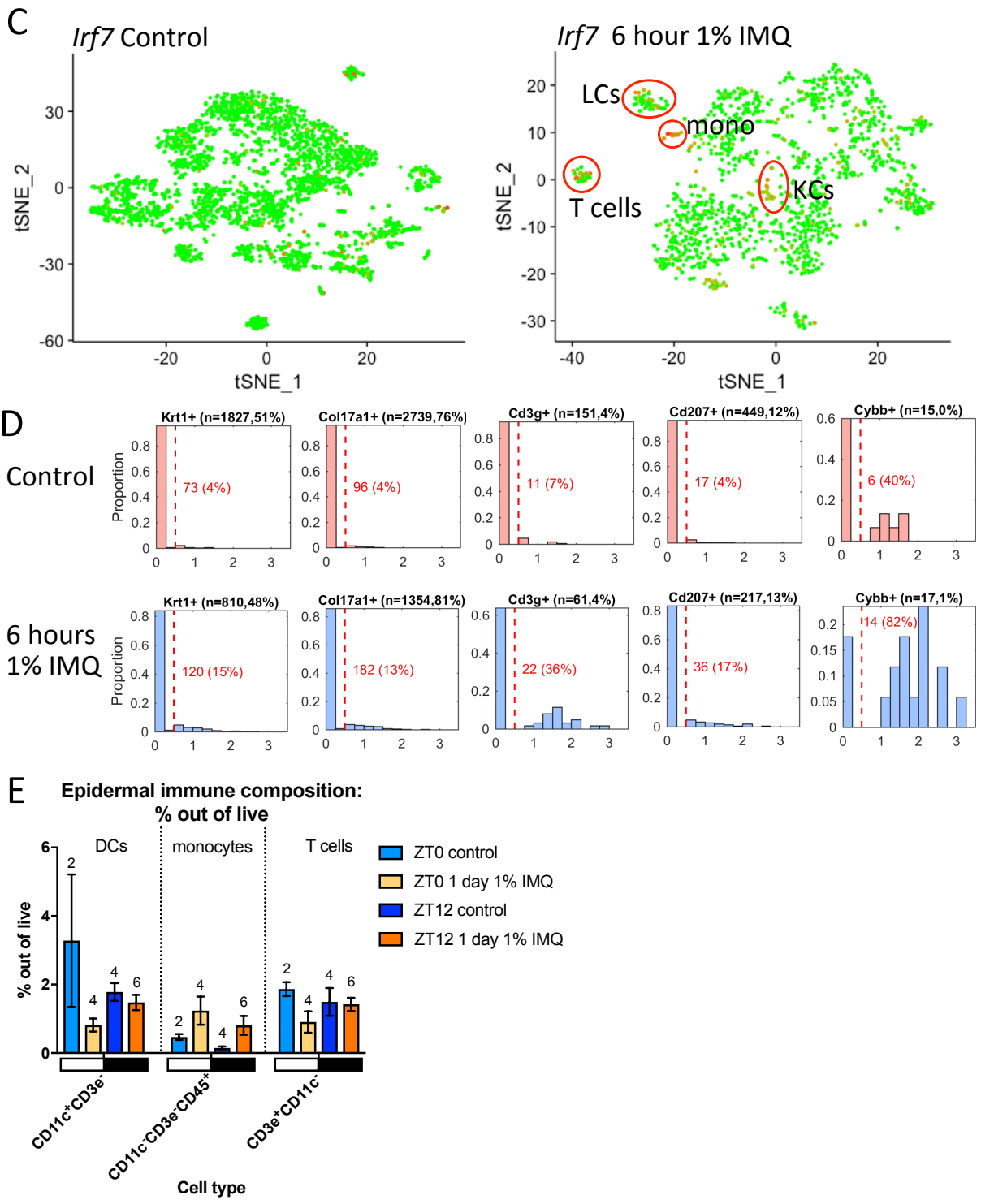

Figure 3.2.3 IMQ upregulates ISG expression in keratinocytes, Langerhan's cells, T cells and monocytes within the epidermis. (A) TSNE data plots from single cell seq on mouse epidermal cells isolated from adult male mice untreated (left) or treated with 1% IMQ for 6 hours (right). differentiated keratinocytes (KC diff), basal keratinocytes (KC basal), basal infundibulum (Infu basal), mitotic keratinocytes (mitotic KCs), hair follicle stem cells (HFSC), Langerhan's cells (LCs), sebaceous gland (SG), melanocytes (MCs), fibroblasts (FBs),

monocytes (mono). **(B)** Output from the Immgen database (Heng et al., 2008), which was used to identify the monocyte cell population within the epidermis. W-plot showing gene expression of the top 50 genes differentially expressed in the monocyte population in various immune cell populations from the Immgen database. Cell types are on the y-axis and means-normalized gene expression is on the x-axis. **(C)** ISG expression represented by *Irf7* expression. Under control conditions, few cells express *Irf7*, while after 6 hours of 1% IMQ, populations of LCs, T cells, TCs, and mono are induced to express the *Irf7*. Green = no expression, red = intensity of expression. **(D)** Multiple epidermal cell types are induced to express *Irf7* mRNA after IMQ. Proportion of differentiated KCs (*Krt1*$^{+}$), basal KCs (*Col17a1*$^{+}$), T cells (*Cd3g*$^{+}$), LCs (*Cd207*$^{+}$) and monocytes (*Cybb*$^{+}$) expressing *Irf7* in in control (untreated) and 6 hour 1% IMQ treated adult mouse epidermal cells analyzed by single cell seq. Relative *Irf7* expression is on the x-axis and proportion of cells expressing *Irf7* mRNA out of each population is on the y-axis. Number of cells analyzed and percent of each population out of total cells analyzed is listed above each graph. Number and percent of cells expressing *Irf7* out of each population is listed on each graph in red. **(E)** Flow cytometry quantification of immune cell populations within the epidermis of Wt male mice treated with 1% IMQ for 24 hours during the day or night (indicated by white and back bars). There were no significant changes across treatments or time points. Data represents mean ± SEM of N = 2-6 Wt male mice per group. The numbers above each group indicate the number of samples analyzed. Statistical significance was determined by Student's paired t-test.

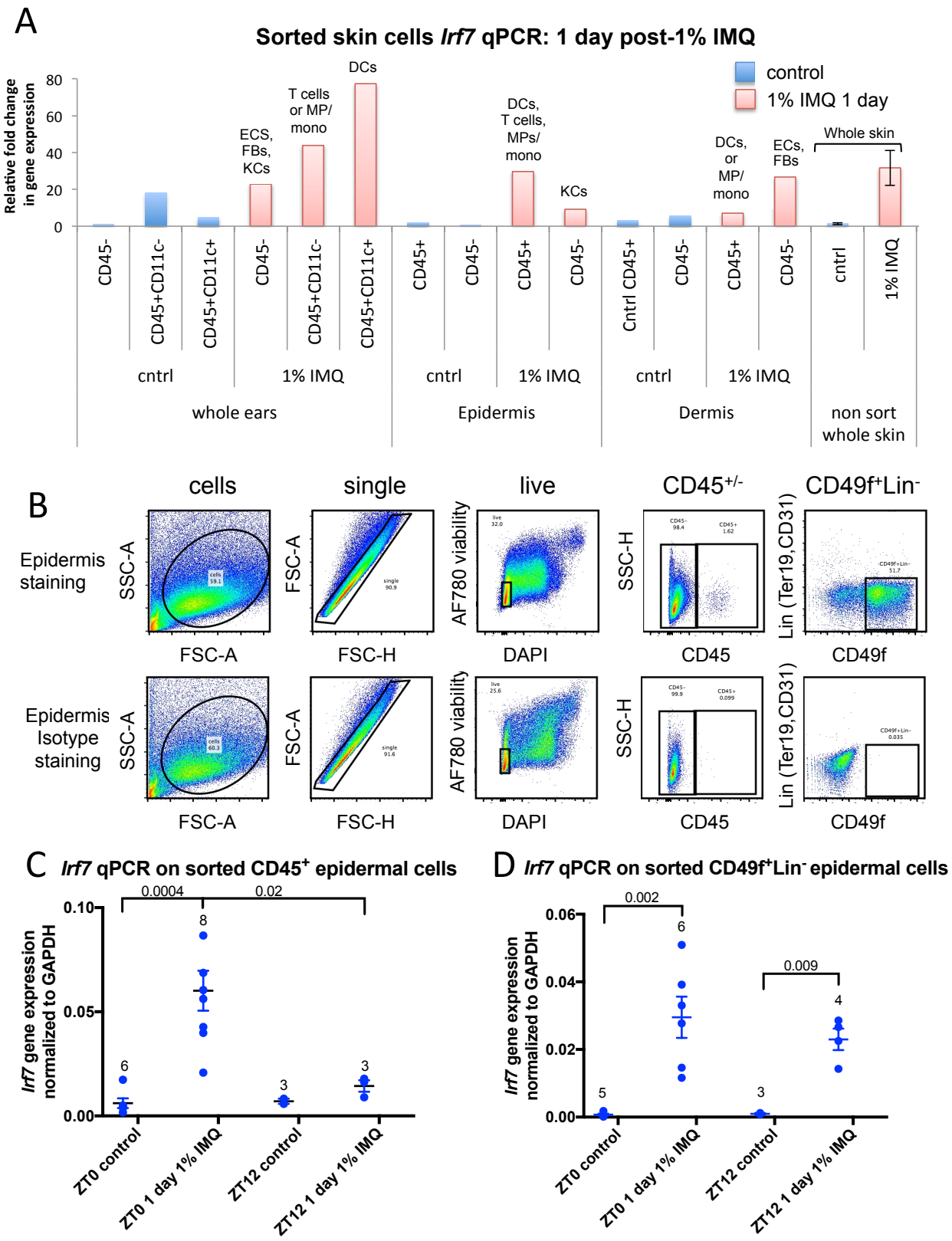

Figure 3.2.4 *Irf7* upregulation is diurnal in epidermal immune cells, but not KCs. Mice were treated with 1% IMQ during the day (ZT0) or night (ZT12) and after 1 day, epidermal cell suspensions were collected, stained, and FACS sorted. **(A)** $CD11c^+$ DCs in the skin are induced

to express *Irf7* most potently out of all skin cell types. Mice were treated with 1% IMQ for 1 day at ZT07 on their backs and ears and whole ear skin, isolated back epidermis, and dermis were FACS sorted for $CD45^-$, $CD45^+$, and/or $CD11c^+$ and qPCR for *Irf7* was performed. Each bar represents cells pooled from 3-5 mice. Whole skin RNA was included as control (N = 3). **(B)** Gating strategy used to FACS sorting epidermal $CD45^+$ immune cells and $CD49f^+CD45^-Lin^-$ KCs. **(C)** QPCR for *Irf7* was performed on FACS-sorted immune cells ($CD45^+$) and **(D)** Keratinocytes ($CD49f^+CD45^-Lin^-$). **(B-D)** Data represents mean ± SEM of N = 3-8 Wt male mice per group. The numbers above each group indicate the number of samples analyzed. Statistical significance was determined by Student's paired t-test and significant P-values are shown.

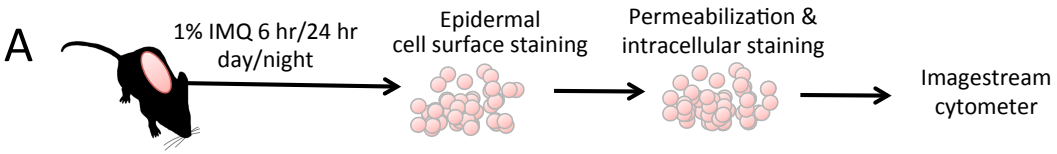
A
1% IMQ 6 hr/24 hr day/night
Epidermal cell surface staining
Permeabilization & intracellular staining
Imagestream cytometer

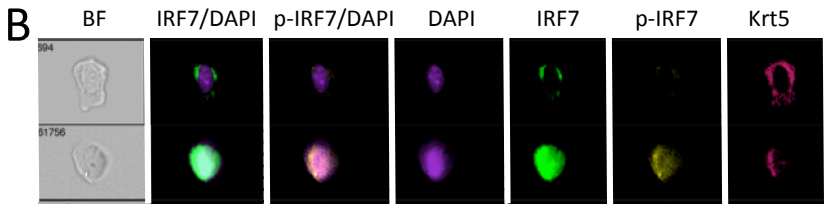
B
BF
IRF7/DAPI
p-IRF7/DAPI
DAPI
IRF7
p-IRF7
Krt5

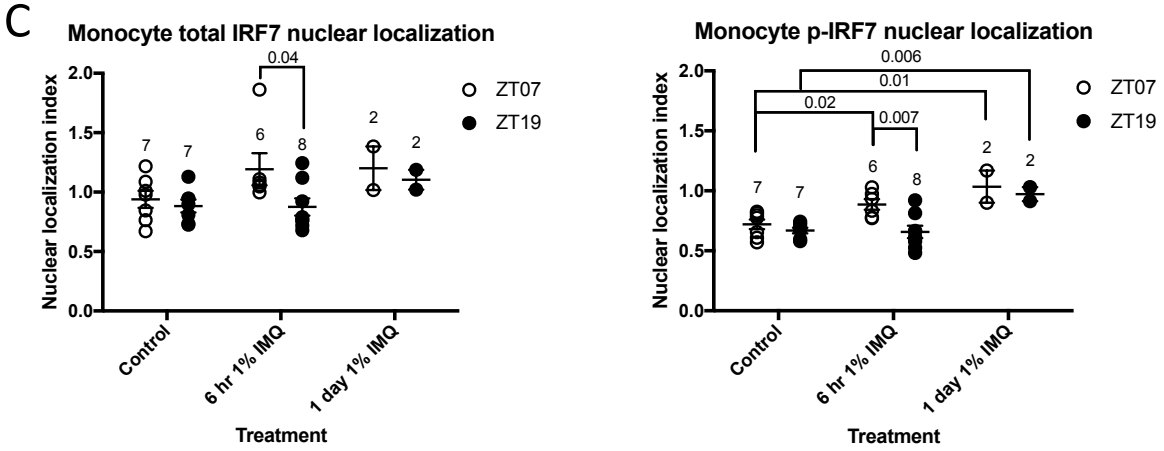
C
Monocyte total IRF7 nuclear localization
Nuclear localization index
ZT07
ZT19
0.04
Control
6 hr 1% IMQ
1 day 1% IMQ
Treatment
Monocyte p-IRF7 nuclear localization
0.006
0.01
0.02
0.007

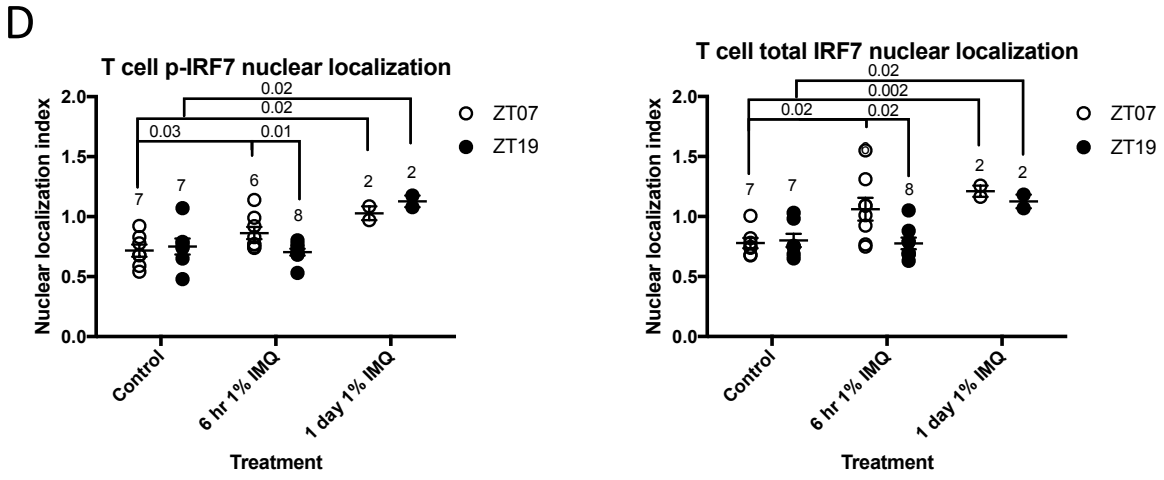
D
T cell p-IRF7 nuclear localization
0.02
0.02
0.03
0.01
T cell total IRF7 nuclear localization
0.02
0.002
0.02
0.02

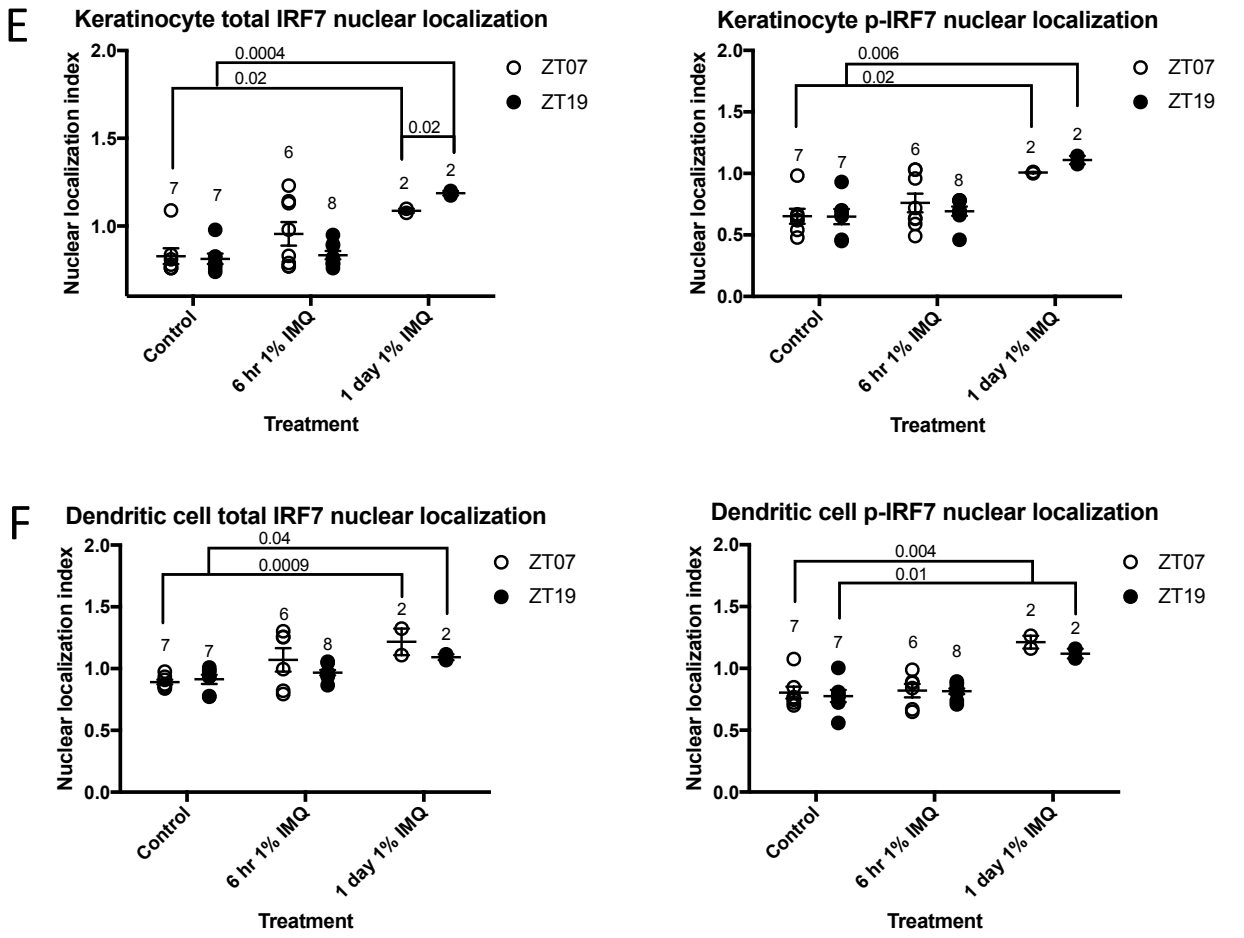

Figure 3.2.5 IMQ induced nuclear localization of total and phosphorylated IRF7 is diurnal in epidermal T cells and monocytes. (A) Experimental design. Male Wt mice were treated with 1% IMQ for 6 hours or 24 hours during the day (ZT07) or night (ZT19) and back epidermis was dissociated, stained for cell surface markers and intracellular IRF7 and p-IRF7, and analyzed on the Imagestream Flow Cytometer as described in the Methods section. Nuclear localization index was calculated using IDEAS software. **(B)** Example images (60x) taken during ImageStream fluorescence imaging, showing a keratinocyte with no p-IRF7 nuclear localization (top) and one with p-IRF7 nuclear localization (bottom). **(C)** Average nuclear translocation index for total IRF7 (left) and p-IRF7 (right) in monocytes ($CD45^+CD11c^-CD3e^-$). **(D)** Average nuclear translocation index for total IRF7 (left) and p-IRF7 (right) in T cells ($CD45^+$ $CD3e^+CD11c^-$). **(E)** Average nuclear translocation index for total IRF7 (left) and p-IRF7 (right) in KCs ($CD45^-$). **(F)** Average nuclear translocation index for total IRF7 (left) and p-IRF7 (right) in DCs ($CD45^+CD11c^+CD3e^-$). **(A-F)** Each data point represents 1 mouse and Mean ± SEM is indicated. Statistical significance was determined by Student's paired t-test and significant or near-significant P-values are shown.

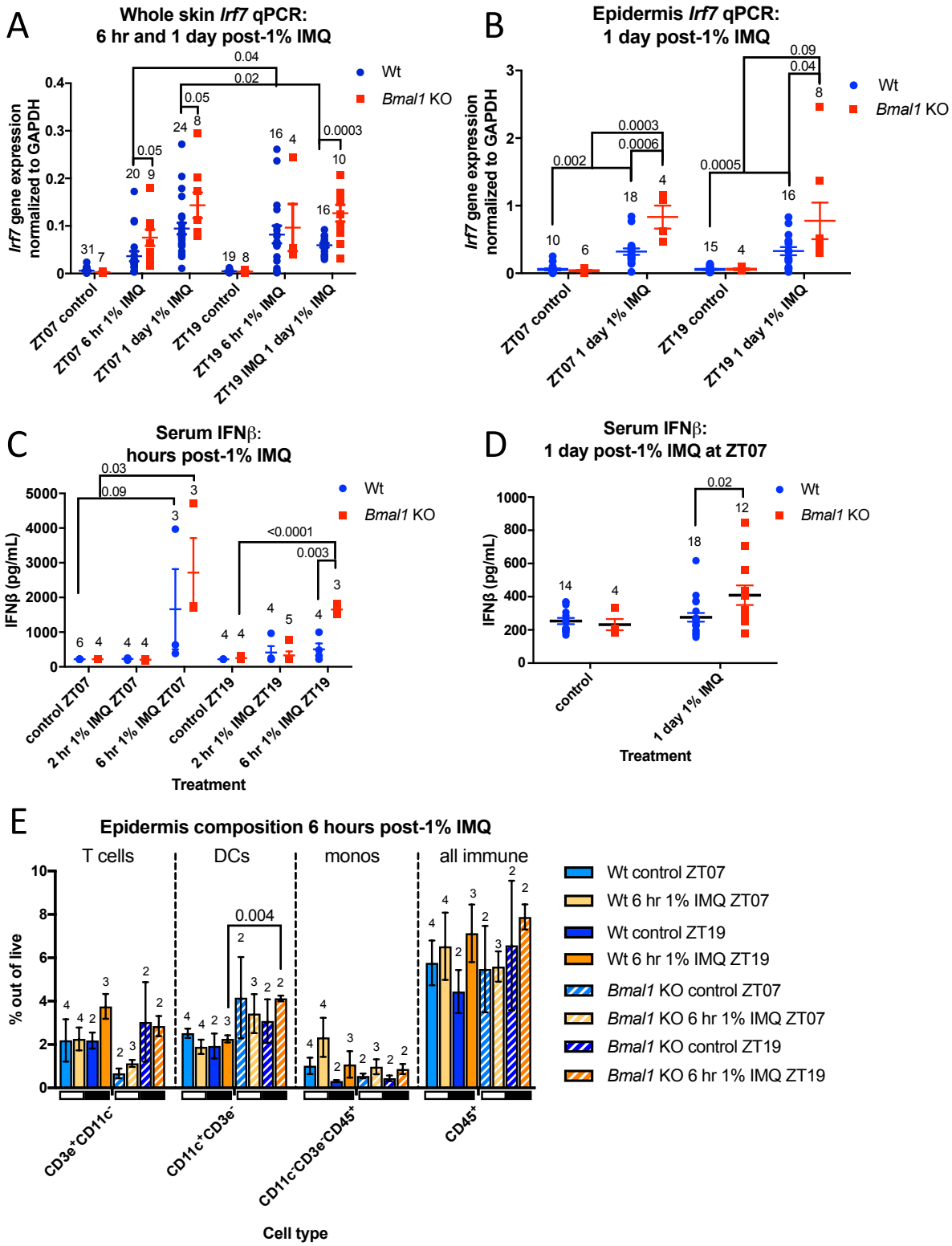

Figure 3.2.6 Systemic *Bmal1* deletion results in exacerbated IMQ-induced serum IFN-β and ISG expression in the skin. (A) *Irf7* mRNA is exacerbated in the skin of *Bmal1* KO mice after 1% IMQ. *Irf7* expression measured by qPCR on whole back skin RNA from Wt (blue, N = 17-30) and *Bmal1* KO (red, N = 6-9) mice untreated, or treated with 1% IMQ during the day (ZT07)

or night (ZT19) for 6 hours or 1 day. **(B)** *Irf7* mRNA is exacerbated in the epidermis of *Bmal1* KO mice after 1% IMQ. *Irf7* expression measured by qPCR on isolated back epidermis RNA from Wt (blue, N = 10-18) and *Bmal1* KO (red, N = 4-8) untreated mice or mice treated with 1% IMQ during the day (ZT07) or night (ZT19) for 1 day. **(C)** *Bmal1* KO mice have higher serum IFN-β compared to Wt after 6 hours of 1% IMQ at night. Mice were untreated, or treated with 1% IMQ for 2 hours or 6 hours during the day (ZT07) or night (ZT19) and serum was collected and IFN-β ELISA was performed. **(D)** *Bmal1* KO mice have exacerbated serum IFN-β after 1 day of 1% IMQ compared to Wt. Male Wt and *Bmal1* KO mice were untreated or treated with 1% IMQ during the day (ZT07) similar to (C), and serum was collected after 1 day. **(E)** Flow cytometry quantification of immune cell populations within the epidermis in Wt and *Bmal1* KO mice treated with 1% IMQ for 6 hours during the day or night (indicated by white and back bars). There were no significant changes across treatments, time points or genotypes (One-way ANOVA). **(A-D)** Each data point represents 1 mouse and Mean ± SEM is indicated. The numbers above each group indicate the number of samples analyzed. Statistical significance was determined by Student's paired t-test and significant or near-significant P-values are shown.

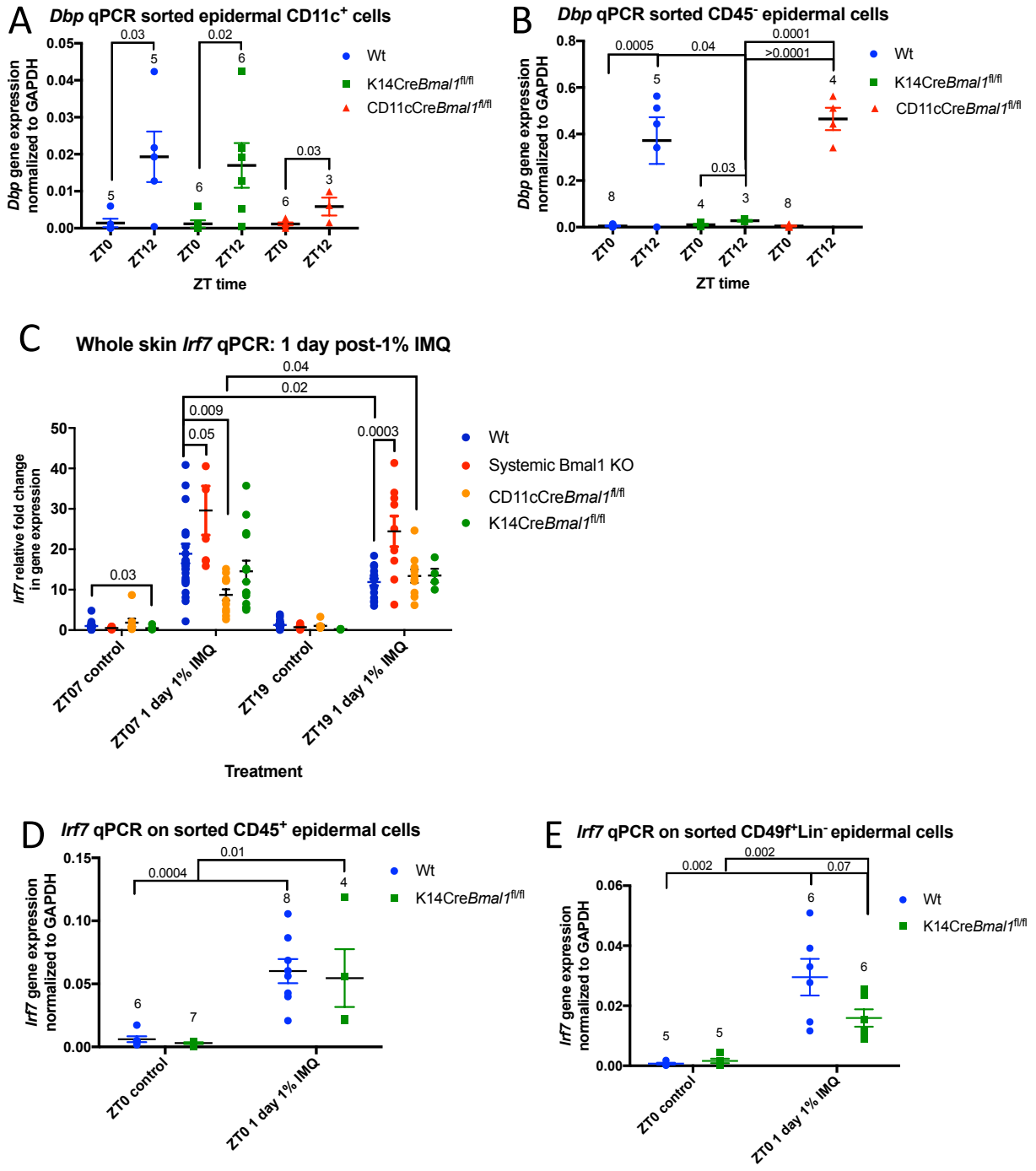

Figure 3.2.7 Keratinocyte (KC)- or dendritic cell (DC)-specific *Bmal1* deletion is not sufficient to cause exacerbated ISG expression after 1 day of 1% IMQ. Efficient disruption in clock-controlled gene expression in cell type-specific *Bmal1* KO epidermal cells. **(A-B)** QPCR for clock-controlled gene, *Dbp*, was performed on sorted CD45$^-$ epidermal cells (mainly KCs), **(A)** and CD11c$^+$ DCs **(B)** from Wt, KC-specific, and DC-specific *Bmal1* KO epidermis collected during the day (ZT0) or night (ZT12). **(C)** Whole skin *Irf7* is exacerbated in the skin of systemic *Bmal1* KO mice, but not KC- or DC-specific *Bmal1* KO mice, after 1 day of 1% IMQ applied during the day (ZT07) or night (ZT19). *Irf7* expression was measured by qPCR on whole

back skin of Wt (blue bars, N = 14-28), systemic *Bmal1* KO (orange bars, N = 3-10), KC-specific *Bmal1* KO (green bars, N = 4-14), and DC-specific *Bmal1* KO (red bars, N = 8-11). Each data point represents 1 mouse and Mean ± SEM is indicated. **(D)** FACS-sorted immune ($CD45^+$) cells and **(E)** KCs ($CD45^-CD49f^+Lin^-$) from isolated epidermis of Wt (Blue bars, N = 3-8) and KC-specific *Bmal1* KO (K14Cre*Bmal1*$f^{fl/fl}$) (green bars, N = 3-8) mice treated with 1% IMQ for 1 day and collected at ZT09. Data represents Mean ± SEM. **(A-E)** Statistical significance was determined by Student's paired t-test and significant P-values are shown.

Table 3.2.1. GSEA pathways enriched after 1 dose, or 5 repeated doses of 1% IMQ versus control

GSEA for single dose of 1% IMQ vs control					
MSigDB Hallmark Pathways	**ES**	**NES**	**NOM p-val**	**FDR q-val**	**FWER p-val**
ALLOGRAFT_REJECTION	0.61	2.05	0.00	0.00	0.00
IL6_JAK_STAT3_SIGNALING	0.64	2.04	0.00	0.00	0.00
INFLAMMATORY_RESPONSE	0.60	2.02	0.00	0.00	0.00
COMPLEMENT	0.57	1.94	0.00	0.00	0.01
INTERFERON_GAMMA_RESPONSE	0.88	1.97	0.00	0.00	0.01
INTERFERON_ALPHA_RESPONSE	0.91	1.75	0.00	0.01	0.07
KRAS_SIGNALING_UP	0.52	1.61	0.02	0.03	0.20
COAGULATION	0.41	1.49	0.04	0.09	0.38
IL2_STAT5_SIGNALING	0.42	1.43	0.05	0.12	0.47

GSEA for 5 days of 1% IMQ vs control					
MSigDB Hallmark Pathways	**ES**	**NES**	**NOM p-val**	**FDR q-val**	**FWER p-val**
PROTEIN_SECRETION	0.44	2.59	0.01	0.02	0.17
G2M_CHECKPOINT	0.40	2.55	0.00	0.02	0.19
CHOLESTEROL_HOMEOSTASIS	0.47	2.60	0.01	0.02	0.16
MYC_TARGETS_V1	0.41	2.61	0.00	0.02	0.16
MITOTIC_SPINDLE	0.37	2.40	0.00	0.03	0.26
E2F_TARGETS	0.38	2.41	0.00	0.03	0.25
FATTY_ACID_METABOLISM	0.42	2.62	0.00	0.03	0.16
PI3K_AKT_MTOR_SIGNALING	0.39	2.30	0.01	0.03	0.33
MTORC1_SIGNALING	0.41	2.66	0.00	0.03	0.14
P53_PATHWAY	0.34	2.22	0.01	0.03	0.39
COMPLEMENT	0.35	2.24	0.01	0.03	0.38
DNA_REPAIR	0.35	2.18	0.02	0.04	0.44
HEME_METABOLISM	0.34	2.13	0.02	0.04	0.48
INTERFERON_ALPHA_RESPONSE	0.46	2.66	0.01	0.04	0.14
UNFOLDED_PROTEIN_RESPONSE	0.34	2.05	0.01	0.04	0.53
XENOBIOTIC_METABOLISM	0.34	2.13	0.02	0.04	0.48
PEROXISOME	0.35	2.07	0.01	0.04	0.51
ADIPOGENESIS	0.42	2.69	0.00	0.05	0.13
INTERFERON_GAMMA_RESPONSE	0.42	2.73	0.00	0.06	0.12
OXIDATIVE_PHOSPHORYLATION	0.45	2.90	0.00	0.08	0.08

Table 3.2.2. GSEA pathways enriched in control night versus day, or control day versus night

GSEA for control night versus day					
MSigDB Hallmark pathways	**ES**	**NES**	**NOM p-val**	**FDR q-val**	**FWER p-val**
KRAS_SIGNALING_DN	0.25	2.58	0.00	0.00	0.00
PANCREAS_BETA_CELLS	0.28	1.76	0.01	0.03	0.46
SPERMATOGENESIS	0.19	1.78	0.01	0.04	0.40

GSEA for control day versus night					
MSigDB Hallmark pathways	**ES**	**NES**	**NOM p-val**	**FDR q-val**	**FWER p-val**
MYC_TARGETS_V1	0.43	3.95	0.00	0.00	0.00
G2M_CHECKPOINT	0.40	3.68	0.00	0.00	0.00
E2F_TARGETS	0.40	3.62	0.00	0.00	0.00
HTGF_BETA_SIGNALING	0.52	3.22	0.00	0.00	0.00
P53_PATHWAY	0.35	3.21	0.00	0.00	0.00
PROTEIN_SECRETION	0.40	3.11	0.00	0.00	0.00
MITOTIC_SPINDLE	0.34	3.08	0.00	0.00	0.00
MTORC1_SIGNALING	0.34	3.04	0.00	0.00	0.00
OXIDATIVE_PHOSPHORYLATION	0.33	3.02	0.00	0.00	0.00
UNFOLDED_PROTEIN_RESPONSE	0.38	3.02	0.00	0.00	0.00
DNA_REPAIR	0.33	2.74	0.00	0.00	0.01
PI3K_AKT_MTOR_SIGNALING	0.35	2.73	0.00	0.00	0.01
GLYCOLYSIS	0.28	2.57	0.00	0.00	0.02
APICAL_JUNCTION	0.29	2.57	0.00	0.00	0.02
EMT	0.27	2.48	0.00	0.00	0.04
HEME_METABOLISM	0.27	2.46	0.00	0.00	0.05
ESTROGEN_RESPONSE_LATE	0.26	2.35	0.00	0.01	0.08
APOPTOSIS	0.26	2.30	0.00	0.01	0.11
UV_RESPONSE_DN	0.25	2.20	0.00	0.01	0.17
HYPOXIA	0.24	2.16	0.00	0.01	0.20

Table 3.2.3. GSEA pathways enriched after 1 dose of 1% IMQ during the night versus day or day versus night

GSEA for 1 day 1% IMQ night versus day					
MSigDB Hallmark pathways	**ES**	**NES**	**NOM p-val**	**FDR q-val**	**FWER p-val**
KRAS_SIGNALING_DN	0.24	2.08	0.00	0.01	0.07
SPERMATOGENESIS	0.22	1.73	0.02	0.03	0.50

GSEA for 1 day 1% IMQ day versus night					
MSigDB Hallmark pathways	**ES**	**NES**	**NOM p-val**	**FDR q-val**	**FWER p-val**
MYC_TARGETS_V1	0.47	4.46	0.00	0.00	0.00
OXIDATIVE_PHOSPHORYLATION	0.45	4.24	0.00	0.00	0.00
MTORC1_SIGNALING	0.42	4.03	0.00	0.00	0.00
ADIPOGENESIS	0.43	4.01	0.00	0.00	0.00
G2M_CHECKPOINT	0.50	3.92	0.00	0.00	0.00
PROTEIN_SECRETION	0.49	3.81	0.00	0.00	0.00
INTERFERON_ALPHA_RESPONSE	0.40	3.80	0.00	0.00	0.00
MITOTIC_SPINDLE	0.39	3.68	0.00	0.00	0.00
INTERFERON_GAMMA_RESPONSE	0.39	3.63	0.00	0.00	0.00
E2F_TARGETS	0.40	3.54	0.00	0.00	0.00
DNA_REPAIR	0.43	3.51	0.00	0.00	0.00
UNFOLDED_PROTEIN_RESPONSE	0.38	3.35	0.00	0.00	0.00
FATTY_ACID_METABOLISM	0.41	3.29	0.00	0.00	0.00
PI3K_AKT_MTOR_SIGNALING	0.34	3.25	0.00	0.00	0.00
P53_PATHWAY	0.37	3.22	0.00	0.00	0.00
UV_RESPONSE_DN	0.34	3.22	0.00	0.00	0.00
GLYCOLYSIS	0.33	3.06	0.00	0.00	0.00
EMT	0.32	3.02	0.00	0.00	0.00
MYOGENESIS	0.33	3.00	0.00	0.00	0.00
APOPTOSIS	0.33	2.96	0.00	0.00	0.00

Red text indicates pathways uniquely identified as enriched during the day after 24 hours IMQ (i.e. pathways not identified as enriched during the day under homeostasis).

Table 3.2.4 GSEA pathways enriched after 5 repeated doses of 1% IMQ during the night versus day or day versus night

GSEA for 5 repeated IMQ doses during the night versus day					
MSigDB Hallmark Pathways	**ES**	**NES**	**NOM p-val**	**FDR q-val**	**FWER p-val**
G2M_CHECKPOINT	0.32	3.99	0.00	0.00	0
E2F_TARGETS	0.31	3.92	0.00	0.00	0
MYC_TARGETS_V2	0.43	3.39	0.00	0.00	0
UNFOLDED_PROTEIN_RESPONSE	0.26	2.68	0.00	0.00	0
MTORC1_SIGNALING	0.20	2.44	0.00	0.00	0.003
MITOTIC_SPINDLE	0.19	2.34	0.00	0.00	0.007
TNFA_SIGNALING_VIA_NFKB	0.18	2.23	0.00	0.00	0.015
PI3K_AKT_MTOR_SIGNALING	0.19	1.88	0.01	0.05	0.309
UV_RESPONSE_UP	0.16	1.83	0.01	0.05	0.407
MYC_TARGETS_V1	0.15	1.84	0.01	0.05	0.382
IL2_STAT5_SIGNALING	0.14	1.79	0.01	0.06	0.481
CHOLESTEROL_HOMEOSTASIS	0.21	1.76	0.02	0.06	0.539
ESTROGEN_RESPONSE_EARLY	0.14	1.77	0.02	0.06	0.523
HYPOXIA	0.13	1.65	0.03	0.10	0.746
PROTEIN_SECRETION	0.17	1.62	0.03	0.11	0.793

GSEA for 5 repeated IMQ doses during the day versus night					
MSigDB Hallmark Pathways	**ES**	**NES**	**NOM p-val**	**FDR q-val**	**FWER p-val**
OXIDATIVE_PHOSPHORYLATION	0.26	3.24	0.00	0.00	0.00
MYOGENESIS	0.20	2.49	0.00	0.00	0.006
FATTY_ACID_METABOLISM	0.20	2.29	0.00	0.00	0.015
ADIPOGENESIS	0.17	2.15	0.00	0.01	0.043

Table 3.2.5 Genes used to annotate epidermal cell clusters

Cell clusters	Genes
Basal KC	*Krt5, Col17a1, Itga6, Sca1(Ly6a), Thbs1, Krt14, Serpinb2*
Differentiated KC (diff KC)	*Krt1, Krt10, Mt4*
Mitotic KC	*Cdk1, Ccnb1, Cdca8, Top2a, Ki67, Cdc20, Krt5*
Basal infundibulum (Infu basal)	*Sostdc1, Aldh3a1, Fst*
Isthmus (upper HF)	*Krt17, Krt79, Cst6, Rbp1, Sprr1a, Defb6, Sox9, Col17a1*
Hair follicle stem cell (HFSC)	*Postn, Sox9, CD34, Krt24, Lhx2*
Langerhan's cells (LC)	*Csf1r, CD207, CD74, Ptgs1, Il1b*
Monocytes (mono)	*Cybb, Fcgr3 (CD16), Ccl6, Lyz2, Ccl4, Bst2, Isg15, Ly6e, Cxcl10, Ptprc, Ifi204*
T cells	*CD3g, Thy1, Cxcr6*
Sebaceous gland (SG)	*Plin2, Mgst1, Ldhb*
Melanocytes (MC)	*Pmel, Tyrp1, Mlana*

Chapter 4: Effect of *Bmal1* deletion and repeated doses of IMQ on diurnal rhythms of inflammatory parameters

Abstract

The pathogenesis of IMQ-induced psoriasis is well studied, however, the role of the circadian clock on such inflammatory pathways in the skin is unclear. The purpose of this study was to investigate the time-of-day specific effects treatment with the immunomodulatory cream, Imiquimod (IMQ), on IMQ-induced psoriasiform inflammation in the mouse skin. We measured cell proliferation, immune cell infiltration, and spleen weight. Our studies show that under homeostasis or after a single dose of 1% IMQ, these parameters differ depending on the time of day in which IMQ is applied; however, after 5 repeated IMQ doses these parameters are constitutively high and lack diurnal gating. We also investigated whether the core clock plays a role in psoriasiform inflammation by treating Wt and *Bmal1* KO mice with IMQ and found that *Bmal1* KO mice have normal immune cell recruitment, spleen weight and cell proliferation, but greater epidermal thickness, after 5 days of 1% IMQ treatment. Investigating how the circadian clock contributes to skin inflammatory responses can provide essential insight into how to treat and prevent dermatological diseases by optimally timing treatment regimens.

4.1 Introduction

As a protective interface against the external environment, the skin defends the internal body from pathogenic organisms and environmental stressors. In addition to its' physical barrier properties, the skin also has immune functions that respond to pathogens or foreign particles: keratinocytes and immune cells mount inflammatory responses through the activation of Toll-

like receptor (TLR) pathways. When applied topically to the skin of mice, Imiquimod (IMQ) acts as a potent immune activator, initiating TLR7 signaling in the skin; upon repeated doses, IMQ treatment leads to psoriasiform inflammation, mirroring human psoriasis, which is characterized by increased cytokine production, massive immune infiltration and epidermal hyperproliferation, and epidermal thickening (Van der Fits et al., 2009).

Previous studies have demonstrated that numerous skin activities are heavily dependent on the circadian rhythm. BMAL1:CLOCK control the transcription of genes involved in inflammatory cell recruitment and/or the ability of immune cells to become activated after pathogen exposure (Chapter 1, Figure 1.4); therefore, the circadian clock may play an important role in the defense response against pathogens and pathogen mimics such as IMQ or RNA/DNA. The severity of sepsis is time-of-day dependent and corresponded with diurnal changes in the expression and function of a toll-like receptor, TLR9, which is responsible for activating the expression and secretion of pro-inflammatory genes leading to inflammatory cell recruitment (Silver et al., 2012; Marpegan et al., 2009). A very recent study showed that neutrophil and macrophage infiltration and chemokine expression was time-of-day dependent during *Leishmania major* infection and that rhythms were abolished in clock-deficient macrophages and when BMAL1 was deleted in immune cells (Kiessling et al., 2017).

One of the key functions of the circadian clock in the skin is controlling the rhythm cell proliferation, or S-phase. The proportion of basal keratinocytes in the mouse skin in S-phase is greater during the early morning hours, and lowest during the afternoon; this rhythm is reversed in humans (Brown et al., 1991). The rhythm of cell proliferation depends on *Bmal1* intrinsic to

keratinocytes, as transgenic mice lacking *Bmal1* specifically in keratinocytes have arrhythmic S-phase, equivalent to the levels of peak S-phase in normal mice (Geyfman et al., 2012).

Although many studies describe the pathogenesis of IMQ-induced psoriasis, few describe the potential role of the circadian clock in the inflammatory pathways in the skin. The circadian clock mediates daily homeostatic cycles in the skin, and it has also been implicated as an integral modulator of the immune response. Nakamura et al. (2011, 2014) have described allergic responses in the skin as circadian regulated and dependent on the cell-intrinsic clock mast cells, which secrete histamines in a diurnal manner in response to IgE (Nakamura et al., 2011); Nakamura et al. (2014). This group has also found that delayed type skin allergic reactions are more severe in mice mutated for *Clock* (Takita et al., 2013). Moreover, ablation of a key entrainment stimulus for the circadian clock, melatonin, caused hamsters to lose diurnal rhythm of antigen-presenting dendritic cell trafficking in the skin and impaired cutaneous antigen-specific delayed-type hypersensitivity reactions (Prendergast et al., 2013). Recently, a role for the circadian clock has been described in a mouse model of psoriasis, an inflammatory skin disease that affects approximately 3% of the population (Ando et al., 2015). *Clock* mutation dampens the development of IMQ-induced dermatitis, whereas the *Per2* mutation results in an exaggeration (Ando et al., 2015). The authors of this study propose that these effects are due to modulation of the IL-23 receptor (IL-23R) expression in γ/δ^+ T cells, however no causal connection was explored. Thus, more research is required to understand the mechanisms by which the circadian clock gates IMQ-induced immune activation. Together, these studies illustrate an important modulatory activity of the circadian clock on immune responses in the skin and suggest that without proper regulation, the immune system may become over-reactive,

resulting in the development of autoimmune diseases. While significant advances have been made to understand the mechanisms by which the circadian clock regulates skin biology and specifically the skins' immune response, much remains to be discovered.

Here we investigate the circadian clock's role in early and late inflammatory immune responses in the mouse skin. To achieve this, we treated mice topically with the chemical immunomodulator IMQ for one day or daily for five days at time points throughout the day-night cycle. To measure inflammation state, we assessed time-of-day dependent changes in the proportion of proliferating (EdU^+) cells in the interfollicular epidermis (IFE) and the epidermal width and found that both parameters were significantly diurnal under homeostasis, and rhythmicity was disrupted after repeated IMQ doses (Figure 4.2.1A). Spleen weight was diurnal under homeostasis and 1 day of 1% IMQ, but lacked rhythmicity after 5 days of 1% IMQ. The proportion of $Ly6G^+$ neutrophils in the whole skin differ across the day/night cycle after one day of IMQ, with greater numbers of cells after daytime IMQ, but no diurnal differences were present by 5 days of 1% IMQ, or for $CD45^+$ or $F4/80^+$ cells. We investigated the mechanism underlying this IMQ-induced elimination of circadian rhythmicity by measuring core clock gene expression after IMQ and found that IMQ downregulates *Dbp* and *Rev-erbα* in a dose dependent manner. We next asked whether the core clock protein BMAL1 plays a direct role in regulating IMQ-induced inflammatory responses. We found that systemic *Bmal1* KO mice exhibited normal inflammatory cell recruitment to the skin after 5 days of 1% IMQ treatment. Although systemic *Bmal1* KO mice had greater epidermal thickness after 5 days of 1% IMQ, epidermal proliferation and spleen weight was consistent with that of Wt. In conclusion, these results support the idea that the early phase of the IMQ-induced inflammatory response is diurnal, while

rhythmicity is dampened or ablated after immense inflammation elicited by repeated IMQ treatments.

Together, the results of this study shed light on the underappreciated role of the circadian clock in regulating immune responses in the skin. Investigating the circadian clock's contributions to skin inflammatory responses can provide essential insight into the optimal treatment and prevention of dermatological diseases such as actinic keratosis and superficial basal cell carcinoma, both of which are treated therapeutically with IMQ in humans.

4.2 Results

4.2.1 Repeated doses of IMQ dampens diurnal rhythms of inflammatory parameters including epidermal proliferation and width, spleen weight, and skin immune cell occupancy

Apart from gene expression changes, we were also interested in determining if the circadian clock gates other inflammatory parameters associated with the early and late phases of IMQ-induced psoriasiform inflammation. We treated mice with 1% IMQ as described in section 3.1 (see also Figure 3.2.1A) for 1 day or 5 days and measured spleen weight, cell proliferation within the IFE, epidermal width, and immune cell occupancy. Without regard to the circadian time, the proportion of proliferating cells (EdU^+ cells) was greater after 5 days of 1% IMQ compared to control (Figure 4.2.1A), and the epidermal width, an indicator inflammation state, was significantly greater after 1 day and 5 days of 1% IMQ, compared to control (Figure 4.2.1B).

Total immune cells ($CD45^+$) and neutrophils and/or monocytes ($Ly6G^+$) in the whole skin increased from control to 5 days 1% IMQ and from 1 day 1% IMQ to 5 days 1% IMQ (Figure 4.2.1D). Macrophages and/or Langerhan's cells ($F4/80^+$) in the whole skin increased from control to 5 days 1% IMQ (Figure 4.2.1D).

We assessed time-of-day dependent changes in the proportion of proliferating (EdU^+) cells in the IFE and epidermal width after IMQ treatments throughout the day/night cycle and found that both parameters differed significantly under homeostasis, however no time-of-day dependent differences were observed after 1 day or 5 days of 1% IMQ (Figure 4.2.1A and B). Spleen weight for control and 1 day of 1% IMQ treatment differed significantly across the day/night cycle, but no diurnal significance was observed after 5 days of 1% IMQ treatment (Figure 4.2.1C). Numbers of $Ly6G^+$ neutrophils in the whole skin differ across the day/night cycle after 1 day of IMQ with greater cells seen after daytime treatment compared to nighttime treatment, but no other significant time-of-day dependent changes were observed under homeostasis or by 5 days of 1% IMQ treatment, or for $CD45^+$ or $F4/80^+$ cells (Figure 4.2.1D).

These results show that a single dose of 1% IMQ elicits time-of-day dependent neutrophil recruitment to the skin, changes in epidermal thickness, and spleen weight. Conversely, repetitive doses of IMQ treatment disrupts diurnal rhythms in epidermal cell proliferation and width, neutrophil recruitment, and spleen weight.

4.2.2 Core clock gene expression is affected by IMQ and *Bmal1* systemic deletion

Considering our observations that repeated doses of IMQ caused robust inflammation and dampened circadian rhythms in inflammatory parameters, we wanted to know whether the core clock itself is affected by IMQ treatment. To this end, we measured the skin mRNA expression level of circadian clock-controlled genes *Dbp* and *Rev-erbα* from mice treated with 1% IMQ for 6 hours during the day or night, as described in Figure 3.2.1A with slight modification (6 hours IMQ only included 1 time point for day (ZT07) and one for night (ZT19)). We found that *Dbp* was downregulated in a dose-dependent manner after 6 hours of one dose of 1% IMQ (Figure 4.2.2A and 4.2.2B). Interestingly, this IMQ-induced suppression was also seen for *Rev-erbα*, which encodes the protein Rev-erbα, a clock-controlled transcription factor that negatively regulates *Bmal1* expression (Figure 4.2.2C and 4.2.2D).

4.2.3 Systemic deletion of *Bmal1* results in normal immune infiltration and cell proliferation, and splenomegaly, but greater epidermal thickness after 5 days of IMQ treatment

To investigate the biological significance of the circadian clock in pro-inflammatory immune responses in the skin, we applied 1% IMQ to the backs of *Bmal1* KO mice for 0 hours (control), 6 hours, 1 day, 3 days, and 5 days and collected back skin and spleen. Through immunofluorescent imaging, we found that *Bmal1* KO mice had no significant difference in total immune ($CD45^+$) or $Ly6G^+$ neutrophils and/or monocytes in the whole skin compared to Wt, while there was significantly less $F4/80^+$ macrophages in the whole skin in *Bmal1* KO mice compared to Wt after 1 day of 1% IMQ (Figure 4.2.3A and B). We also found that by 5 days of 1% IMQ, Wt treated ears had a trend toward higher proportion of $CD11c^+$ DCs and $CD3e^+$ T

cells compared to control and there was no significant difference between Wt and *Bmal1* KO under control, 24 hour 1% IMQ, or 5 day 1% IMQ (Figure 4.2.3C). Similarly, there was no difference in spleen weight between *Bmal1* KO and Wt by 5 days of 1% IMQ (Figure 4.2.4A). While epidermal cell proliferation was heightened in *Bmal1* KO mice under homeostasis, it was not significantly different compared to Wt after 5 days of 1% IMQ (Figure 4.2.4B). Interestingly, we observed an increase in epidermal thickness in *Bmal1* KO compared to Wt at this time point (Figure 4.2.4C).

4.3 Discussion

Investigating the circadian clock's contributions to skin inflammatory responses can provide essential insight into the treatment of dermatological diseases such as actinic keratosis and superficial basal cell carcinoma. Our study shows that under homeostasis or after a single dose of 1% IMQ, the proportion of proliferating cells in the IFE, the epidermal width, and spleen weight are significantly diurnal in Wt mice, and this rhythmicity is disrupted after 5 daily doses of 1% IMQ. Numbers of $Ly6G^+$ neutrophils in the whole skin differ across the day/night cycle after one day of 1% IMQ treatment, but no diurnal differences are present after 5 daily doses of 1% IMQ. These results oppose the results of a study by Ando and colleagues which show that IMQ treatment during the night versus the day results in greater ear thickening, suggesting a diurnal rhythm in inflammatory cell infiltration (Ando et al., 2015). The difference in results between the current study and their study may be due to their use of 2.5% IMQ cream, which is twice the dose used in the current study. They also use ICR Albino (also known as CD1) female mice while we use male C57/B6J mice; these strains have been shown to have different inflammatory

responses to repetitive IMQ treatment (Swindell et al., 2017). For example, ICR mice have greater IMQ-induced splenomegaly compared to C57/B6J, but C57/B6J have greater epidermal thickness and weight loss in response to IMQ than ICR mice (Swindell et al., 2017).

We hypothesized that the lack of diurnal rhythmicity of inflammatory parameters seen after repeated IMQ treatments may be due to altered expression of core clock machinery. Our data suggests that this is the case, as clock-controlled genes *Dbp* and *Rev-erbα* are downregulated after IMQ. This finding is supported by previous studies in which inflammatory disease pathology was correlated with suppression of clock-controlled gene expression (Ehlers et al., 2017; Haspel et al., 2014; Haimovich et al., 2010).

Previous studies show discordant results regarding the effect of circadian disruption on psoriatic inflammation. In humans, the incidence of psoriasis is greater in shift workers (Li et al., 2013). Consistent with this, disrupting the circadian clock through altered sleep-wake cycles elevates pro-inflammatory cytokine secretion (Hirotsu et al., 2012) and diminishes barrier function (Matsui et al., 2016) in mouse models of psoriasis. On the other hand, Ando and colleagues show that mutation of the core clock gene, *Clock*, lessens IMQ-induced ear swelling and inflammatory recruitment to skin draining lymph nodes, while mutation of *Per2* (an inhibitor of BMAL1:CLOCK) results in the opposite phenotype (Ando et al., 2015).

While IMQ-induced ISG expression in the skin and IFN-β serum levels are exacerbated in *Bmal1* KO mice (Chapter 3), the current study illustrates that inflammatory infiltrate as a result of daily repeated 1% IMQ treatment is relatively unaffected by *Bmal1* deletion. The idea that

local inflammation is independent of type I IFN signaling has been described in other studies (Guiducci et al., 2010; Wohn et al., 2013; Kader et al., 2013). In fact, skin inflammation is unaffected after blocking IFN-α signaling in pDCs in the IMQ-induced psoriasis mouse model (Wohn et al., 2013). In addition, inhibition of PI3K, an essential complex for TLR-activated IRF7 nuclear location and IFN-α production in pDCs, does not affect inflammatory cytokines or maturation of pDCs in response to TLR7/9 triggering. Thus, while the circadian clock is an important regulator of IMQ-induced ISG expression and type I IFN levels, it does not affect IMQ-induced inflammatory cell recruitment.

A hallmark of psoriasiform inflammation is an epidermal cell proliferation, accompanied by an increase in epidermal thickness. Our results show that, while *Bmal1* KO mice have greater epidermal thickness after 5 days of 1% IMQ, their cell proliferation within the IFE is similar to Wt at this time point. The discrepancy between the epidermal thickness and cell proliferation results may be due to the fact that BMAL1 expression regulates cell cycle progression within the basal cells of the IFE; deletion of *Bmal1* results in increased cell proliferation under homeostasis (Figure 4.2.4B). It is also possible that other factors contributing to epidermal thickness may be heightened in the *Bmal1* KO mice independent of cell proliferation, such as hydropic cell swelling, which is common in virally infected KCs.

The current study illustrates that under homeostasis and early on after 1% IMQ treatment, the circadian rhythm of cell proliferation in basal epidermal keratinocytes, epidermal thickness, spleen weight, and neutrophil occupancy is maintained. However, as psoriasiform inflammation progresses with repeated IMQ treatments, these parameters are heightened and the diurnal

rhythmicity is dampened. Understanding the effect of time of day on the time course dynamics of IMQ-induced inflammatory activation is important for designing optimal treatment regimens centered on harnessing the body's natural circadian rhythms.

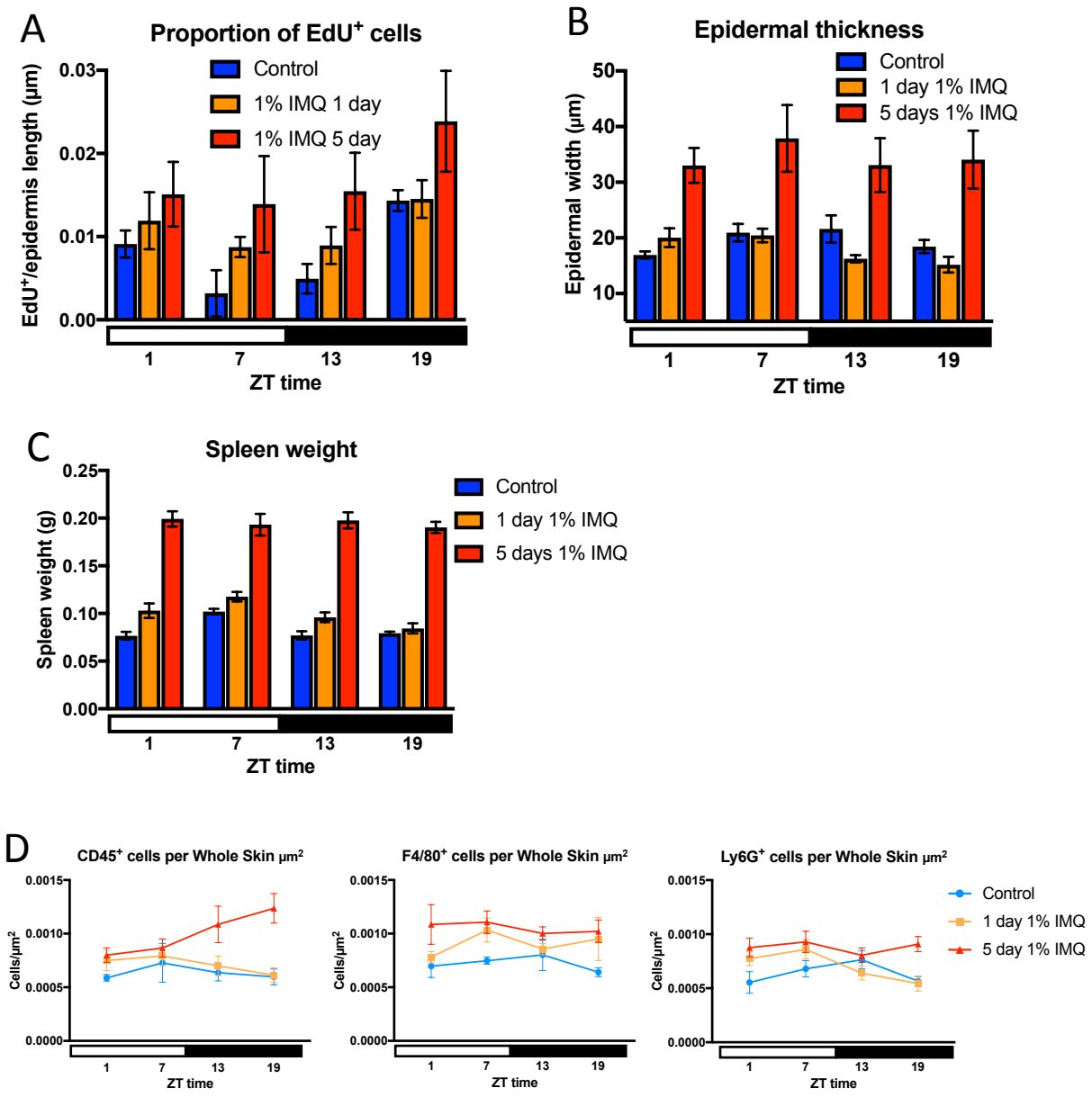

Figure 4.2.1 Repeated doses of 1% IMQ dampens diurnal rhythms of inflammatory parameters including epidermal proliferation and width, spleen weight, and skin immune cell occupancy. (A) Wt mice were treated with IMQ at circadian time points for one day or consecutively for five days as described in 3.2.1A. Two hours prior to collection, mice were IP injected with EdU and skin samples were prepared as described in the methods section. Control mice were untreated (blue, N = 5), 1 day 1% IMQ (orange, N = 7), and 5 days 1% IMQ (red, N = 5-7). Data presented as mean ± SEM. Two-way ANOVA test shows significance between treatments (P = 0.02) and time points (P = 0.005). Tukey's post-hoc test for control vs 5 day 1% IMQ P = 0.01. One-way ANOVA for control across ZT times was P < 0.003, but no significance was found for the different treatments. **(B)** Wt male mice were treated as described in 4.2.1A and epidermal thickness was measured in H&E stained skin sections. Epidermal thickness was significantly different between treatments (Two-way ANOVA P < 0.0001), for both control

versus 5 day IMQ, and 1 day IMQ versus 5 day IMQ (Tukey's post-hoc test $P < 0.0001$ for both). Epidermal thickness after 1 day IMQ differed across ZT time (one-way ANOVA $P = 0.01$), but no significance was found under homeostasis or after 5 days of 1% IMQ. Control mice treated with control cream (blue, N = 5), 1 day 1% IMQ (orange, N = 7), and 5 days 1% IMQ (red, N = 5-7). **(C)** Male mice were treated as described in (A) and spleen weights were measured upon sacrifice. Spleen weight differed across ZT time and treatments (Two way ANOVA $P = 0.028$ and $P < 0.0001$). Spleens weighed more after 1 day 1% IMQ and 5 day 1% IMQ compared to controls (Tukey's post-hoc test, $P = 0.004$ and $P < 0.0001$). Spleen weight changed across ZT time in controls, and after 1 day 1% IMQ (One-way ANOVA $P = 0.0002$ and $P = 0.003$, respectively) but not after 5 days of IMQ. **(D)** Male mice were treated as described in 3.2.1A and whole back skin sections were imaged by IF microscopy after staining for immune markers; cells were counted as described in Methods. There was a significant difference in the proportion of $CD45^+$, $F4/80^+$, $Ly6G^+$ cells within the whole skin between treatments (two-way ANOVA $P < 0.0001$, 0.0009, and 0.0002, respectively). $CD45^+$ and $Ly6G^+$ cells increase from control to 5 day 1% IMQ (Tukey's post-hoc test $P < 0.0001$ and $P = 0.0006$), and from 1 day IMQ to 5 day IMQ (Tukey's post-hoc test $P < 0.0001$ and $P = 0.007$), while $F4/80^+$ cells only increase from control to 5 day 1% IMQ (Tukey's post-hoc test $P = 0.0006$). No significant difference was seen in $CD45^+$ and $F4/80^+$ cells across ZT time in control, 1 day 1% IMQ, and 5 day 1% IMQ, while the proportion of $Ly6G^+$ cells in the whole skin differed across ZT time after 1 day 1% IMQ (one-way ANOVA $P = 0.03$), with greater cells seen after daytime treatment compared to nighttime treatment. Data points represent mean ± SEM for control (blue, N = 4 or 5), 1 day 1% IMQ (green, N = 5 or 6) and 5 day 1% IMQ (red, N = 5 or 6).

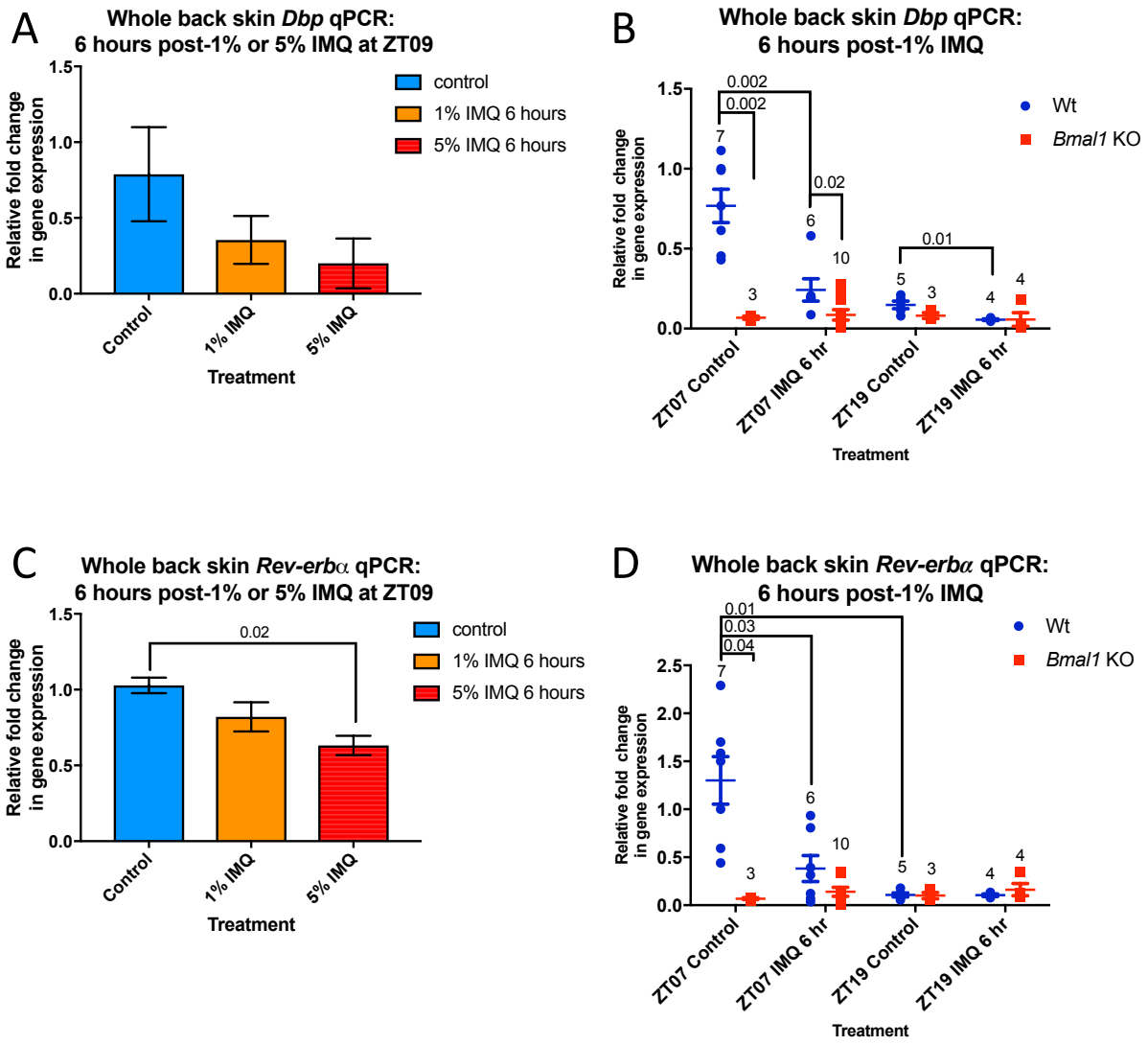

Figure 4.2.2 Clock-controlled gene expression is affected by IMQ and *Bmal1* systemic deletion. **(A)** Clock-controlled gene *Dbp* is downregulated after 6 hours of IMQ, in a dose-dependent fashion. Wt male mice were untreated (blue, N = 4), or treated as described in Methods for 6 hours with 1% IMQ (pink, N = 3), or 5% IMQ (red, N = 2). *Dbp* expression in whole skin was measured by qPCR. **(B)** Six hours of 1% IMQ downregulates *Dbp* to a similar extent as systemic *Bmal1* deletion. Wt (Blue, N = 5-7), and systemic *Bmal1* KO mice (red, N = 5-7) were treated during the day or night with 1% IMQ for 6 hours *Dbp* expression in whole skin was measured by qPCR. **(C)** The clock-controlled gene, *Rev-erb*α, is downregulated after 6 hours of 1% IMQ, in a dose-dependent fashion. The same samples used in (A) were subject to qPCR for *Rev-erb*α. **(D)** Six hours of 1% IMQ downregulates *Rev-erb*α to a similar extent as systemic *Bmal1* deletion. The same samples from (B) were subject to qPCR for *Rev-erb*α. **(B and D)** Each data point represents 1 mouse and Mean ± SEM is indicated. Statistical significance was determined by Student's paired t-test and significant P-values are shown.

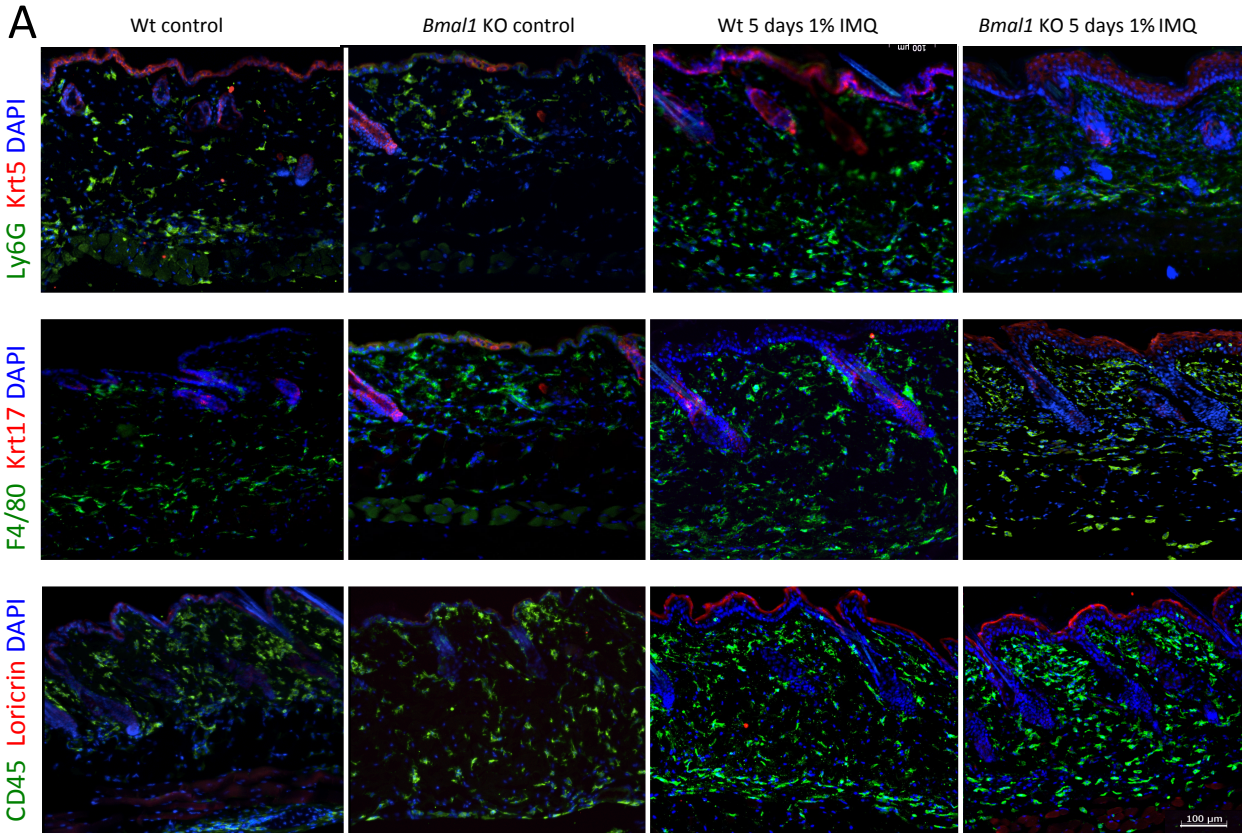
A
Wt control
Bmal1 KO control
Wt 5 days 1% IMQ
Bmal1 KO 5 days 1% IMQ
Ly6G Krt5 DAPI
F4/80 Krt17 DAPI
CD45 Loricrin DAPI
100 µm

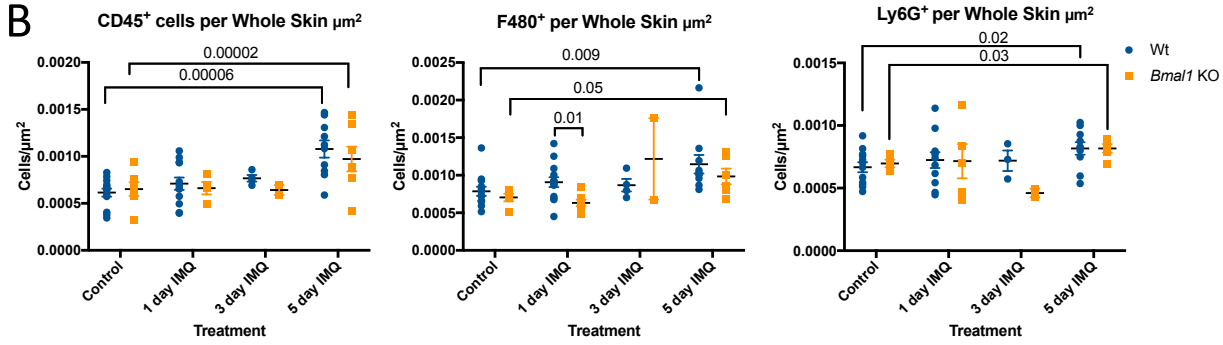
B
CD45+ cells per Whole Skin µm2
F480+ per Whole Skin µm2
Ly6G+ per Whole Skin µm2
Cells/µm2
Treatment
Control
1 day IMQ
3 day IMQ
5 day IMQ
0.00002
0.00006
0.009
0.05
0.01
0.02
0.03
Wt
Bmal1 KO

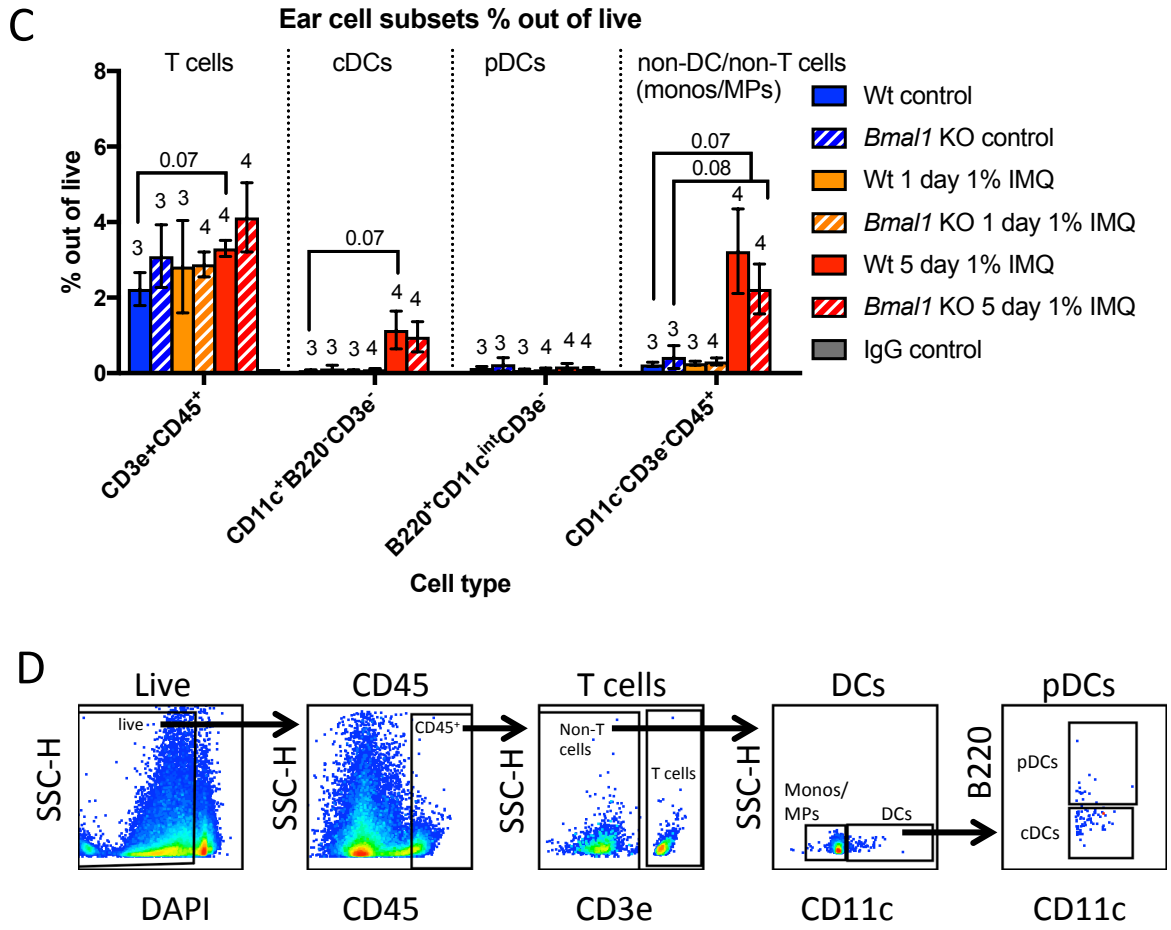

Figure 4.2.3 Systemic *Bmal1* deletion does not affect inflammatory cell recruitment after daily IMQ. (A) IMQ-induced immune cell recruitment to the skin is unaffected by *Bmal1* deletion. Mice were treated as described in 3.2.1A and whole back skin sections were imaged by immunofluorescent microscopy after staining for immune markers. Representative images are shown. **(B)** Quantification of the proportion of immune cells in the skin from the images shown in (A). **(C)** Flow cytometry quantification of whole ear skin immune cells, T cells ($CD3e^+$), non-T cells immune cells ($CD3e^-CD45^+$), cDCs ($CD11c^+B220^-CD3e^-$) and pDCs ($B220^+CD11c^{int}CD3e^-$) in Wt (solid bars) and *Bmal1* KO (striped bars) under control (blue), 1 day 1% IMQ (orange) and 5 days of 1% IMQ (red), isotype control-stained samples (grey), presented as percentage out of all live cells. The numbers above each bar indicate the number of samples analyzed. Mean ± SEM is indicated. Statistical significance was determined by Student's paired t-test, and significant or near-significant P-values are shown. **(D)** Gating strategy used to quantify the proportion of immune cell subsets in the ear skin shown in (C).

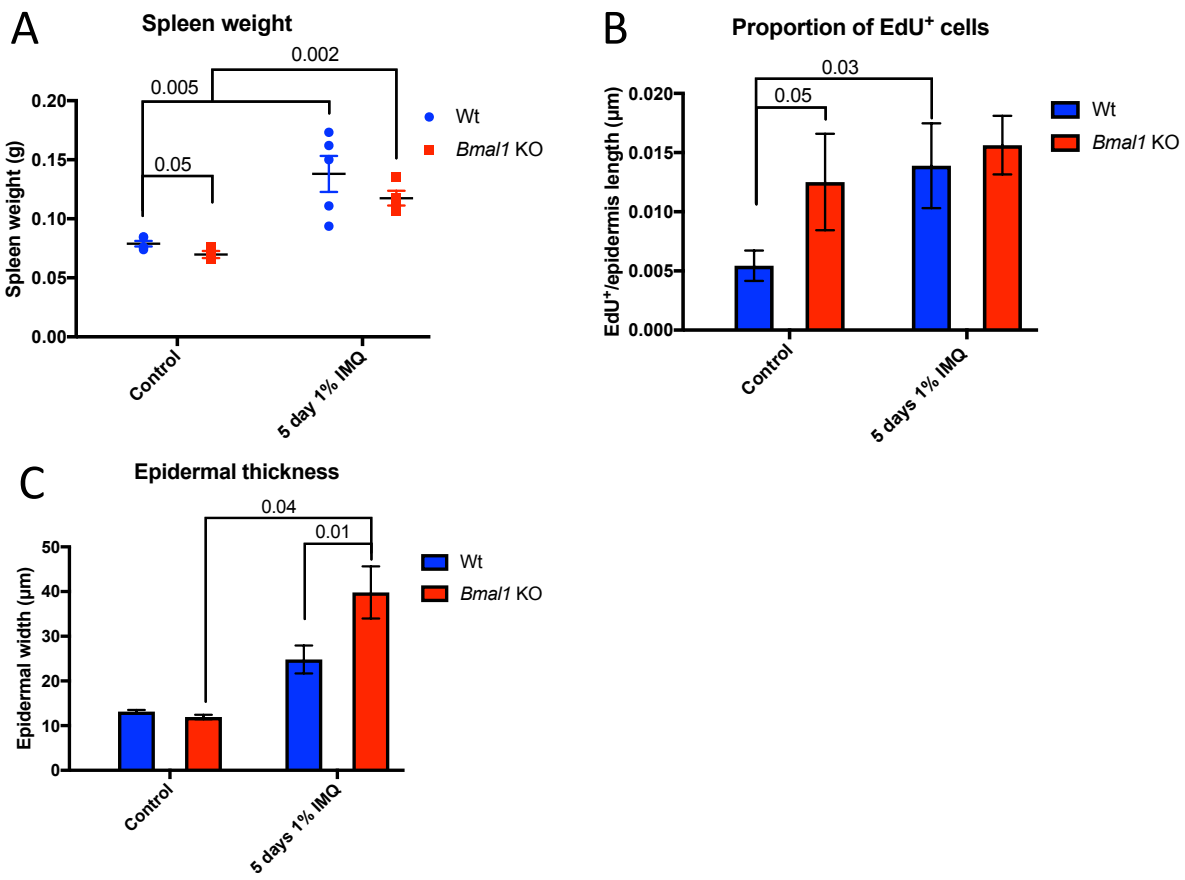

Figure 4.2.4 *Bmal1* deletion does not affect IMQ-induced splenomegaly and epidermal hyperproliferation, results in elevated epidermal thickness. (A) IMQ-induced splenomegaly is similar in *Bmal1* KO and Wt mice. Wt (blue) and *Bmal1* KO mice (red) were untreated or treated for 5 days with IMQ and spleens were collected and weighed. Values represent mean ± SEM for Wt control (N = 3M, 2F), *Bmal1* KO control (N = 1M, 2F), Wt 5 day 1% IMQ (N = 2M, 3F), *Bmal1* KO 5 day 1% IMQ (N = 2M, 2F). **(B)** Cell proliferation is similar in *Bmal1* KO compared to Wt after 5 day 1% IMQ. Wt (blue) and *Bmal1* KO mice (red) were untreated or treated for 5 days with 1% IMQ and EdU^+ cells were counted and normalized to the length of epidermis. Values represent mean ± SEM for Wt control (N = 9M, 4F), *Bmal1* KO control (N = 6M, 1F), Wt IMQ 5 day (N = 11M, 2F), *Bmal1* KO IMQ 5 day (N = 5M, 5F). **(C)** Epidermal thickness is greater in *Bmal1* KO mice after 5 days of 1% IMQ. Wt and *Bmal1* KO mice were untreated or treated with 1% IMQ for 5 days and epidermal thickness was measured by immunofluorescence microscopy after DAPI staining. Values represent mean ± SEM for Wt control (N = 2), *Bmal1* KO control (N = 2), Wt 5 day 1% IMQ (N = 7M, 16F), *Bmal1* KO 5 day 1% IMQ (N = 7M, 6F). Each data point represents 1 mouse and Mean ± SEM is indicated. **(A-E)** Statistical significance was determined by Student's paired t-test and significant P-values are shown.

Chapter 5: Conclusions and Perspectives

5.1 The circadian clock and feeding schedules regulate skin UVB-induced DNA damage

The circadian clock is a mechanism that allows organisms to anticipate daily changes in their environment for better survival. It enables organisms to better capitalize on environmental resources (e.g. light and food) compared to those that cannot predict such availability. All phyla of life, from Archaea to Eukarya, have circadian clocks, and all cells of an organism express the molecular core clock machinery. Approximately 10% of all genes are regulated either directly or indirectly by the core clock proteins Clock and BMAL1, as described in Chapter 1. It was thought that the core clock in the SCN was the sole pacemaker in charge of setting the rhythm of clocks in peripheral organs. In the past few decades, however, studies have emerged showing that food intake can shift the phase of the clock in the liver independently of the phase of the SCN (Damiola et al., 2000). It can be expected that the phase of an organ responsible for organismal metabolism would be responsive to food intake; however, our work shows that the skin, the most distal organ, is acutely responsive to food intake and that eating at different times of day changes which genes are diurnally expressed in the skin (Chapter 2).

The circadian clock within the skin regulates important functions such as cellular metabolism, DNA damage repair, immune defense, cell proliferation and barrier properties. On the cellular level, the skin clock temporally gates discordant biological processes from occurring in parallel. A prime example of this is seen in the rhythms in ox. phos. metabolism and cell cycle within the basal IFE and HFSCs. In mice, these cells proliferate with S-phase occurring at night, anti-phasic to the rhythm of ox. phos. metabolism, which occurs during the day. Ox. phos. produces ROS,

which may damage DNA, and cells are more sensitive to DNA damage during the S-phase of the cell cycle (Geyfman et al., 2012), when chromatin is euchromatic. When damaged DNA is passed down in proliferating cells, mutations will accumulate which may result in cancer formation. By temporally gating these discordant cellular processes, the circadian clock promotes organismal fitness.

On the other hand, there are also nucleotide excision repair enzymes within the skin and other organs that act as a control mechanism by finding DNA lesions and repairing them. Of these repair proteins, XPA exhibits circadian rhythms in the skin of mice, anti-phasic to the sensitivity of UVB-induced DNA damage (Gaddameedhi et al., 2011). Thus, we believe that sensitivity to DNA damage within the skin, especially that caused UVB-radiation, depends on not only the stage of the cell cycle, but also the expression of *XPA*. In our experiments from Chapter 2 we find that the rhythm of UVB induced damage is reversed in daytime-fed mice, and all RF-fed mice had lower levels of overall lower proportion of cells in S-phase while the phase of S-phase cycles remained the same. We also observed lower levels and somewhat shifted phase of the expression of *XPA*. Since these experiments were only carried out for a month-long RF program, and a single exposure to UVB immediately before collection, it would be useful to perform experiments in a context similar to what we would see in humans. For example, if we did more long-term RF experiments followed by repeated doses of UVB, we could determine if UVB-induced melanoma development is more aggressive when mice eat at abnormal times throughout the day-night cycle. Because the circadian clocks and activity patterns in mice and humans are opposite for the most part, it would also be enlightening to perform these UVB-induced DNA damage experiments on biopsies from patients undergoing reductive procedures.

5.2 BMAL1 regulates the diurnal interferon-sensitive gene response to TLR7 activation

The skin is the foremost barrier in charge of protecting us against invading bacterial and viral pathogens, and studies suggest that certain immune-mediated processes in the skin vary depending on the time of day (described in Chapter 1). In Chapter 3, we investigated how the circadian clock and timing of food may regulate IFN-associated immune responses in the skin. We found that interferon-sensitive genes (ISGs) are induced in a time-of-day dependent manner, with greater magnitude of expression after daytime than nighttime treatment with the TLR7 agonist Imiquimod (IMQ). Shifting the clock by daytime RF effectively reversed the rhythm of the ISG response. The diurnal rhythm in ISG induction was prominent in epidermal immune cells rather than KCs. In support of this finding, we observed greater total and p-IRF7 nuclear localization after daytime than nighttime IMQ treatment in T cells and monocytes from the epidermis. We also found that mice systemically lacking *Bmal1* exhibited exaggerated expression of ISGs in response to IMQ that could not be recapitulated by DC- or KC-specific *Bmal1* deletion. These findings reveal that BMAL1 expression in immune cells, particularly monocytes and T cells, is an important regulator in the skin's ISG response after TLR activation.

Since ISGs polarize cells to fight off potential invading microbial pathogens and/or tumor cells, the results of this study suggest that, in mice, therapeutic activation of this pathway during the day may be more beneficial than at night. This idea is supported by a previous study in which tumor-bearing mice injected with IFN-β during the day (9 a.m.) experienced a slower rate of tumor growth and prolonged survival compared to mice injected at night (9 p.m.) (Takane et al.,

2000). Future experiments will utilize skin viral models to determine if skin is more protected against viral exposure during the day than night. As viral infections contribute to approximately 15% of human cancers worldwide (zur Hausen et al., 1991), and anti-viral treatments such as IMQ are commonly used to treat cancer, these findings will be significant in the fields of both virology as well as oncology. Understanding the mechanism(s) by which the circadian clock mediates ISG responses in the skin is of direct translational relevance; this knowledge can be used to develop time-of-day-specific treatment regimens for skin cancers currently treated with IMQ (e.g. superficial basal cell carcinoma).

5.3 BMAL1 binds to sites within ISG gene sequences

In chapter 3.2.6 we describe how systemic *Bmal1* deletion results in exacerbated IMQ-induced ISG expression in the mouse skin, including the epidermis. We aimed to identify the possible mechanism(s) by which BMAL1 restrains IMQ-induced ISG expression; we found data from two BMAL1 ChIP experiments that were performed at time points throughout the day/night cycle in mouse liver. In Rey et al. (2011), there were 13 BMAL1-bound ISGs (Figure 5.1A) and in Koike et al. (2012) there were 32 BMAL1-bound ISGs (Figure 5.1B), 11 of which exhibited diurnal mRNA expression in the liver (Koike et al., 2012). Out of these genes, we have identified genes whose encoded proteins participate in the IFN-induced feed-forward loop promoting ISG expression (Table 5.1). Thus it is possible that, by binding to the promoter(s) of one or more of these genes in a diurnal fashion, BMAL1 acts as a negative regulator of ISG expression. The normalized expression of these BMAL1-bound and -unbound ISGs from our previous microarray experiment in the whole skin illustrates that BMAL1 bound ISGs generally have

higher gene expression compared to the genes that are not BMAL1 targets (Figure 5.1C; data originally plotted in Figure 3.2.1C and 3.2.6). In Wt mice, 77 ISGs were upregulated on average 1.2 fold or more after 1 day of 1% IMQ applied during the day (ZT01, ZT07) compared to the night (ZT13, ZT19), as described in Figure 3.2.1. Out of these diurnally-induced genes, 58 of them were upregulated by 1.2 fold or greater in *Bmal1* KO mice compared to Wt after 1 day of 1% IMQ treatment, and 12 of them were shown to be targets for BMAL1 binding (Koike et al., 2012, Rey et al., 2011). The genes *Cfb, Ddx58, Parp9, Uba7, Rtp4, Gch1* were identified as BMAL1 binding targets (Koike et al., 2012), upregulated in *Bmal1* KO mice compared to Wt after 1 day of 1% IMQ, and were induced 1.2 fold or more after 1 day of daytime 1% IMQ treatment compared to nighttime 1% IMQ treatment. Thus, the proteins encoded by these genes are attractive candidates for BMAL1-regulated mediators of the IMQ-induced ISG response. In the sections below, we summarize these genes and associated pathways. These results are also summarized in Table 5.1.

PI3K pathway

TLR7/8-mediated ISG expression depends on the activation and translocation of IRF7 and STAT1 to the nucleus and the Phosphatidylinositide-3-kinase (PI3K) pathway is critical for the nuclear translocation of IRF7, at least in human pDCs (Guiducci et al., 2008; Rhee et al., 2003). We identified two PI3K subunits, *Pik3r1* and *Pik3ap1* that are bound by BMAL1 and have diurnally oscillating mRNA levels in mouse liver under homeostasis (Koike et al., 2012) (Figure 5.1E). *Pik3ap1*, but not *Pik3r1*, also has diurnally oscillating mRNA in the mouse skin under homeostasis (Geyfman et al., 2012). In our experiments, *Pik3ap1* was induced 2 fold after 1 day

of 1% IMQ in Wt mice, and was 3 fold higher in *Bmal1* KO skin compared to Wt after 1 day of 1% IMQ (Figure 5.1D).

IFN/JAK/STAT Pathway

IMQ induces type I IFNs which bind to IFN receptors (IFNAR1/2) in a paracrine and/or autocrine manner, leading to activation of JAK1 and TYK2, STAT1/2 phosphorylation and nuclear translocation, and formation of the ISGF3 complex (STAT1-STAT2-IRF9) which directly activates the transcription of ISGs. There is evidence that genes encoding proteins within this pathway may be directly regulated by BMAL1. *Ifnar2* has been identified as a target for BMAL1 binding (Koike et al., 2012) and its mRNA is diurnally expressed in both the mouse liver and skin under homeostasis (Koike et al., 2012; Geyfman et al., 2012).

PARP9 acts as a chaperone facilitating the interaction between DTX3L and STAT1 thereby enhancing STAT1-mediated ISG expression through a currently unknown mechanism (Zhang et al., 2015). BMAL1 binds to the *Parp9* gene in a diurnal fashion; and *Parp9* mRNA oscillates in mouse liver (Koike et al., 2012) (Figure 5.1F). In our experiments, *Parp9* was induced 1.75 fold in the skin of *Bmal1* KO mice compared to Wt after 1 day IMQ (Figure 5.1D). BMAL1 also binds to the *Jak1* gene (Koike et al. 2012; Rey et al. 2011); however, *Jak1* mRNA does not oscillate diurnally in the liver or skin under homeostasis (Koike et al., 2012; Geyfman et al., 2012; Wang et al., 2017).

ISGylation pathway

ISGylation is a process similar to ubiquitination that involves the protein ISG15 directly binding to protein targets, thereby increasing the stability and/or activity of some proteins, including Irf3, JAK1, STAT1 and inhibiting the activity of others, for example, *Trim25* (Zhang et al., 2011). When IRF3 is stabilized, it complexes with IRF7 and binds to the IFN-β promoter and induces its expression (Wathelet et al., 1998). IRF3 can also directly activate a subset of ISGs in the absence of IFN (Guo et al., 2000; Mossman et al., 2001). The importance of the ISGylation pathway in the IFN/JAK/STAT pathway is highlighted in studies in which ISGylation is constitutively active (in the absence of de-ISGylation proteins), JAK1 and STAT1 exhibit prolonged phosphorylation activation, as well as DNA binding of STAT1 (Malahkova et al., 2003). Furthermore, mice lacking the ability to ISGylate fare worse when faced with influenza B virus infection due to an inability to mount anti-viral responses (Malahkova et al., 2003).

Uba7 (also known as UbE1L) is an important player in the ISGylation pathway as it activates the key ISGylation factor, ISG15 (Wathelet et al., 1998; Malahkova et al., 2003). We identified *Uba7* as target for BMAL1 binding; *Uba7* also exhibits oscillating mRNA levels in mouse liver (Koike et al., 2012). In our experiments, *Uba7* and *Isg15* were upregulated 2 fold and 1.2 fold, respectively, in *Bmal1* KO compared to Wt after 1 day of 1% IMQ treatment (Figure 5.1D). In addition, *Jak1* and *Stat1* are direct targets of ISG15 (Malakhov et al., 2003).

5.4 Conclusions and Future Directions

Mice with disturbed circadian rhythms have increased susceptibility to viral infections (Edgar et al., 2016; Ehlers et al., 2016; Msjumdar et al., 2017). It has been suggested that this effect may

be due to BMAL1 controlling the expression of host anti-viral genes (or suppressing pro-viral genes) (Msjumdar et al., 2017). However, our data and a study by Ehlers et al. (2017) show the opposite, in that, mice lacking *Bmal1* have exacerbated ISG expression after TLR stimulation. In our IMQ model, we are able to separate the effects of intrinsic TLR/IFN pathway activation from the influence of ongoing viral replication. Our study also uses an agonist specific for a single TLR (TLR7), while viral infections quite often activate multiple TLRs, cytosolic RNA helicases (e.g. MDA5, RIG-I, LGP2) and NOD-like receptors, yielding pleotropic effects. Thus, we are the first to show that the increased susceptibility to viral infection in *Bmal1* KO mice is not due to intrinsic defects in activation of the IFN pathway, as previously suggested (Msjumdar et al., 2017; Edgar et al., 2016). We speculate that one or more of the following situations may explain the increased susceptibility to viral infections observed in the *Bmal1* KOs: **(1)** While IFN-activated pathways protect against pathogens and cancer, excessive IFN responses make pathologies worse by reducing the killing strength of the adaptive immune system; thus, the anti-viral power of the IFN-activated pathways requires a balance between activating signals and inhibitory mechanisms (Porritt et al., 2015). For example, during lymphocytic choriomeningitis virus infection, chronic IFN signaling suppresses the adaptive immune system, allowing more virally infected cells to survive (Teijaro et al., 2013). Additional evidence supporting the immunosuppressive function of type I IFNs is seen when patients with relapsing-remitting multiple sclerosis are treated with recombinant IFN-β, which suppresses T cell activity and leads to better prognosis (Dhib-Jalbut and Marks, 2010). **(2)** *Bmal1* deletion results in upregulation of the core clock gene CLOCK (Lin et al., 2009; Geyfman et al., 2012); CLOCK has been shown to associate with the viral transcriptional complex of the herpes virus to mediate viral gene expression (Kalamvoki et al., 2010, 2011). **(3)** The circadian clock controls the expression of

approximately 10% of the genome, including genes important for protein biosynthesis. Cells lacking circadian clocks have elevated expression of certain protein biosynthesis enzymes which may facilitate greater production of viral gene products (Edgar et al., 2016).

Further ChIP experiments on immune cell populations from IMQ-treated Wt and control mice are necessary in order to address the potential regulatory interaction(s) of BMAL1 with genes encoding master regulators of the TLR-activated ISG response. These studies will shed light on previously unknown functions of the core clock protein in modulating important biological processes including protection against cancers, viral, and bacterial infections. Our study illustrates for the first time that BMAL1 negatively regulates ISG expression in the context of TLR activation.

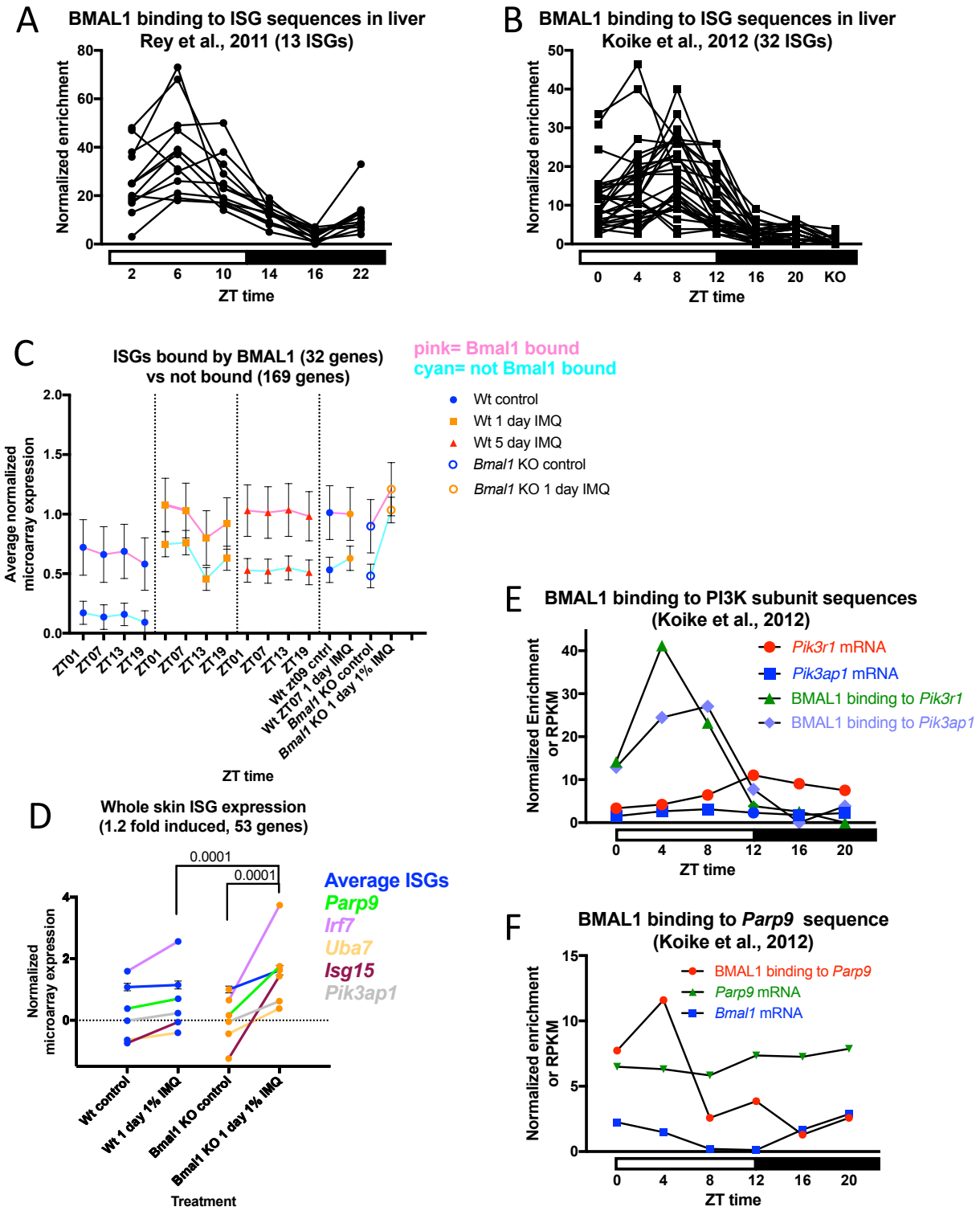

Figure 5.1 BMAL1 binds to interferon-sensitive genes. **(A)** BMAL1 binding strength to ISG gene sequences identified as BMAL1 bound at time points throughout the day-night cycle in mouse liver. Original BMAL1 ChIP data published by Rey et al., 2011. **(B)** BMAL1 binding strength to ISG gene sequences identified as BMAL1 bound at time points throughout the day-night cycle in mouse liver, and in *Bmal1* KO (KO) liver. **(C)** Average normalized whole skin

microarray expression of ISGs (from Figure 3.2.1C and Figure 3.2.7A). Genes identified as BMAL1 binding targets in (A) and/or (B) are averaged and connected by pink lines, and genes not identified as BMAL1 bound are averaged and connected by cyan lines. **(D)** Average normalized whole skin microarray expression of ISGs from Wt and systemic *Bmal1* KO mice treated with 1% IMQ for 1 day at ZT09 (blue lines). Expression of individual BMAL1-bound ISGs: *Parp9* (green lines), *Uba7* (gold lines), *Pik3ap1* (grey lines), and ISGs without BMAL1 binding: *Irf7* (pink lines), *Isg15* (purple lines), are plotted. **(E)** BMAL1 ChIP reads for PI3K subunit genes (*Pi3kr1* and *Pik3ap1*) and PI3K subunit mRNA expression throughout the day-night cycle in mouse liver. **(F)** BMAL1 binding strength to *Parp9* and *Bmal1* gene and *Parp9* mRNA expression throughout the day-night cycle in mouse liver. (B, E, F) Original BMAL1 ChIP and mRNA data published by Koike et al., 2012.

Table 5.1 Candidate BMAL1-regulated TLR7/IFN pathway activators

Pathway/ Genes	Gene	Protein function	Bmal1 bound in liver under homeostasis	Diurnal mRNA in liver under homeostasis	Diurnal mRNA in whole skin under homeostasis	Upregulated in *Bmal1* KO after IMQ	mRNA upregulated in the skin by IMQ
PI3K pathway	*Pik3r1*	nuclear trafficking of IRF7[6]	yes[5]	yes[5]	yes[4,8]	no	no
	Pik3ap1		yes[5]	yes[5]	yes[4,8]	3 fold	2 fold
ISGylation pathway	*Uba7*	Activates ISG15	Yes[5,7]	no	yes[8]	2 fold	2 fold
	Isg15	targets Jak1 and Stat1[1], Stabilizes certain ISGs (IRF3)[2]	no	no	yes[8]	1.5 fold	2.5 fold
IFNAR/ JAK/STAT pathway	*Ifnar2*	Senses IFN-α/β	yes[5]	no	yes[4,8]	1.18 fold	1.5 fold
	Parp9	STAT1 nuclear localization[3]	yes[5]	yes[5]	yes[4,8]	2.3 fold	4 fold
	Jak1	Signal transduction	yes[5,7]	yes[5]	no	no	no
	Jak2		no	yes[5]	no	no	no

[1] Giannakopoulos et al., 2005
[2] Shi et al., 2010
[3] Zhang et al., 2015
[4] Geyfman et al., 2012
[5] Kioke et al., 2012
[6] Guidducci et al., 2008
[7] Rey et al., 2011
[8] Wang et al., 2017

Chapter 6: Methods

Restricted feeding protocol

Twenty-three day old male C57BL/6NCrl mice (Charles River Laboratories, strain code 027) were acclimated to the mouse facility for 1 to 2 weeks before starting the RF experiments. The mice were housed under 12h:12h light/dark cycles (Light on at 6:30am, ZT0, and off at 6:30pm, ZT12) with free access to water during the whole experiment, and free access to food before initiation of the RF experiments. Regular chow was used in all experiments. The RF schedules were carried out for 18 to 21 days for the RNA-seq, qPCR and cell proliferation experiments (the first RF experiment from Chapter 2) and 21 to 26 days for the DNA damage and body weight/food intake data (the second RF experiment from Chapter 2). In the first RF experiment, EN mice had free access to food from ZT12 for 4 hours during the first 8 days, but after that were given the same amount food as was eaten by ED mice. Slight modifications to the RF schedules in the second RF experiment were as follows: The mice were weighed every other day immediately prior to daily food availability. Each day, ED and MD mice were given access to 20g of chow for 4 hours and leftover food was measured. The average food consumed per mouse in ED and MD was given to EN mice beginning at ZT12. Because EN mice ate all the food they received during the first 4 hours of food availability, EN food intake (Figure 2.2.2A) was represented as the food weight they received. In both experiments, skin was sampled at the end of the experiment during the second telogen when mice were at around postnatal day 54; the telogen state of the skin was verified by histology. All procedures were approved by the Institutional Animal Care and Use Committee of the University of California, Irvine (approval number 2001-2239).

Cell proliferation assays

Four hours prior to sampling, 50 μg/g BrdU was injected intraperitoneally. The histological staining for BrdU was performed as previously described (Geyfman et al., 2012). BrdU-positive and BrdU-negative cells were quantified with ImageJ with the observer blind to experimental conditions.

Quantitative PCR

Total RNA from whole dorsal back skin was purified with TRIzol Reagent (Life Technologies), cDNA was synthesized with iScript cDNA Synthesis Kit (Bio-Rad) and qPCR was performed with SsoFast EvaGreen/Probes Supermix (Bio-Rad). The Taqman probes for *Per2* (Mm00478113.m1), and *Irf7* (Mm00516793_g1) were from Applied Biosystems. Primers for *Per1* and *Dbp* were from PrimerBank (Wang et al., 2012) (ID: 26349399a1 for *Per1* and 8393240a1 for *Dbp*). The *Xpa* primer sequences for the last exon (exon 6) of *Xpa* were (5'-3') ATTGCGGCGAGCAATAAGAAG and ACAAGGTACAAGTCTTGCGGT (Eurofins). Target genes are normalized to mouse Mouse GAPDH Endogenous Control (Thermo Fisher Scientific).

Phase and peak statistics on qPCR and cell proliferation

The biological replicates of each time point of each RF schedule were assigned to 4 sets of artificial time series by random permutation and the peak time, mean and peak expression of each time series was calculated with the cosinor function of psych package (Revelle, 2016). The peak value was calculated as mean × (1+amplitude). The phase shift between any two RF schedules was calculated using the peak time of the curves in the same set, so that 4 replicates of

the peak time, average value, peak value and peak shift were produced at each permutation. The calculation of the mean and standard deviation of peak time as well as the Watson-Williams test of difference between peak time means and between the shifts was done with the circular package (Agostinelli and Lund, 2013). The calculation and test were done for 100 permutations and the average of the mean, SEM and the P-values were presented.

Stranded total RNA sequencing

Total RNA from mouse whole back skin with RNA integrity number (RIN) higher than 6.5 were pooled, treated with RNase-Free DNase (Qiagen cat. No. 79254), and cleaned with RNeasy Mini Elute Cleanup Kit (Qiagen). Library was constructed with TruSeq Stranded Total RNA Sample Prep Kit (Illumina) and sequenced with Hiseq 2500 (Illumina).

Analysis of RNA-Seq data

RNA-Seq short reads were mapped to mouse genome mm10 by Tophat2 (Kim et al., 2013), and rRNA reads were removed from the bam file via RSeQC (Wang et al., 2012). The reads with mapping quality less than 5 were removed with SAMtools (Li et al., 2009) (Table 2.2.1). Then the exon and intron gene reads and the reads for the antisense region of the whole gene body were counted with HOMER (Heinz et al., 2010). Transcripts were annotated using the UCSC known canonical gene set (31,872 total; 22,526 with introns). The reads were normalized into RPKM (Reads Per Kilobase per Million) by CQN (Hansen et al., 2012). The data analysis thereafter was performed with R (Ihaka and Gentleman, 1996; R Core Team, 2014), if not differently specified.

Identification of diurnal genes in whole skin RNA-seq data

Circadian genes identified in each of four algorithms, ARSER (Yang and Su, 2010), Lomb-Scargle (Glynn et al., 2006; Lomb, 1976), JTK-Cycle (Hughes et al., 2010) and sinusoid curve fitting (Geyfman et al., 2012), were combined to generate one circadian gene list. The exon reads from EN were ranked by the p-value of each method and compared with the genes circadian in telogen skin (Geyfman et al., 2012), or circadian in at least seven other tissues (Yan et al., 2008). The ratio of reference genes (positive found ratio, PFR) was found within a sliding window of 100 genes moving from the top (most significant p-values) for each method. Then, the PFRs of each method's list were smoothed using the loess function in R base. A p-value cutoff was chosen for each method so that the smoothed PFR was high enough to be significant compared to a random ordering of genes, using a permutation test with a p-value cutoff of $P < 0.01$. These cutoffs were applied to all transcripts for each method, and transcripts identified by at least one of these methods were incorporated into the final circadian list. Because each algorithm has pros and cons (Deckard et al., 2013), combining the different methods using PFR to determine the cutoffs in a consistent way yielded a more comprehensive circadian list. The peak time predicted by Lomb-Scargle method (Glynn et al., 2006; Lomb, 1976) was adopted for the phase shift analysis.

Identification of feeding-affected genes

Whole skin RNA-seq exon reads from EN, ED and MD were re-grouped according to the feeding time (FT) (FT0 being the onset of feeding, FT4 being 4 hours after the onset of feeding, FT8 being 8 hours after the onset of feeding, for each particular RF schedule) and then averaged. Feeding-affected genes were identified by comparing RNA-seq expression values at FT0 (ZT4

and ZT28 of MD, ZT12 for EN, ZT0 and ZT24 for ED), FT4 (ZT8 of MD, ZT16 for EN, ZT4 and ZT28 for ED) and FT8 (ZT12 of MD, ZT20 for EN, ZT8 for ED) by one-way ANOVA. The higher ratio out of the FT8/FT0 and FT4/FT0 ratios was used to represent the fold change in gene expression after feeding.

Functional enrichment analysis

Gene ontology annotations were downloaded on Oct 1st 2014 from EBI (ftp://ftp.ebi.ac.uk/pub/databases/GO/goa/MOUSE/gene_association.goa_mouse.gz) and MGI (ftp://ftp.informatics.jax.org/pub/reports/gene_association.mgi). Annotations were combined to get a more comprehensive list of gene sets. Fisher's exact test was employed for enrichment test and the IEA annotations were included.

UVB-induced DNA damage assays

Two days before the end of the RF experiment, mice were anesthetized by intraperitoneal injection of ketamine (100 mg/kg) and xylazine (10 mg/kg) and then their back skin was shaved using electric clippers during a time that would not interfere with their feeding schedules. A single dose of 500 J/m^2 was applied to the mice 15 minutes before sampling as described previously (Geyfman et al., 2012), at ZT9 or ZT19. Whole back skin DNA was isolated with QIAamp DNA Mini Kit (Qiagen cat. No. 51306). ELISA was employed to detect CPDs and (6-4)PP and with antibodies from Cosmo Bio Co. (NMDND001 for CPDs and NMDND002 for (6-4)PPs) following the manufacture's protocol.

Skin histology measurement

The dorsal skin of the mice used in the second RF experiment was collected, fixed in 10% formalin for 48 hours, ethanol dehydrated and embedded in paraffin. After sectioning, dewaxing and rehydrating, staining with H&E was performed. Twenty-fold magnified mosaic images were acquired on a BZ-X710 All-in-one Fluorescence Microscope (Keyence), with at least 1,000 μm skin length per image. Histological measurements were performed by a blinded researcher using ImageJ software. At least 2 images per mouse were analyzed and 15 measurements for each skin compartment per image were averaged.

Accession Numbers for whole skin RNA-seq data

RNA-Seq data is archived in a publicly accessible database at Gene Expression Omnibus (http://www.ncbi.nlm.nih.gov/geo) with accession number GEO: GSE83855.

Animals for 1% IMQ experiments

Mice were housed under 12:12 LD cycles with food and water *ad libidum*. Lights were switched on at 6 a.m. and off at 6 p.m.. Zeitgeber time (ZT) refers to lights on = ZT0 and lights off = ZT12. All mice used in microarray experiments were male C57BL/6J from Jackson Laboratories. Mice were housed under 12:12 LD cycles for at least 7 days prior to the beginning of experiments. Animal handling after lights off was in red light. Mice with signs of skin injury were removed from the study. The *K14Cre* mouse was generated as described in (Andl et al., 2004). *Bmal1* germline KO mice were generated as described in (Bunger et al. 2000). The *Bmal1* floxed mouse was generated as described in (Marcheva *et al*. 2010). To produce CD11cCre*Bmal1*$^{fl/fl}$ mice, C57BL/6J-Tg(Itgaxcre,-EGFP)4097Ach/J mice (Jackson Laboratories) were bred with *Bmal1* floxed mice. Mice were maintained according National

Institutes of Health guidelines and approved by the Institutional Animal Care and Use Committee of the University of California, Irvine (protocol number 2001-2239).

IMQ Treatment

All mice (including controls) were anesthetized by intraperitoneal (i.p.) injection with ketamine (100mg/kg) and xylazine (10mg/kg) and shaved two days prior to experiment initiation. To make 1% IMQ cream, 5% pharmaceutical IMQ (Perrigo brand) was diluted in a ratio of 1:4 with CVS Vitamin E Plus Moisturizing Cream™. The 1% of the stock 5% cream was weighed out in 0.0625g aliquots to apply to the back and 0.031g aliquots to apply to the ears and shaved backs of mice. For specimen collection, mice were euthanized by CO_2 followed by cervical dislocation. Whole back skin were collected in 10% formalin, fixed for 2 days at 4° C, and ethanol dehydrated by applying gradients of 25% ethanol, 50% ethanol, 70% ethanol and 80% ethanol at room temperature for every two hours. Samples were then embedded into Optimal Cutting Temperature compound (OCT) and sliced into 8 μm sections onto Superfrost™ Plus™ slide (Thermo Fisher) and stored at -80°C.

Whole skin RNA isolation in IMQ experiments

RNA extraction is performed on whole skin with TRIzol™ reagent (Invitrogen, Carlsbad, CA) following manufacturers' recommendations; briefly, skin is suspended in 1-2ml of trizol and homogenized using Precellys tubes (Burtin), cellular debris is then removed by centrifugation at 12,000g for 10 minutes, total RNA is then extracted using chloroform followed by purification using Zymogen's Direct-zol RNA Isolation kit. RNA was resuspended in RNase-free water (Ambion) and the quality is checked on an Agilent Bioanalyzer 2100 (Agilent Technologies).

Microarray analysis of whole skin RNA

Whole skin RNA from 4-7 mice with RNA Integrity numbers (RINs) above 7 were pooled. 200 ng of total RNA was hybridized to an Affymetrix Mouse Gene 1.0 ST arrays. All reads were Plier normalized, and duplicate reads and genes with expression level below 50 were removed. Expression was Log_2 transformed and mean centered across all arrays being compared.

Single cell sequencing of adult mouse epidermal cells

Adult male mice were treated as described in Methods and epidermal cells were isolated after 6 hours of 1% IMQ treatment. Live (double negative for DAPI and BV510 Viability dye (Tonbo Biosciences)), single epidermal cells were sorted and resuspended at 1x 10^6 cells/mL in 0.04% UltraPure BSA and loaded into the Chromium™ Single Cell platform at a target yield of 6,000 cells. Sequencing was performed multiple times if necessary to obtain a depth of approximately 2,000 median genes per cell. Alignment and data filtering was done using Cell Ranger (10x Genomics). Genes were filtered based on being expressed by a minimum of 4 cells. Cells were filtered based on having at least 600-5,300 genes expressed, with less than 10% of expressed genes being mitochondria-associated genes. Cells were clustered based on global gene expression using Seurat (Satija et al., 2015) and t-distributed stochastic neighbor embedding (t-SNE) plots were annotated by hand using the data set by Jooste and colleagues (2016) as a reference.

Single cell sequencing Irf7 graphs

In epidermal samples from IMQ treated and control mice, expression of a gene is defined as

($\log_2$(UMI (unique molecular identifier) +1) > 0.5). The number of cells expressing a gene characteristic of a specific cell population of interest (such as *Krt5* for basal KCs, or *Krt1* for differentiated KCs, *Cd207* for LCs, ect.) was denoted by n1. Among these "positive" cells (e.g. *Krt5*+ cells), the number of cells expressing *Irf7* was denoted by n2. Thus, the percentage of *Irf7*+ cells among the cells positive for a gene of interest (for example, *Krt5*+ cells) was calculated with the equation n2/n1*100%. The expression levels of *Irf7* was divided into different bins (bin size = 0.25). Then the proportion of cells in each bin was counted and the histogram plot of *Irf7* was created for each cell cluster specified.

Immunofluorescent (IF) staining of back skin sections

Superfrost™ Plus™ slides stored at -80°C containing three 8 μm sections of mouse back skin were placed in a 37°C incubator for 10 minutes before they were submerged in acetone for 10 minutes at -20°C. The slides were washed in PBS twice, and the skin samples on each slide were incubated at room temperature for 1 hour in blocking buffer containing 2% BSA and 0.1% Tween 20 with 1:200 Fc block (Anti-CD16/32; Tonbo Biosciences), and 10% goat serum (Vector Labs). Slices of skin were then stained at 4°C overnight with 1:200 rat anti-CD45 (Life Technologies) and 1:500 Rabbit Anti-mouse Loricrin (Abcam), 1:200 Anti-mouse Ly-6G (Gr-1) (eBioscience) and 1:500 Anti- Rabbit anti-Mouse Keratin 5 (Abcam) or, 1:250 Rat Anti-Mouse F4/80 (Life Technologies) and 1:500 Rabbit Anti-mouse Keratin 17 (Cell Signaling). The next day, slides were rinsed 3 times in PBS and then secondary antibodies (all from Invitrogen) were applied at 1:1000. The slides were rinsed again then mounted with HardSet™ Mounting media with DAPI (Vectashield®). All slides were imaged within 48 hours.

Immune Cell Quantification by Immunofluorescence microscopy of skin sections

ImageJ was used to quantify the number of immune cells. All data represents cells counted per unit area in μm^2. The statistical analyses were performed in Graphpad Prism using the paired Student's t-test for two-group comparisons (e.g. Wt versus *Bmal1* KO, or control versus IMQ). Two-way ANOVA was used to test significant differences between treatments (control, 1 day 1% IMQ, 5 days 1% IMQ), and one-way ANOVA was used to test significant differences across the day-night cycle.

5-ethynyl-2′-deoxyuridine (EdU) Incorporation Assay to Measure DNA Synthesis

Two hours prior to sacrifice, mice were weighed and injected with EdU at 5 mg/kg of body weight. Mice were euthanized by cervical dislocation. Back skin was fixed in 10% formalin for 2 days at 4°C, and ethanol-dehydrated by applying solutions of 25% ethanol, 50% ethanol, 70% ethanol and 80% ethanol at room temperature for every two hours. Samples were then embedded into paraffin and sectioned into a measurement of 8 μm.

Cell Proliferation Measurement

To measure cell proliferation induced by IMQ, paraffin sections were stained for EdU using the Click-iT® EdU Imaging kit (Thermo Fisher Scientific). Slides were first dipped in xylene and multiple rounds of ethyl alcohol followed by blocking in phosphate buffered saline (PBS) containing 3% bovine serum albumin (BSA) and 0.1% Tween-20 (PBT). After permeabilizing with 1x PBS containing 0.5% Triton X-100, samples were washed with a PBT and 3% BSA mixture. The Click-iT™ reaction cocktail was made following the EdU kit protocol. After applying the reaction cocktail, the slides were incubated for 30 minutes in the dark then washed

in 1x PBS with 3% BSA. Images of the samples were taken at 10x magnification using a Spinning Disk Confocal Microscope™ (Zeiss). EdU^+ cells were counted with ImageJ software. The epidermal lengths and cell count were recorded and used to calculate the average cell proliferation per length of epidermis for each mouse.

Epidermal Width Measurement

H&E staining was used to determine epidermal width changes as indications of inflammation. Paraffin sections (8 μm) were first put into a 65°C incubator for 1 hour. They are then dipped in the order of xylene, ethyl alcohol, distilled water, hematoxylin, water, bluing agent, 1% diluted eosin, water, ethyl alcohol, isopropyl, and xylene. After mounting and drying, epidermal widths were measured in 15 equally proportioned segments across the length of the photos taken using Leica™ light microscope at 10x magnification. The data was averaged for each sample.

IFN-β Serum ELISA

Two or 6 hours after 1% IMQ treatment, mice were sacrificed by C02 inhalation and peripheral blood was collected by cardiac puncture. Blood was allowed to clot and then centrifuged at 5,000g for 10 minutes. The serum was collected and stored at 80°C until ready for further use. The serum was later run on ELISA plates: IFNα/IFNβ 2Plex Mouse ProcartaPlex Panel (eBioscience) (for 2 and 6 hours post-1% IMQ samples), or Mouse IFN Beta ELISA kit (TCM, Serum) (PBL assay science) (for 1 day 1% IMQ samples). A standard curve was run to determine the concentrations of IFNα/β.

FACS sorting and flow cytometry of ear, dermis, and epidermal cells

For epidermal samples, mouse back skin was excised and dermal fat was scraped off with forceps. Skin was cut into 10cm^2 pieces and floated epidermal side upwards in 0.25% trypsin (Gibco™) for 2 hours at 37°C. Epidermis was then scraped into Accutase® Cell Detachment Solution and then disrupted using 3 mL syringes (BD). Dermal samples were further dissociated for two hours at 37°C in RPMI media (Gibco) containing 25 ug/mL Liberase TL (Sigma), 12 mM Sodium Pyruvate, 0.5M HEPES, 0.116 ug/mL DNAse I, and then processed with the GentleMACS machine (Miltenyi Biotec) on the mouse tumor setting. Epidermal or dermal cells were filtered 2 times through 70 μm filters, spun down at 600 g for 6 min, resuspended in 50 uL of 1:200 Fc block (anti-CD16/32 from Tonbo Biosciences):FACS buffer containing PBS, 2mM EDTA and 5% FBS, and Penicillin/Streptomycin. Cells were blocked on ice for 15 minutes, then 1 uL of each antibody (combinations of: Brilliant Violet 605™ Anti-mouse/human CD45R/B220 (Biolegend), APC Rat Anti-Mouse CD45 (BD Biosciences), Anti-Mouse CD11c PE-Cy7 (Tonbo Biosciences), PE/Dazzle™ 594 Anti-human/mouse CD49f (BioLegend), Anti-Mouse Ly-6G (Gr-1) redFluor™ 710 (Tonbo Bioscience), Anti-Mouse CD3e PerCP-Cy5.5 (Tonbo Biosciences), and in some experiments, antibodies against lineage (Lin) markers Anti-Mouse Ter19-PE and Anti-Mouse CD31-PE (both from eBioscience), were added and cells were incubated 25 minutes on ice in the dark. During the last 5 minutes of incubation, 1 mL of PBS was added and DAPI was added at a final concentration of 500 ng/uL, and 0.5 uL of BV510 viability dye (Tonbo Biosciences) was added. Cells were fixed with 1% paraformaldehyde and run on the Novoyte flow cytometer within 24 hours, or immediately FACS-sorted on the FACSaria Fusion (BD).

For ear cell analysis, mice were sacrificed and ears were collected and pulled dorsal and ventral halves were pulled apart with forceps. Ears were minced up in RPMI media (Gibco) containing 25 ug/mL Liberase TL (Sigma), 12 mM Sodium Pyruvate, 0.5M HEPES, 0.116 ug/mL DNAse I. Cell suspensions were shaken at 200 g for 45 minutes at 37°C, then run on the GentleMACS™ (Miltenyi Biotec) on the mouse tumor setting. Samples were incubated an additional 15 minutes at 37°C prior to neutralizing the dissociation by adding 10% FBS and 2 mM EDTA. Ear cells were centrifuged, filtered twice through 70 μm filters, blocked with Anti-CD16/32, stained and run on the cytometer(s) as described above.

Assessment of IRF7 nuclear translocation within skin cell subsets

Epidermal cell suspensions were prepared and stained for cell surface markers as described in *FACS sorting and flow cytometry of ear, dermis, and epidermal cells*. For viability staining, cells were incubated 1:1000 with 0.5 uL of BV510 viability dye (Tonbo Biosciences), rinsed, rinsed twice in FACS buffer and then permeabilized using the Foxp3 permeabilization kit (eBiosciences) and stained with Anti-IRF-7 (pS477/pS479) PE, human and mouse (Miltenyi Biotec) and AlexaFluor® 488 anti-IRF7 (BioLegend). Immediately prior to acquisition on the ImageStream technology flow cytometer (Amnis Corporation), cells were incubated in 5,000 ng/uL DAPI to label all nuclei. To quantify nuclear translocation of total and p-IRF7, we used the. IDEAS® analysis software was used to calculate the nuclear translocation index (a measurement for amount of nuclear translocation of a marker in cells) of total IRF7 and p-IRF7, independent of nuclear shape or cytoplasmic size. Statistical analysis was performed using Student's paired t-test.

REFERENCES

Adamovich, Y., Rousso-Noori, L., Zwighaft, Z., Neufeld-Cohen, A., Golik, M., Kraut-Cohen, J., . . . Asher, G. (2014). Circadian clocks and feeding time regulate the oscillations and levels of hepatic triglycerides. *Cell Metab, 19*(2), 319-330. doi:10.1016/j.cmet.2013.12.016

Agostinelli, C., & Lund, U. (2013). R package 'circular': Circular Statistics (version 0.4-7) (Version 0.4-7). Retrieved from https://r-forge.r-project.org/projects/circular/

Akira, S., & Takeda, K. (2004). Toll-like receptor signalling. *Nat Rev Immunol, 4*(7), 499-511. doi:10.1038/nri1391

Andl, T., Ahn, K., Kairo, A., Chu, E. Y., Wine-Lee, L., Reddy, S. T., . . . Millar, S. E. (2004). Epithelial Bmpr1a regulates differentiation and proliferation in postnatal hair follicles and is essential for tooth development. *Development, 131*(10), 2257-2268. doi:10.1242/dev.01125

Ando, N., Nakamura, Y., Aoki, R., Ishimaru, K., Ogawa, H., Okumura, K., . . . Nakao, A. (2015). Circadian Gene Clock Regulates Psoriasis-Like Skin Inflammation in Mice. *J Invest Dermatol, 135*(12), 3001-3008. doi:10.1038/jid.2015.316

Armstrong, A. W., Harskamp, C. T., & Armstrong, E. J. (2013). Psoriasis and metabolic syndrome: a systematic review and meta-analysis of observational studies. *J Am Acad Dermatol, 68*(4), 654-662. doi:10.1016/j.jaad.2012.08.015

Armstrong, B. K., & Kricker, A. (2001). The epidemiology of UV induced skin cancer. *J Photochem Photobiol B, 63*(1-3), 8-18.

Atkinson, H. J., & Babbitt, P. C. (2009). Glutathione transferases are structural and functional outliers in the thioredoxin fold. *Biochemistry, 48*(46), 11108-11116. doi:10.1021/bi901180v

Barnes, P. J. (1985). Circadian variation in airway function. *Am J Med, 79*(6A), 5-9.

Bass, J. (2012). Circadian topology of metabolism. *Nature, 491*(7424), 348-356. doi:10.1038/nature11704

Baumann, A., Gönnenwein, S., Bischoff, S. C., Sherman, H., Chapnik, N., Froy, O., & Lorentz, A. (2013). The circadian clock is functional in eosinophils and mast cells. *Immunology, 140*(4), 465-474. doi:10.1111/imm.12157

Baydas, G., Gursu, M. F., Yilmaz, S., Canpolat, S., Yasar, A., Cikim, G., & Canatan, H. (2002). Daily rhythm of glutathione peroxidase activity, lipid peroxidation and glutathione levels in tissues of pinealectomized rats. *Neurosci Lett, 323*(3), 195-198.

Baydas, G., Yilmaz, O., Celik, S., Yasar, A., & Gursu, M. F. (2002). Effects of certain micronutrients and melatonin on plasma lipid, lipid peroxidation, and homocysteine levels in rats. *Arch Med Res, 33*(6), 515-519.

Bego, M. G., Mercier, J., & Cohen, E. A. (2012). Virus-activated interferon regulatory factor 7 upregulates expression of the interferon-regulated BST2 gene independently of interferon signaling. *J Virol, 86*(7), 3513-3527. doi:10.1128/JVI.06971-11

Bellet, M. M., Deriu, E., Liu, J. Z., Grimaldi, B., Blaschitz, C., Zeller, M., . . . Sassone-Corsi, P. (2013). Circadian clock regulates the host response to Salmonella. *Proc Natl Acad Sci U S A, 110*(24), 9897-9902. doi:10.1073/pnas.1120636110

Birmachu, W., Gleason, R. M., Bulbulian, B. J., Riter, C. L., Vasilakos, J. P., Lipson, K. E., & Nikolsky, Y. (2007). Transcriptional networks in plasmacytoid dendritic cells stimulated with synthetic TLR 7 agonists. *BMC Immunol, 8*, 26. doi:10.1186/1471-2172-8-26

Bjarnason, G. A., & Jordan, R. (2002). Rhythms in Human Gastrointestinal Mucosa and Skin. *Chronobiology International, 19*(1), 129-140. doi:10.1081/CBI-120002595

Blanpain, C., & Fuchs, E. (2009). Epidermal homeostasis: a balancing act of stem cells in the skin. *Nat Rev Mol Cell Biol, 10*(3), 207-217. doi:10.1038/nrm2636

Brown, S. A., Zumbrunn, G., Fleury-Olela, F., Preitner, N., & Schibler, U. (2002). Rhythms of mammalian body temperature can sustain peripheral circadian clocks. *Curr Biol, 12*(18), 1574-1583.

Brown, W. R. (1991). A review and mathematical analysis of circadian rhythms in cell proliferation in mouse, rat, and human epidermis. *J Invest Dermatol, 97*(2), 273-280.

Buchakjian, M. R., & Kornbluth, S. (2010). The engine driving the ship: metabolic steering of cell proliferation and death. *Nat Rev Mol Cell Biol, 11*(10), 715-727. doi:10.1038/nrm2972

Buhr, E. D., & Takahashi, J. S. (2013). Molecular components of the Mammalian circadian clock. *Handb Exp Pharmacol*(217), 3-27. doi:10.1007/978-3-642-25950-0_1

Bunger, M. K., Wilsbacher, L. D., Moran, S. M., Clendenin, C., Radcliffe, L. A., Hogenesch, J. B., . . . Bradfield, C. A. (2000). Mop3 is an essential component of the master circadian pacemaker in mammals. *Cell, 103*(7), 1009-1017.

Burholt, D. R., Etzel, S. L., Schenken, L. L., & Kovacs, C. J. (1985). Digestive Tract Cell Proliferation and Food Consumption Patterns of Ha/Icr Mice. *18*(4), 369-386.

Calverley, P. M., & Walker, P. (2003). Chronic obstructive pulmonary disease. *Lancet, 362*(9389), 1053-1061.

Cho, H. Y., Jedlicka, A. E., Reddy, S. P., Kensler, T. W., Yamamoto, M., Zhang, L. Y., & Kleeberger, S. R. (2002). Role of NRF2 in protection against hyperoxic lung injury in mice. *Am J Respir Cell Mol Biol, 26*(2), 175-182. doi:10.1165/ajrcmb.26.2.4501

Chouela, E., Abeldaño, A., Pellerano, G., & Hernández, M. I. (2002). Diagnosis and treatment of scabies: a practical guide. *Am J Clin Dermatol, 3*(1), 9-18.

Clausen, O. P. F., Thorud, E., Bjerknes, R., & Elgjo, K. Circadian Rhythms in Mouse Epidermal Basal Cell Proliferation. doi:10.1111/j.1365-2184.1979.tb00154.x

Cleaver, J. E. (1968). Defective Repair Replication of DNA in Xeroderma Pigmentosum. *Nature, 218*(5142), 652-656.

Cretenet, G., Le Clech, M., & Gachon, F. (2010). Circadian clock-coordinated 12 Hr period rhythmic activation of the IRE1alpha pathway controls lipid metabolism in mouse liver. *Cell Metab, 11*(1), 47-57. doi:10.1016/j.cmet.2009.11.002

Damiola, F., Le Minh, N., Preitner, N., Kornmann, B., Fleury-Olela, F., & Schibler, U. (2000). Restricted feeding uncouples circadian oscillators in peripheral tissues from the central pacemaker in the suprachiasmatic nucleus. *Genes Dev, 14*(23), 2950-2961.

Dhib-Jalbut S., Marks S. (2010). Interferon-beta mechanisms of action in multiple sclerosis. *Neurology*, 74(Suppl 1):S17–S24.

Di Domizio, J., Blum, A., Gallagher-Gambarelli, M., Molens, J. P., Chaperot, L., & Plumas, J. (2009). TLR7 stimulation in human plasmacytoid dendritic cells leads to the induction of early IFN-inducible genes in the absence of type I IFN. *Blood, 114*(9), 1794-1802. doi:10.1182/blood-2009-04-216770

Dibner, C., Schibler, U., & Albrecht, U. (2010). The mammalian circadian timing system: organization and coordination of central and peripheral clocks. *Annu Rev Physiol, 72*, 517-549. doi:10.1146/annurev-physiol-021909-135821

Edgar, R. S., Stangherlin, A., Nagy, A. D., Nicoll, M. P., Efstathiou, S., O'Neill, J. S., & Reddy,

A. B. (2016). Cell autonomous regulation of herpes and influenza virus infection by the circadian clock. *Proc Natl Acad Sci U S A, 113*(36), 10085-10090. doi:10.1073/pnas.1601895113

Finkel, T. (2011). Signal transduction by reactive oxygen species. *J Cell Biol, 194*(1), 7-15. doi:10.1083/jcb.201102095

Fischer, T. W., Kleszczyński, K., Hardkop, L. H., Kruse, N., & Zillikens, D. (2013). Melatonin enhances antioxidative enzyme gene expression (CAT, GPx, SOD), prevents their UVR-induced depletion, and protects against the formation of DNA damage (8-hydroxy-2'-deoxyguanosine) in ex vivo human skin. *J Pineal Res, 54*(3), 303-312. doi:10.1111/jpi.12018

Fisher, G. J., Kang, S., Varani, J., Bata-Csorgo, Z., Wan, Y., Datta, S., & Voorhees, J. J. (2002). Mechanisms of photoaging and chronological skin aging. *Arch Dermatol, 138*(11), 1462-1470.

Fritz, V., & Fajas, L. (2010). Metabolism and proliferation share common regulatory pathways in cancer cells. *Oncogene, 29*(31), 4369-4377. doi:10.1038/onc.2010.182

Froy, O., Chapnik, N., & Miskin, R. (2005). Mouse intestinal cryptdins exhibit circadian oscillation. *FASEB J, 19*(13), 1920-1922. doi:10.1096/fj.05-4216fje

Gaddameedhi, S., Selby, C. P., Kaufmann, W. K., Smart, R. C., & Sancar, A. (2011). Control of skin cancer by the circadian rhythm. *Proc Natl Acad Sci U S A, 108*(46), 18790-18795. doi:10.1073/pnas.1115249108

Gaddameedhi, S., Selby, C. P., Kemp, M. G., Ye, R., & Sancar, A. (2015). The circadian clock controls sunburn apoptosis and erythema in mouse skin. *J Invest Dermatol, 135*(4), 1119-1127. doi:10.1038/jid.2014.508

George, T. C., Fanning, S. L., Fitzgerald-Bocarsly, P., Fitzgeral-Bocarsly, P., Medeiros, R. B., Highfill, S., . . . Lynch, D. H. (2006). Quantitative measurement of nuclear translocation events using similarity analysis of multispectral cellular images obtained in flow. *J Immunol Methods, 311*(1-2), 117-129. doi:10.1016/j.jim.2006.01.018

Geyfman, M., Kumar, V., Liu, Q., Ruiz, R., Gordon, W., Espitia, F., . . . Andersen, B. (2012). Brain and muscle Arnt-like protein-1 (BMAL1) controls circadian cell proliferation and susceptibility to UVB-induced DNA damage in the epidermis. *Proc Natl Acad Sci U S A, 109*(29), 11758-11763. doi:10.1073/pnas.1209592109

Gillette, M., & Sejnowski, T. (2005). *PHYSIOLOGY: Biological Clocks Coordinately Keep Life on Time*.

Girardi, M., Oppenheim, D. E., Steele, C. R., Lewis, J. M., Glusac, E., Filler, R., . . . Hayday, A. C. (2001). Regulation of cutaneous malignancy by gammadelta T cells. *Science, 294*(5542), 605-609. doi:10.1126/science.1063916

Glynn, E. F., Chen, J., & Mushegian, A. R. (2006). Detecting periodic patterns in unevenly spaced gene expression time series using Lomb-Scargle periodograms. *Bioinformatics, 22*(3), 310-316. doi:10.1093/bioinformatics/bti789

Guiducci, C., Ghirelli, C., Marloie-Provost, M. A., Matray, T., Coffman, R. L., Liu, Y. J., . . . Soumelis, V. (2008). PI3K is critical for the nuclear translocation of IRF-7 and type I IFN production by human plasmacytoid predendritic cells in response to TLR activation. *J Exp Med, 205*(2), 315-322. doi:10.1084/jem.20070763

Guo, J., Peters, K. L., & Sen, G. C. (2000). Induction of the human protein P56 by interferon, double-stranded RNA, or virus infection. *Virology, 267*(2), 209-219. doi:10.1006/viro.1999.0135

Haimovich, B., Calvano, J., Haimovich, A. D., Calvano, S. E., Coyle, S. M., & Lowry, S. F. (2010). In vivo endotoxin synchronizes and suppresses clock gene expression in human peripheral blood leukocytes. *Crit Care Med, 38*(3), 751-758. doi:10.1097/CCM.0b013e3181cd131c

Hansen, K. D., Irizarry, R. A., & Wu, Z. (2012). Removing technical variability in RNA-seq data using conditional quantile normalization. *Biostatistics, 13*(2), 204-216. doi:10.1093/biostatistics/kxr054

Hara, R., Wan, K., Wakamatsu, H., Aida, R., Moriya, T., Akiyama, M., & Shibata, S. (2001). Restricted feeding entrains liver clock without participation of the suprachiasmatic nucleus. *Genes Cells, 6*(3), 269-278.

Harden, J. L., Krueger, J. G., & Bowcock, A. M. (2015). The immunogenetics of Psoriasis: A comprehensive review. *J Autoimmun, 64*, 66-73. doi:10.1016/j.jaut.2015.07.008

Heib, V., Becker, M., Warger, T., Rechtsteiner, G., Tertilt, C., Klein, M., . . . Stassen, M. (2007). Mast cells are crucial for early inflammation, migration of Langerhans cells, and CTL responses following topical application of TLR7 ligand in mice. *Blood, 110*(3), 946-953. doi:10.1182/blood-2006-07-036889

Heinz, S., Benner, C., Spann, N., Bertolino, E., Lin, Y. C., Laslo, P., . . . Glass, C. K. (2010). Simple combinations of lineage-determining transcription factors prime cis-regulatory elements required for macrophage and B cell identities. *Mol Cell, 38*(4), 576-589. doi:10.1016/j.molcel.2010.05.004

Hemmi, H., Kaisho, T., Takeuchi, O., Sato, S., Sanjo, H., Hoshino, K., . . . Akira, S. (2002). Small anti-viral compounds activate immune cells via the TLR7 MyD88-dependent signaling pathway. *Nat Immunol, 3*(2), 196-200. doi:10.1038/ni758

Heng, T. S., Painter, M. W., & Consortium, I. G. P. (2008). The Immunological Genome Project: networks of gene expression in immune cells. *Nat Immunol, 9*(10), 1091-1094. doi:10.1038/ni1008-1091

Hirotsu, C., Rydlewski, M., Araújo, M. S., Tufik, S., & Andersen, M. L. (2012). Sleep loss and cytokines levels in an experimental model of psoriasis. *PLoS One, 7*(11), e51183. doi:10.1371/journal.pone.0051183

Hornung, V., Rothenfusser, S., Britsch, S., Krug, A., Jahrsdörfer, B., Giese, T., . . . Hartmann, G. (2002). Quantitative expression of toll-like receptor 1-10 mRNA in cellular subsets of human peripheral blood mononuclear cells and sensitivity to CpG oligodeoxynucleotides. *J Immunol, 168*(9), 4531-4537.

Huang, P., Ceccatelli, S., Håkansson, H., Grandison, L., & Rannug, A. (2002). Constitutive and TCDD-induced expression of Ah receptor-responsive genes in the pituitary. *Neurotoxicology, 23*(6), 783-793. doi:10.1016/S0161-813X(02)00040-2

Hughes, M. E., Hogenesch, J. B., & Kornacker, K. (2010). JTK_CYCLE: an efficient nonparametric algorithm for detecting rhythmic components in genome-scale data sets. *J Biol Rhythms, 25*(5), 372-380. doi:10.1177/0748730410379711

Ihaka, R., & Gentleman, R. (1996). R: A Language for Data Analysis and Graphics. *Journal of Computational and Graphical Statistics, 5*(3), 299-314.

Ikuta, T., Namiki, T., Fujii-Kuriyama, Y., & Kawajiri, K. (2009). AhR protein trafficking and function in the skin. *Biochem Pharmacol, 77*(4), 588-596. doi:10.1016/j.bcp.2008.10.003

Izumo, M., Pejchal, M., Schook, A. C., Lange, R. P., Walisser, J. A., Sato, T. R., . . . Takahashi, J. S. (2014). Differential effects of light and feeding on circadian organization of peripheral clocks in a forebrain Bmal1 mutant. *Elife, 3*. doi:10.7554/eLife.04617

Janich, P., Pascual, G., Merlos-Suárez, A., Batlle, E., Ripperger, J., Albrecht, U., . . . Benitah, S. A. (2011). The circadian molecular clock creates epidermal stem cell heterogeneity. *Nature, 480*(7376), 209-214. doi:10.1038/nature10649

Joost, S., Zeisel, A., Jacob, T., Sun, X., La Manno, G., Lönnerberg, P., . . . Kasper, M. (2016). Single-Cell Transcriptomics Reveals that Differentiation and Spatial Signatures Shape Epidermal and Hair Follicle Heterogeneity. *Cell Syst, 3*(3), 221-237.e229. doi:10.1016/j.cels.2016.08.010

Jouffe, C., Cretenet, G., Symul, L., Martin, E., Atger, F., Naef, F., & Gachon, F. (2013). The circadian clock coordinates ribosome biogenesis. *PLoS Biol, 11*(1), e1001455. doi:10.1371/journal.pbio.1001455

Kader, M., Smith, A. P., Guiducci, C., Wonderlich, E. R., Normolle, D., Watkins, S. C., . . . Barratt-Boyes, S. M. (2013). Blocking TLR7- and TLR9-mediated IFN-α production by plasmacytoid dendritic cells does not diminish immune activation in early SIV infection. *PLoS Pathog, 9*(7), e1003530. doi:10.1371/journal.ppat.1003530

Kalamvoki, M., Roizman, B. (2010). Circadian CLOCK histone acetyl transferase localizes at ND10 nuclear bodies and enables herpes simplex virus gene expression. *Proc Natl Acad Sci U S A,* 107(41):17721–17726. doi: 10.1073/pnas.1012991107

Kalamvoki, M., Roizman, B. (2011). The histone acetyltransferase CLOCK is an essential component of the herpes simplex virus 1 transcriptome that includes TFIID, ICP4, ICP27, and ICP22. *J Virol*, 85(18):9472–9477. doi: 10.1128/JVI.00876-11

Kang, T. H., Lindsey-Boltz, L. A., Reardon, J. T., & Sancar, A. (2010). Circadian control of XPA and excision repair of cisplatin-DNA damage by cryptochrome and HERC2 ubiquitin ligase. *Proc Natl Acad Sci U S A, 107*(11), 4890-4895. doi:10.1073/pnas.0915085107

Kaur, S., Zilmer, M., Eisen, M., Kullisaar, T., Rehema, A., & Vihalemm, T. (2001). Patients with allergic and irritant contact dermatitis are characterized by striking change of iron and oxidized glutathione status in nonlesional area of the skin. *J Invest Dermatol, 116*(6), 886-890. doi:10.1046/j.0022-202x.2001.01374.x

Khapre, R. V., Kondratova, A. A., Susova, O., & Kondratov, R. V. (2011). Circadian clock protein BMAL1 regulates cellular senescence in vivo. *Cell Cycle, 10*(23), 4162-4169. doi:10.4161/cc.10.23.18381

Kiessling, S., Dubeau-Laramée, G., Ohm, H., Labrecque, N., Olivier, M., & Cermakian, N. (2017). The circadian clock in immune cells controls the magnitude of Leishmania parasite infection. *Sci Rep, 7*(1), 10892. doi:10.1038/s41598-017-11297-8

Kiley, P. J., & Storz, G. (2004). Exploiting thiol modifications. *PLoS Biol, 2*(11), e400. doi:10.1371/journal.pbio.0020400

Kim, D., Pertea, G., Trapnell, C., Pimentel, H., Kelley, R., Salzberg, S. L., . . . Wold, B. (2013). TopHat2: accurate alignment of transcriptomes in the presence of insertions, deletions and gene fusions. *14*(4), R36.

Koca, R., Altin, R., Konuk, N., Altinyazar, H. C., & Kart, L. (2006). Sleep disturbance in patients with lichen simplex chronicus and its relationship to nocturnal scratching: A case control study. *South Med J, 99*(5), 482-485. doi:10.1097/01.smj.0000215640.97668.3f

Kojima, H., Sakamoto, J., & Yasue, M. (1999). Circadian rhythm-modulated chemotherapy with high dose 5-fluorouracil against gastrointestinal cancers: evaluation and case report. *Nagoya J Med Sci, 62*(1-2), 29-38.

Kondratov, R. V., Kondratova, A. A., Gorbacheva, V. Y., Vykhovanets, O. V., & Antoch, M. P.

(2006). Early aging and age-related pathologies in mice deficient in BMAL1, the core component of the circadian clock. *Genes Dev, 20*(14), 1868-1873. doi:10.1101/gad.1432206

Kondratov, R. V., Vykhovanets, O., Kondratova, A. A., & Antoch, M. P. (2009). Antioxidant N-acetyl-L-cysteine ameliorates symptoms of premature aging associated with the deficiency of the circadian protein BMAL1. *Aging (Albany NY), 1*(12), 979-987. doi:10.18632/aging.100113

Koren, S., & Fleischmann, W. R. (1993). Optimal circadian timing reduces the myelosuppressive activity of recombinant murine interferon-gamma administered to mice. *J Interferon Res, 13*(3), 187-195.

Koren, S., Whorton, E. B., & Fleischmann, W. R. (1993). Circadian dependence of interferon antitumor activity in mice. *J Natl Cancer Inst, 85*(23), 1927-1932.

Kowalska, E., Ripperger, J. A., Hoegger, D. C., Bruegger, P., Buch, T., Birchler, T., . . . Brown, S. A. (2013). NONO couples the circadian clock to the cell cycle. *Proc Natl Acad Sci U S A, 110*(5), 1592-1599. doi:10.1073/pnas.1213317110

Kuroda, H., Tahara, Y., Saito, K., Ohnishi, N., Kubo, Y., Seo, Y., . . . Shibata, S. (2012). Meal frequency patterns determine the phase of mouse peripheral circadian clocks. *Sci Rep, 2*, 711. doi:10.1038/srep00711

Köllisch, G., Kalali, B. N., Voelcker, V., Wallich, R., Behrendt, H., Ring, J., . . . Ollert, M. (2005). Various members of the Toll-like receptor family contribute to the innate immune response of human epidermal keratinocytes. *Immunology, 114*(4), 531-541. doi:10.1111/j.1365-2567.2005.02122.x

Lamia, K. A., Papp, S. J., Yu, R. T., Barish, G. D., Uhlenhaut, N. H., Jonker, J. W., . . . Evans, R. M. (2011). Cryptochromes mediate rhythmic repression of the glucocorticoid receptor. *Nature, 480*(7378), 552-556. doi:10.1038/nature10700

Lapenna, D., De Gioia, S., Mezzetti, A., Porreca, E., Ciofani, G., Marzio, L., . . . Cuccurullo, F. (1992). Circadian variations in antioxidant defences and lipid peroxidation in the rat heart. *Free Radic Res Commun, 17*(3), 187-194.

Laporte, D., Lebaudy, A., Sahin, A., Pinson, B., Ceschin, J., Daignan-Fornier, B., & Sagot, I. (2011). Metabolic status rather than cell cycle signals control quiescence entry and exit. *J Cell Biol, 192*(6), 949-957. doi:10.1083/jcb.201009028

Le Belle, J. E., Orozco, N. M., Paucar, A. A., Saxe, J. P., Mottahedeh, J., Pyle, A. D., . . . Kornblum, H. I. (2011). Proliferative neural stem cells have high endogenous ROS levels that regulate self-renewal and neurogenesis in a PI3K/Akt-dependant manner. *Cell Stem Cell, 8*(1), 59-71. doi:10.1016/j.stem.2010.11.028

Lebre, M. C., van der Aar, A. M., van Baarsen, L., van Capel, T. M., Schuitemaker, J. H., Kapsenberg, M. L., & de Jong, E. C. (2007). Human keratinocytes express functional Toll-like receptor 3, 4, 5, and 9. *J Invest Dermatol, 127*(2), 331-341. doi:10.1038/sj.jid.5700530

Lengyel, Z., Battyáni, Z., Szekeres, G., Csernus, V., & Nagy, A. D. (2013). Circadian clocks and tumor biology: what is to learn from human skin biopsies? *Gen Comp Endocrinol, 188*, 67-74. doi:10.1016/j.ygcen.2013.03.033

Levi, F., & Schibler, U. (2007). Circadian rhythms: mechanisms and therapeutic implications. *Annu Rev Pharmacol Toxicol, 47*, 593-628. doi:10.1146/annurev.pharmtox.47.120505.105208

Li, H., Handsaker, B., Wysoker, A., Fennell, T., Ruan, J., Homer, N., . . . Subgroup, G. P. D. P.

(2009). The Sequence Alignment/Map format and SAMtools. *Bioinformatics, 25*(16), 2078-2079. doi:10.1093/bioinformatics/btp352

Li, W., Hofer, M. J., Songkhunawej, P., Jung, S. R., Hancock, D., Denyer, G., & Campbell, I. L. (2017). Type I interferon-regulated gene expression and signaling in murine mixed glial cells lacking signal transducers and activators of transcription 1 or 2 or interferon regulatory factor 9. *J Biol Chem, 292*(14), 5845-5859. doi:10.1074/jbc.M116.756510

Li, W. Q., Qureshi, A. A., Schernhammer, E. S., & Han, J. (2013). Rotating night-shift work and risk of psoriasis in US women. *J Invest Dermatol, 133*(2), 565-567. doi:10.1038/jid.2012.285

Li, Z., Musich, P. R., Serrano, M. A., Dong, Z., & Zou, Y. (2011). XPA-mediated regulation of global nucleotide excision repair by ATR Is p53-dependent and occurs primarily in S-phase. *PLoS One, 6*(12), e28326. doi:10.1371/journal.pone.0028326

Libert, S., Bonkowski, M. S., Pointer, K., Pletcher, S. D., & Guarente, L. (2012). Deviation of innate circadian period from 24 h reduces longevity in mice. *Aging Cell, 11*(5), 794-800. doi:10.1111/j.1474-9726.2012.00846.x

Lin, K. K., Kumar, V., Geyfman, M., Chudova, D., Ihler, A. T., Smyth, P., . . . Andersen, B. (2009). Circadian clock genes contribute to the regulation of hair follicle cycling. *PLoS Genet, 5*(7), e1000573. doi:10.1371/journal.pgen.1000573

Liu, J., Malkani, G., Mankani, G., Shi, X., Meyer, M., Cunningham-Runddles, S., . . . Sun, Z. S. (2006). The circadian clock Period 2 gene regulates gamma interferon production of NK cells in host response to lipopolysaccharide-induced endotoxic shock. *Infect Immun, 74*(8), 4750-4756. doi:10.1128/IAI.00287-06

Lomb, N. R. (1976). Least-squares frequency analysis of unequally spaced data. *Astrophysics and Space Science, 39*(2), 447-462. doi:10.1007/bf00648343

Lowrey, P. L., & Takahashi, J. S. (2011). Genetics of circadian rhythms in Mammalian model organisms. *Adv Genet, 74*, 175-230. doi:10.1016/B978-0-12-387690-4.00006-4

Lévi, F., Filipski, E., Iurisci, I., Li, X. M., & Innominato, P. (2007). Cross-talks between circadian timing system and cell division cycle determine cancer biology and therapeutics. *Cold Spring Harb Symp Quant Biol, 72*, 465-475. doi:10.1101/sqb.2007.72.030

Majumdar, T., Dhar, J., Patel, S., Kondratov, R., & Barik, S. (2017). Circadian transcription factor BMAL1 regulates innate immunity against select RNA viruses. *Innate Immun, 23*(2), 147-154. doi:10.1177/1753425916681075

Malakhova, O. A., Yan, M., Malakhov, M. P., Yuan, Y., Ritchie, K. J., Kim, K. I., . . . Zhang, D. E. (2003). Protein ISGylation modulates the JAK-STAT signaling pathway. *Genes Dev, 17*(4), 455-460. doi:10.1101/gad.1056303

Mancuso, G., Gambuzza, M., Midiri, A., Biondo, C., Papasergi, S., Akira, S., . . . Beninati, C. (2009). Bacterial recognition by TLR7 in the lysosomes of conventional dendritic cells. *Nat Immunol, 10*(6), 587-594. doi:10.1038/ni.1733

Marcheva, B., Ramsey, K. M., Buhr, E. D., Kobayashi, Y., Su, H., Ko, C. H., . . . Bass, J. (2010). Disruption of the clock components CLOCK and BMAL1 leads to hypoinsulinaemia and diabetes. *Nature, 466*(7306), 627-631. doi:10.1038/nature09253

Marié, I., Durbin, J. E., & Levy, D. E. (1998). Differential viral induction of distinct interferon-alpha genes by positive feedback through interferon regulatory factor-7. *EMBO J, 17*(22), 6660-6669. doi:10.1093/emboj/17.22.6660

Marpegan, L., Leone, M. J., Katz, M. E., Sobrero, P. M., Bekinstein, T. A., & Golombek, D. A.

(2009). Diurnal variation in endotoxin-induced mortality in mice: correlation with proinflammatory factors. *Chronobiol Int, 26*(7), 1430-1442. doi:10.3109/07420520903408358

Martín, V., Sainz, R. M., Mayo, J. C., Antolín, I., Herrera, F., & Rodríguez, C. (2003). Daily rhythm of gene expression in rat superoxide dismutases. *Endocr Res, 29*(1), 83-95.

Masri, S., Cervantes, M., & Sassone-Corsi, P. (2013). The circadian clock and cell cycle: interconnected biological circuits. *Curr Opin Cell Biol, 25*(6), 730-734. doi:10.1016/j.ceb.2013.07.013

Matsu-Ura, T., Dovzhenok, A., Aihara, E., Rood, J., Le, H., Ren, Y., . . . Hong, C. I. (2016). Intercellular Coupling of the Cell Cycle and Circadian Clock in Adult Stem Cell Culture. *Mol Cell, 64*(5), 900-912. doi:10.1016/j.molcel.2016.10.015

Matsui, M. S., Pelle, E., Dong, K., & Pernodet, N. (2016). Biological Rhythms in the Skin. *Int J Mol Sci, 17*(6). doi:10.3390/ijms17060801

Maurice, D. V., Lightsey, S. F., Hsu, K. T., & Rhoades, J. F. (1991). Comparison of glutathione S-transferase activity in the rat and birds: tissue distribution and rhythmicity in chicken (Gallus domesticus) liver. *Comp Biochem Physiol B, 100*(3), 471-474.

Mauvoisin, D., Wang, J., Jouffe, C., Martin, E., Atger, F., Waridel, P., . . . Naef, F. (2014). Circadian clock-dependent and -independent rhythmic proteomes implement distinct diurnal functions in mouse liver. *Proc Natl Acad Sci U S A, 111*(1), 167-172. doi:10.1073/pnas.1314066111

Menet, J. S., Pescatore, S., & Rosbash, M. (2014). CLOCK:BMAL1 is a pioneer-like transcription factor. *Genes Dev, 28*(1), 8-13. doi:10.1101/gad.228536.113

Miller, L. S., Sørensen, O. E., Liu, P. T., Jalian, H. R., Eshtiaghpour, D., Behmanesh, B. E., . . . Modlin, R. L. (2005). TGF-alpha regulates TLR expression and function on epidermal keratinocytes. *J Immunol, 174*(10), 6137-6143.

Miyamoto, I., Miura, N., Niwa, H., Miyazaki, J., & Tanaka, K. (1992). Mutational analysis of the structure and function of the xeroderma pigmentosum group A complementing protein. Identification of essential domains for nuclear localization and DNA excision repair. *J Biol Chem, 267*(17), 12182-12187.

Mohawk, J. A., Green, C. B., & Takahashi, J. S. (2012). Central and peripheral circadian clocks in mammals. *Annu Rev Neurosci, 35*, 445-462. doi:10.1146/annurev-neuro-060909-153128

Mohty, M., Vialle-Castellano, A., Nunes, J. A., Isnardon, D., Olive, D., & Gaugler, B. (2003). IFN-α Skews Monocyte Differentiation into Toll-Like Receptor 7-Expressing Dendritic Cells with Potent Functional Activities. *The Journal of Immunology, 171*(7), 3385.

Moriwaki, S., & Takahashi, Y. (2008). Photoaging and DNA repair. *J Dermatol Sci, 50*(3), 169-176. doi:10.1016/j.jdermsci.2007.08.011

Mossman, K. L., Macgregor, P. F., Rozmus, J. J., Goryachev, A. B., Edwards, A. M., & Smiley, J. R. (2001). Herpes simplex virus triggers and then disarms a host antiviral response. *J Virol, 75*(2), 750-758. doi:10.1128/JVI.75.2.750-758.2001

Mukherji, A., Kobiita, A., Ye, T., & Chambon, P. (2013). Homeostasis in intestinal epithelium is orchestrated by the circadian clock and microbiota cues transduced by TLRs. *Cell, 153*(4), 812-827. doi:10.1016/j.cell.2013.04.020

Naik, S., Bouladoux, N., Linehan, J. L., Han, S. J., Harrison, O. J., Wilhelm, C., . . . Belkaid, Y. (2015). Commensal-dendritic-cell interaction specifies a unique protective skin immune signature. *Nature, 520*(7545), 104-108. doi:10.1038/nature14052

Nakamura, Y., Harama, D., Shimokawa, N., Hara, M., Suzuki, R., Tahara, Y., . . . Nakao, A. (2011). Circadian clock gene Period2 regulates a time-of-day-dependent variation in cutaneous anaphylactic reaction. *J Allergy Clin Immunol, 127*(4), 1038-1045.e1031-1033. doi:10.1016/j.jaci.2011.02.006

Nakamura, Y., Nakano, N., Ishimaru, K., Hara, M., Ikegami, T., Tahara, Y., . . . Nakao, A. (2014). Circadian regulation of allergic reactions by the mast cell clock in mice. *J Allergy Clin Immunol, 133*(2), 568-575. doi:10.1016/j.jaci.2013.07.040

Ning, S., Huye, L. E., & Pagano, J. S. (2005). Regulation of the transcriptional activity of the IRF7 promoter by a pathway independent of interferon signaling. *J Biol Chem, 280*(13), 12262-12270. doi:10.1074/jbc.M404260200

Ohdo, S., Wang, D. S., Koyanagi, S., Takane, H., Inoue, K., Aramaki, H., . . . Higuchi, S. (2000). Basis for dosing time-dependent changes in the antiviral activity of interferon-alpha in mice. *J Pharmacol Exp Ther, 294*(2), 488-493.

Pai, M. P., & Hunt, T. K. (1972). Effect of varying oxygen tensions on healing of open wounds. *Surg Gynecol Obstet, 135*(5), 756-758.

Pan, X., & Hussain, M. M. (2009). Clock is important for food and circadian regulation of macronutrient absorption in mice. *J Lipid Res, 50*(9), 1800-1813. doi:10.1194/jlr.M900085-JLR200

Panda, S., Antoch, M. P., Miller, B. H., Su, A. I., Schook, A. B., Straume, M., . . . Hogenesch, J. B. (2002). Coordinated transcription of key pathways in the mouse by the circadian clock. *Cell, 109*(3), 307-320.

Pantazis, P. (1980). Sensitivity of DNA synthetic phase to near-ultraviolet radiation: chromatid damage at early and late replication periods. *Cancer Lett, 10*(3), 253-259.

Pasparakis, M., Haase, I., & Nestle, F. O. (2014). Mechanisms regulating skin immunity and inflammation. *Nat Rev Immunol, 14*(5), 289-301. doi:10.1038/nri3646

Pekovic-Vaughan, V., Gibbs, J., Yoshitane, H., Yang, N., Pathiranage, D., Guo, B., . . . Meng, Q. J. (2014). The circadian clock regulates rhythmic activation of the NRF2/glutathione-mediated antioxidant defense pathway to modulate pulmonary fibrosis. *Genes Dev, 28*(6), 548-560. doi:10.1101/gad.237081.113

Pendergast, J. S., Yeom, M., Reyes, B. A., Ohmiya, Y., & Yamazaki, S. (2010). Disconnected circadian and cell cycles in a tumor-driven cell line. *Commun Integr Biol, 3*(6), 536-539. doi:10.4161/cib.3.6.12841

Plikus, M. V., Van Spyk, E. N., Pham, K., Geyfman, M., Kumar, V., Takahashi, J. S., & Andersen, B. (2015). The circadian clock in skin: implications for adult stem cells, tissue regeneration, cancer, aging, and immunity. *J Biol Rhythms, 30*(3), 163-182. doi:10.1177/0748730414563537

Plikus, M. V., Vollmers, C., de la Cruz, D., Chaix, A., Ramos, R., Panda, S., & Chuong, C. M. (2013). Local circadian clock gates cell cycle progression of transient amplifying cells during regenerative hair cycling. *Proc Natl Acad Sci U S A, 110*(23), E2106-2115. doi:10.1073/pnas.1215935110

Pluquet, O., Dejeans, N., & Chevet, E. (2014). Watching the clock: endoplasmic reticulum-mediated control of circadian rhythms in cancer. *Ann Med, 46*(4), 233-243. doi:10.3109/07853890.2013.874664

Porritt, R. A., & Hertzog, P. J. Dynamic control of type I IFN signalling by an integrated network of negative regulators. *Trends in Immunology, 36*(3), 150-160.

Preitner, N., Damiola, F., Lopez-Molina, L., Zakany, J., Duboule, D., Albrecht, U., & Schibler,

U. (2002). The orphan nuclear receptor REV-ERBalpha controls circadian transcription within the positive limb of the mammalian circadian oscillator. *Cell, 110*(2), 251-260.

Prendergast, B. J., Cable, E. J., Patel, P. N., Pyter, L. M., Onishi, K. G., Stevenson, T. J., . . . Bradley, S. P. (2013). Impaired leukocyte trafficking and skin inflammatory responses in hamsters lacking a functional circadian system. *Brain Behav Immun, 32*, 94-104. doi:10.1016/j.bbi.2013.02.007

Rannug, A., & Fritsche, E. (2006). The aryl hydrocarbon receptor and light. In *Biological Chemistry* (Vol. 387, pp. 1149).

Renn, C. N., Sanchez, D. J., Ochoa, M. T., Legaspi, A. J., Oh, C. K., Liu, P. T., . . . Modlin, R. L. (2006). TLR activation of Langerhans cell-like dendritic cells triggers an antiviral immune response. *J Immunol, 177*(1), 298-305.

Reppert, S. M., & Weaver, D. R. (2002). Coordination of circadian timing in mammals. *Nature, 418*(6901), 935-941. doi:10.1038/nature00965

Revelle, W. (2016). psych: Procedures for Psycological, Psychometric, and Personality Research (Version 1.6.9). Evanston, Illinois: Northwestern University. Retrieved from https://CRAN.R-project.org/package=psych

Rey, G., Cesbron, F., Rougemont, J., Reinke, H., Brunner, M., & Naef, F. (2011). Genome-wide and phase-specific DNA-binding rhythms of BMAL1 control circadian output functions in mouse liver. *PLoS Biol, 9*(2), e1000595. doi:10.1371/journal.pbio.1000595

Reznick, J., Preston, E., Wilks, D. L., Beale, S. M., Turner, N., & Cooney, G. J. (2013). Altered feeding differentially regulates circadian rhythms and energy metabolism in liver and muscle of rats. *Biochim Biophys Acta, 1832*(1), 228-238. doi:10.1016/j.bbadis.2012.08.010

Rhee, S. H., Jones, B. W., Toshchakov, V., Vogel, S. N., & Fenton, M. J. (2003). Toll-like receptors 2 and 4 activate STAT1 serine phosphorylation by distinct mechanisms in macrophages. *J Biol Chem, 278*(25), 22506-22512. doi:10.1074/jbc.M208633200

Sancar, A., Lindsey-Boltz, L. A., Gaddameedhi, S., Selby, C. P., Ye, R., Chiou, Y. Y., . . . Ozturk, N. (2015). Circadian clock, cancer, and chemotherapy. *Biochemistry, 54*(2), 110-123. doi:10.1021/bi5007354

Satija, R., Farrell, J. A., Gennert, D., Schier, A. F., & Regev, A. (2015). Spatial reconstruction of single-cell gene expression data. *Nat Biotechnol, 33*(5), 495-502. doi:10.1038/nbt.3192

Sato, M., Suemori, H., Hata, N., Asagiri, M., Ogasawara, K., Nakao, K., . . . Taniguchi, T. (2000). Distinct and essential roles of transcription factors IRF-3 and IRF-7 in response to viruses for IFN-alpha/beta gene induction. *Immunity, 13*(4), 539-548.

Scheurmann, J., Treiber, N., Weber, C., Renkl, A. C., Frenzel, D., Trenz-Buback, F., . . . Weiss, J. M. (2014). Mice with heterozygous deficiency of manganese superoxide dismutase (SOD2) have a skin immune system with features of "inflamm-aging". *Arch Dermatol Res, 306*(2), 143-155. doi:10.1007/s00403-013-1389-7

Scheving, L. E. (1959). Mitotic activity in the human epidermis. *135*(1), 7-19.

Sherman, B. T., Huang, d. W., Tan, Q., Guo, Y., Bour, S., Liu, D., . . . Lempicki, R. A. (2007). DAVID Knowledgebase: a gene-centered database integrating heterogeneous gene annotation resources to facilitate high-throughput gene functional analysis. *BMC Bioinformatics, 8*, 426. doi:10.1186/1471-2105-8-426

Sigurdardottir, L. G., Valdimarsdottir, U. A., Fall, K., Rider, J. R., Lockley, S. W., Schernhammer, E., & Mucci, L. A. (2012). Circadian disruption, sleep loss, and prostate cancer risk: a systematic review of epidemiologic studies. *Cancer Epidemiol Biomarkers*

Prev, 21(7), 1002-1011. doi:10.1158/1055-9965.EPI-12-0116
SINCLAIR, W. K., & MORTON, R. A. (1965). X-RAY AND ULTRAVIOLET SENSITIVITY OF SYNCHRONIZED CHINESE HAMSTER CELLS AT VARIOUS STAGES OF THE CELL CYCLE. *Biophys J, 5*, 1-25.
Stokkan, K.-A., Yamazaki, S., Tei, H., Sakaki, Y., & Menaker, M. (2001). Entrainment of the Circadian Clock in the Liver by Feeding. *Science, 291*(5503), 490.
Stringari, C., Wang, H., Geyfman, M., Crosignani, V., Kumar, V., Takahashi, J. S., . . . Gratton, E. (2015). In vivo single-cell detection of metabolic oscillations in stem cells. *Cell Rep, 10*(1), 1-7. doi:10.1016/j.celrep.2014.12.007
Sugiura, K. (2013). Unfolded protein response in keratinocytes: impact on normal and abnormal keratinization. *J Dermatol Sci, 69*(3), 181-186. doi:10.1016/j.jdermsci.2012.12.002
Sumaria, N., Roediger, B., Ng, L. G., Qin, J., Pinto, R., Cavanagh, L. L., . . . Weninger, W. (2011). Cutaneous immunosurveillance by self-renewing dermal gammadelta T cells. *J Exp Med, 208*(3), 505-518. doi:10.1084/jem.20101824
Swindell, W. R., Michaels, K. A., Sutter, A. J., Diaconu, D., Fritz, Y., Xing, X., . . . Ward, N. L. (2017). Imiquimod has strain-dependent effects in mice and does not uniquely model human psoriasis. *Genome Med, 9*(1), 24. doi:10.1186/s13073-017-0415-3
Takita, E., Yokota, S., Tahara, Y., Hirao, A., Aoki, N., Nakamura, Y., . . . Shibata, S. (2013). Biological clock dysfunction exacerbates contact hypersensitivity in mice. *Br J Dermatol, 168*(1), 39-46. doi:10.1111/j.1365-2133.2012.11176.x
Tan, D. X., Reiter, R. J., Manchester, L. C., Yan, M. T., El-Sawi, M., Sainz, R. M., . . . Hardeland, R. (2002). Chemical and physical properties and potential mechanisms: melatonin as a broad spectrum antioxidant and free radical scavenger. *Curr Top Med Chem, 2*(2), 181-197.
Tanimura, N., Kusunose, N., Matsunaga, N., Koyanagi, S., & Ohdo, S. (2011). Aryl hydrocarbon receptor-mediated Cyp1a1 expression is modulated in a CLOCK-dependent circadian manner. *Toxicology, 290*(2-3), 203-207. doi:10.1016/j.tox.2011.09.007
Tanioka, M., Yamada, H., Doi, M., Bando, H., Yamaguchi, Y., Nishigori, C., & Okamura, H. (2009). Molecular clocks in mouse skin. *J Invest Dermatol, 129*(5), 1225-1231. doi:10.1038/jid.2008.345
Team, R. C. (2014). R: A language and environment for statistical computing. Vienna, Austria: R Foundation for Statistical Computing. Retrieved from http://www.r-project.org/
Teijaro, J. R., Ng, C., Lee, A. M., Sullivan, B. M., Sheehan, K. C., Welch, M., . . . Oldstone, M. B. (2013). Persistent LCMV infection is controlled by blockade of type I interferon signaling. *Science, 340*(6129), 207-211. doi:10.1126/science.1235214
Terasima, T., & Tolmach, L. J. (1961). Changes in X-ray Sensitivity of HeLa Cells during the Division Cycle. *190*(4782), 1210-1211.
Tomasetti, C., & Vogelstein, B. (2015). Cancer etiology. Variation in cancer risk among tissues can be explained by the number of stem cell divisions. *Science, 347*(6217), 78-81. doi:10.1126/science.1260825
Valacchi, G., Sticozzi, C., Pecorelli, A., Cervellati, F., Cervellati, C., & Maioli, E. (2012). Cutaneous responses to environmental stressors. *Ann N Y Acad Sci, 1271*, 75-81. doi:10.1111/j.1749-6632.2012.06724.x
Velarde, M. C., Flynn, J. M., Day, N. U., Melov, S., & Campisi, J. (2012). Mitochondrial oxidative stress caused by Sod2 deficiency promotes cellular senescence and aging phenotypes in the skin. *Aging (Albany NY), 4*(1), 3-12. doi:10.18632/aging.100423

Vollmers, C., Gill, S., DiTacchio, L., Pulivarthy, S. R., Le, H. D., & Panda, S. (2009). Time of feeding and the intrinsic circadian clock drive rhythms in hepatic gene expression. *Proc Natl Acad Sci U S A, 106*(50), 21453-21458. doi:10.1073/pnas.0909591106

Wang, H., van Spyk, E., Liu, Q., Geyfman, M., Salmans, M. L., Kumar, V., . . . Andersen, B. (2017). Time-Restricted Feeding Shifts the Skin Circadian Clock and Alters UVB-Induced DNA Damage. *Cell Rep, 20*(5), 1061-1072. doi:10.1016/j.celrep.2017.07.022

Wang, L., Wang, S., & Li, W. (2012). RSeQC: quality control of RNA-seq experiments. *Bioinformatics, 28*(16), 2184-2185. doi:10.1093/bioinformatics/bts356

Wang, X., Spandidos, A., Wang, H., & Seed, B. (2012). PrimerBank: a PCR primer database for quantitative gene expression analysis, 2012 update. *Nucleic Acids Res, 40*(Database issue), D1144-1149. doi:10.1093/nar/gkr1013

Wathelet, M. G., Lin, C. H., Parekh, B. S., Ronco, L. V., Howley, P. M., & Maniatis, T. (1998). Virus infection induces the assembly of coordinately activated transcription factors on the IFN-beta enhancer in vivo. *Mol Cell, 1*(4), 507-518.

Wilking, M., Ndiaye, M., Mukhtar, H., & Ahmad, N. (2013). Circadian rhythm connections to oxidative stress: implications for human health. *Antioxid Redox Signal, 19*(2), 192-208. doi:10.1089/ars.2012.4889

Xu, C. X., Krager, S. L., Liao, D. F., & Tischkau, S. A. (2010). Disruption of CLOCK-BMAL1 transcriptional activity is responsible for aryl hydrocarbon receptor-mediated regulation of Period1 gene. *Toxicol Sci, 115*(1), 98-108. doi:10.1093/toxsci/kfq022

Yan, J., Wang, H., Liu, Y., & Shao, C. (2008). Analysis of gene regulatory networks in the mammalian circadian rhythm. *PLoS Comput Biol, 4*(10), e1000193. doi:10.1371/journal.pcbi.1000193

Yang, G., Chen, L., Grant, G. R., Paschos, G., Song, W. L., Musiek, E. S., . . . FitzGerald, G. A. (2016). Timing of expression of the core clock gene Bmal1 influences its effects on aging and survival. *Sci Transl Med, 8*(324), 324ra316. doi:10.1126/scitranslmed.aad3305

Yang, R., & Su, Z. (2010). Analyzing circadian expression data by harmonic regression based on autoregressive spectral estimation. *Bioinformatics, 26*(12), i168-174. doi:10.1093/bioinformatics/btq189

Yeom, M., Pendergast, J. S., Ohmiya, Y., & Yamazaki, S. (2010). Circadian-independent cell mitosis in immortalized fibroblasts. *Proc Natl Acad Sci U S A, 107*(21), 9665-9670. doi:10.1073/pnas.0914078107

Yoon, J. A., Han, D. H., Noh, J. Y., Kim, M. H., Son, G. H., Kim, K., . . . Cho, S. (2012). Meal time shift disturbs circadian rhythmicity along with metabolic and behavioral alterations in mice. *PLoS One, 7*(8), e44053. doi:10.1371/journal.pone.0044053

Yosipovitch, G., Goon, A., Wee, J., Chan, Y. H., & Goh, C. L. (2000). The prevalence and clinical characteristics of pruritus among patients with extensive psoriasis. *Br J Dermatol, 143*(5), 969-973.

Yosipovitch, G., & Tang, M. B. (2002). Practical management of psoriasis in the elderly: epidemiology, clinical aspects, quality of life, patient education and treatment options. *Drugs Aging, 19*(11), 847-863.

Zarrinpar, A., Chaix, A., Yooseph, S., & Panda, S. (2014). Diet and feeding pattern affect the diurnal dynamics of the gut microbiome. *Cell Metab, 20*(6), 1006-1017. doi:10.1016/j.cmet.2014.11.008

Zhang, J., Raper, A., Sugita, N., Hingorani, R., Salio, M., Palmowski, M. J., . . . Crocker, P. R. (2006). Characterization of Siglec-H as a novel endocytic receptor expressed on murine

plasmacytoid dendritic cell precursors. *Blood, 107*(9), 3600-3608. doi:10.1182/blood-2005-09-3842

Zhang, L. J., Sen, G. L., Ward, N. L., Johnston, A., Chun, K., Chen, Y., . . . Gallo, R. L. (2016). Antimicrobial Peptide LL37 and MAVS Signaling Drive Interferon-β Production by Epidermal Keratinocytes during Skin Injury. *Immunity, 45*(1), 119-130. doi:10.1016/j.immuni.2016.06.021

Zhang, Y., Mao, D., Roswit, W. T., Jin, X., Patel, A. C., Patel, D. A., . . . Holtzman, M. J. (2015). PARP9-DTX3L ubiquitin ligase targets host histone H2BJ and viral 3C protease to enhance interferon signaling and control viral infection. *Nat Immunol, 16*(12), 1215-1227. doi:10.1038/ni.3279

zur Hausen, H. (1991). Viruses in human cancers. *Science, 254*(5035), 1167-1173.